Analysis and Control of Dynamical Systems with Quasi-Periodic Coefficients

by

Ashu Sharma

A dissertation submitted to the Graduate Faculty of
Auburn University
in partial fulfillment of the
requirements for the Degree of
Doctor of Philosophy

Auburn, Alabama
August 03, 2019

Keywords: Quasi-periodic, Lyapunov-Perron Transformation
Floquet theory, Stability, Chaos Control, Instability pockets

Approved by

Subhash C. Sinha, Chair, Alumni Professor Emeritus of Mechanical Engineering
George T. Flowers, Professor of Mechanical Engineering
John Y. Hung, Professor of Electrical and Computer Engineering
Dan Marghitu, Professor of Mechanical Engineering

Abstract

Parametrically excited linear systems with oscillatory coefficients have been generally modeled by Mathieu or Hill equations (periodic coefficients) because their stability and response can be determined by Floquét theory. However, in many cases the parametric excitation is not periodic but consists of frequencies that are incommensurate, making them quasi-periodic. Unfortunately, there is no complete theory for linear dynamic systems with quasi-periodic coefficients. Motivated by this fact, in this work, an approximate approach has been proposed to determine the stability and response of quasi-periodic systems. It is suggested here that a quasi-periodic system may be replaced by a periodic system with an appropriate large principal period and thus making it suitable for an application of the Floquét theory. Based on this premise, a systematic approach has been developed and applied to three typical quasi-periodic systems. The approximate boundaries in stability charts obtained from the proposed method are very close to the exact boundaries of original quasi-periodic equations computed numerically using maximal Lyapunov exponents. Further, the frequency spectra of solutions generated near approximate and exact boundaries are found to be almost identical ensuring a high degree of accuracy. In addition, state transition matrices are also computed symbolically in terms of system parameters using Chebyshev polynomials and Picard iteration method. The coefficients of parametric excitation terms are not necessarily small in all cases.

A detailed analysis of ‘instability pockets’ appearing in stability diagrams of parametrically excited systems is also discussed. The alterations in ‘instability pockets’ and stability diagrams, in

general, due to addition of damping is systematically studied. In particular, the results for some typical cases of Mathieu, Meissner, three-frequency Hill and Quasi-Periodic Hill equations are presented in detail.

A methodology to control general nonlinear systems to desired periodic or quasi-periodic motions is also presented. The desired motion could be a periodic orbit, a quasi-periodic motion or a fixed point and does not need to be a solution of the nonlinear system. The applicability of the approach is demonstrated by controlling chaotic systems to desired motions. The controller design is achieved using a combination of a nonlinear feedforward controller and a linear feedback controller.

Acknowledgments

The author is gratefully indebted to Dr. Subhash C. Sinha, Professor, Department of Mechanical Engineering, for his invaluable guidance, encouragement and patience in all stages of this work. He would also like to thank Dr. George T. Flowers, Professor, Department of Mechanical Engineering, Dr. John Y. Hung, Professor, Department of Electrical and Computer Engineering and Dr. Dan Marghitu, Professor, Department of Mechanical Engineering, for serving on his committee.

Finally, the author would like to dedicate this work to his parents, Ajay and Mridula; his wife, Vipasha; and his sister, Richa, for all their love and support, without which this endeavor would never have been successful.

Table of Contents

List of Tables

List of Figures

Chapter 1

Introduction

1.1 Motivation

Linear ordinary differential equations with time-periodic coefficients have a wide range of applications in various fields of science and engineering. Some of their applications include structures subjected to periodic loads [1], helicopter rotor blades in forward flight [2], asymmetric rotor bearing systems [3], robots performing repetitive tasks [4], ship dynamics [5], attitude stability of satellites [6], heart rhythms [7] and quantum mechanics [8], among others. These systems are also called 'parametrically excited systems' since system parameters in mathematical models are no longer constants but become periodic functions of time. These periodic functions can cause instability known as 'parametric resonance'.

In 1883, Gaston Floquét developed a complete theory [9] (now known as the 'Floquét Theory') that determines stability and response of linear ordinary differential equations with periodic coefficients. Since then several numerical, analytical and symbolic techniques have been developed to compute stability and response of periodic systems using the Floquét theory. Some authors approximated the periodic coefficient matrix (periodic functions) by piecewise constant, linear and quadratic matrix (functions) [10, 11] in order to generate approximate solutions. Using Hammond's improved integration scheme [12], Friedmann *et al*. [13] employed Hsu's approach and suggested a numerically

efficient method that requires only a single integration pass scheme. Analytical techniques such as perturbation [14] & averaging [15] have been used by a number of authors to determine stability of periodic systems. However, their effectiveness is restricted by the requirement of existence of a small parameter and a generating solution. To overcome the above limitations, Sinha and his associates developed an efficient technique to compute the state transition matrix of such systems in semi-analytical [16] as well as in symbolic forms [17, 18]. Design of control systems to drive arbitrary unstable or chaotic motions to a periodic orbit also utilizes Floquét theory [19, 20].

As far as applications are concerned, numerous contributions exist in the literature. In most cases, systems have been modeled by Mathieu or Hill equations because one is able to predict their stability and response by the use of Floquét Theory. However, in many cases these are oversimplified models since in reality the parametric excitation is not periodic but consists of frequencies that are incommensurate, making it quasi-periodic. For example, parametric excitation occurs when a ship is sailing in longitudinal waves *i.e.*, sea waves are along the length of the ship. Assuming the vertical force due to sea waves as a periodic force, the equation of motion turns out to be a Mathieu/Hill equation. However, sea waves are not periodic in nature, instead contain incommensurate frequencies. Like the sea waves, the motion of Basilar Membrane (BM) in cochlea of the inner ear and the motion of a heart are some other examples where the parametric forcing terms may not be assumed to be periodic. An appropriate modeling of the heart can be helpful in detecting any irregularities/diseases. The dynamics of BM inside cochlea of inner ear has been a mystery for a long time. Lately, some authors [21-23] have established the fact that BM undergoes parametric excitation and in case of a single tone (frequency) stimuli, dynamic analysis

could be performed using the Floquét theory. However, the structure of sound (speech signal) is generally complex and to understand the dynamics under complex stimuli, study of two or three tone dynamics has to be studied first. Robles *et al.* [24] and Ruggero *et al.* [25] investigated the response of BM to two tone stimuli and established the presence of distortion products (combination of tones). The origin of quasi-periodic solution can also be traced back to Hopf bifurcation of a fixed point that leads to a periodic solution (limit cycle) whose subsequent bifurcation, generally known as the Secondary Hopf bifurcation (or Neimark-Sacker bifurcation), gives birth to either a periodic or a quasi-periodic motion. In order to study the stability of resulting quasi-periodic motion, one has to construct the variational equation about this motion which gives rise to a quasi-periodic Hill equation.

The control of instabilities in these systems is as much important as the determination of stable/unstable regions. In order to design a proper control system, it is imperative to take into account the quasi-periodic behavior of these parametrically excited systems. Control systems are also used during heart surgery to reduce the motion of a part of beating heart over which surgery has to be performed [26, 27]. All these problems require a theoretical framework to understand their dynamics and control, but unfortunately there is no complete theory for linear differential equations with quasi-periodic coefficients. In this work, an attempt has been made to provide an approximate methodology that can be used for a general class of quasi-periodic systems arising in engineering applications.

1.2 Quasi-Periodic (QP) Hill Equation and Related Work

One of the simplest forms of linear differential equations with quasi-periodic coefficients can be represented by a modified damped Mathieu/Hill equation given by

$$\ddot{x} + d\,\dot{x} + \left(a + b_1 \cos \omega_1 t + b_2 \cos \omega_2 t\right) x = 0 \tag{1.1}$$

where, ω_1 and ω_2 are the two parametric frequencies such that ω_1/ω_2 is an irrational number (incommensurate), a, b_1, b_2 and d are system parameters and t is the time. Stability of this type of system has been studied by various authors in the past. In 1980, Davis and Rosenblat [28] studied the QP Hill equation using multiple scale technique and computed the stability boundaries. According to them, stability boundaries arise from 'a' axis for two sets of families, $a = \left(k_1\omega_1\right)^2/4$ and $a = \left(k_2\omega_2\right)^2/4$, where $k_1, k_2 = 0,1,2,\ldots$. Johnson and Moser [29] showed that in the spectral gaps, the rotation number (α) of an almost periodic function is related to the frequency module (M), $2\alpha \in M$. This relationship is valid in the entire parametric space. Since rotation number is independent of the particular solution and is equal to $\sqrt{a}$ when $b_1 = b_2 = 0$, it has been used by several authors to plot the stability diagrams. Zounes and Rand [30] used the results of Johnson and Moser [29] and investigated the QP Hill equation both numerically and analytically. First, the stability diagrams were developed by direct numerical integration and computation of Lyapunov exponents. Later in their paper, expressions for transition curves were derived using regular perturbation and a technique similar to Hill's method of infinite determinants and a good agreement between analytical and numerical solutions was reported. According to them, regions of instability in $a \sim b$ plane originate from 'a' axis at $a = \left(k_1\omega_1 \pm k_2\omega_2\right)^2/4$; $k_1, k_2 = 0,1,2,\ldots$ where main regions of instability arise from $a = \omega_1^2/4$ $(k_1 = 1,\ k_2 = 0)$ and $a = \omega_2^2/4$ $(k_1 = 0,\ k_2 = 1)$. They also mentioned that the higher order resonances are more affected by the damping as compared to the lower order

resonances. Broer and Simó [31] numerically explored the QP Hill equation with two parametric frequencies: $\omega_1 = 1$ and $\omega_2 = \left(\sqrt{5}+1\right)\big/2$. They numerically examined the stability boundaries for relatively large values of parameter (as compared to Zounes and Rand [30]) using maximal Lyapunov exponent and rotation number. In 2011, Puig and Simó [32] investigated the stability boundaries in a QP Hill's equation with three parametric frequencies $\left(\omega_1 = 1,\ \omega_2 = \sqrt{2} \text{ and } \omega_3 = \sqrt{3}\right)$ and plotted the boundaries using rotation number and maximal Lyapunov exponent.

Perturbation and averaging techniques require existence of small parameters and generating solutions, while the application of the Hill's infinite determinants method to QP Hill equation becomes progressively tedious with higher order systems and with larger number of terms in the generalized Fourier series. Moreover, it is known that the Hill's infinite determinants do not converge in all cases [1, 33]. Stability charts can be plotted using rotation number and Lyapunov exponents, however, they require extensive computational power and do not provide analytical insight. To overcome the shortcomings of the above techniques and due to the unavailability of a rigorous theory for quasi-periodic systems, an approximate technique has been presented here. The basic premise is based on the suggestion that a quasi-periodic system may be approximately replaced by a periodic system with an appropriate large principal period and thus making it suitable for an application of the Floquét theory. Apart from establishing the proof of concept via numerical integration, a symbolic technique is also presented that is accurate for a wide range of system parameters.

1.3 Instability Pockets and Effect of Damping in Parametrically Excited Systems

Parametrically excited systems have been the subject of investigations since 1868, when Mathieu [34] first encountered a second order linear differential equation with periodic coefficients while studying the wave motions of an elliptical lake. Since then, the study of parametrically excited systems has found applications in various fields of science and engineering.

In most applications, parametric excitation is periodic or can be modeled to be periodic as an approximation to the true excitation. An equation of this form is known as Hill equation and it is named after G.W. Hill who came across such a differential equation while investigating the motion of the moon's perigee [35]. A special case of Hill equation is the Mathieu equation in which excitation is sinusoidal. These equations have been used to model several physical systems [1,2,6,36,37]. In general, it is difficult to find closed form solutions of time-periodic systems (periodic coefficients). However, there are some special types of Hill equations that have exact solutions [36]. In 1918, Meissner [38] published a paper on the instability in connecting rods of locomotives based on a model in which excitation was assumed to be a rectangular periodic wave function. This equation is commonly known as Meissner equation & it has an exact solution. A rectangular waveform is also used to model time-periodic variation in mesh stiffness in powertrain and gearing applications [39]. MEMS parametric resonators described by Meissner equation can be used in sensing and clocking applications [40]. Gasparetto & Gazzola [41] recently investigated the stability of the Hill equation where the periodic coefficient is an elliptic cosine function. They showed that for certain values of parameters exact solutions can be determined in terms of Jacobi elliptic functions.

Ships sailing in longitudinal sea waves, motion of a heart and Basilar membrane in cochlea of the inner ear are some of the examples where parametric excitation consists of frequencies that are incommensurate, thus making it quasi-periodic.

In general, stability diagrams of Hill & Quasi-Periodic (QP) Hill equations contain strange geometric features that are formed by the intersections of stability boundaries. These closed sub-regions in the parametric space are commonly known as '*Instability pockets*' or '*Instability loops*'. Such pockets do not exist in the stability diagram of Mathieu equation [42]. In 1995, Broer & Levi [43] provided a geometric explanation for instability pockets in Hill equations using singularity theory. Their work was further extended by Broer & Simó [44] in which they concluded that at the k^{th} order resonance, any number of instability pockets (not exceeding $k-1$) can be generated. In 1998, Broer & Simó [31] examined instability pockets in QP Hill equations using the averaging method. However, since instability pockets exist for relatively large amplitudes of parametric excitation, techniques such as averaging & perturbation have limited value in such analyses. Gan & Zhang [45] studied the global structure of instability pockets in Meissner equation with two step potentials using the rotation number approach. But this method cannot be extended to such an equation with three step potentials. Recently, Franco & Collado [46] introduced a concept of maximum growth rate in order to characterize the coexistence points (where instability boundaries intersect) & determined the minimum damping required for an instability pocket to vanish. However, growth rate of solutions were numerically determined.

Damping plays a significant role in engineering applications. Generally speaking, damping has a stabilizing effect & this idea constitutes the main basis in the design of

control systems. However, in certain situations damping could induce instability. In 1875, Thomson & Tait [47] studied gyroscopic systems where the addition of damping destroyed stability. Ziegler [48] was probably the first who pointed out the destabilizing effect of damping in nonconservative systems. The phenomenon of destabilization due to damping is also observed in periodic systems where instability occurs due to the predominant effect of combination resonance [49]. From these studies, it can be concluded that such an instability can be demonstrated only for systems with two degrees of freedom, or higher. Recently, Franco & Collado [50] presented a numerical study of one degree of freedom systems with time-periodic coefficients & showed the destabilizing effect of damping in Mathieu & Meissner equations.

Although numerical methods can always be employed to explore relatively larger parametric region, they require extensive computation effort and, more importantly, they do not provide analytical insight into the problem. To overcome these shortcomings, a symbolic approach developed by Sinha & Butcher [17], has been utilized to investigate instability pockets in several parametrically excited systems. Influence of damping on stability diagrams, in general, and on instability pockets has also been explored using the symbolic technique.

1.4 Control of Nonlinear Systems to Desired Motions

Generally speaking, nonlinear systems have much richer and more complex dynamics than linear systems and some of the interesting behaviors include multiple equilibrium solutions, limit cycles (periodic motions), bifurcations, and chaos, among others. These behaviors may be desirable in some cases but, undesirable in many others. For instance, assembly robots in several manufacturing processes require periodic motions

and it could be realized by a limit cycle of a nonlinear system with low energy consumption [51]. On the other hand, a limit cycle with large amplitude caused by the interaction of aerodynamic forces and structural vibrations in an aircraft wing can be dangerous. Similarly, chaos is desirable in industrial mixing processes and encrypting communications while it is considered undesirable for sensors as it restricts their signal strength and output energy [52]. These desirable/ undesirable dynamics can be controlled with the help of linear or nonlinear active controllers.

The problem of driving nonlinear systems to desired motions leads to equations with time-dependent coefficients. Active control systems can be designed by using existing control techniques applicable to time-varying systems. Pole placement approach for state feedback control design for time-varying systems was first introduced by Follinger [53]. The technique requires either special canonical transformations or iterative schemes [54, 55]. In 1988, Alfhaid and Lee [56] suggested the use of a transformation matrix to convert the time-varying problem into time-invariant form. However, all the examples were restricted to the class of commutative systems. Optimal control theory can also be used for controller design but, it requires the solution of a time-varying matrix Riccati equation [57]. In 1994, Sinha & Joseph [58] introduced a technique based on Floquet theory for the design of controllers for linear dynamical systems with periodic coefficients. Using Lyapunov-Floquet transformation, they reduced the time-periodic system to a time-invariant form to which standard time-invariant methods of control theory can be applied. Due to the presence of generalized inverse in the expression of control law, asymptotic stability cannot be guaranteed by Sinha & Joseph method [59, 60]. In 1988, Middleton & Goodwin [61] presented global and robust BIBS (bounded input and bounded state) stability theory for

adapting controllers applied to time-varying linear systems. In 2006, Zhang & Sinha [62] generalized the idea of feedback linearization for systems with periodic coefficients. Their control scheme was based on Lyapunov-Floquet transformation & normal forms.

One of the applications of control of desirable/ undesirable behaviors of nonlinear systems is chaos control. Pettini [63] first provided the theoretical understanding of the suppression of chaos in Duffing-Holmes oscillator using parametric excitation. Some open problems regarding this approach can be found in Lima and Pettini [64]. In 1989, Hübler & Lüscher [65] presented an open loop strategy to drive chaos to periodic orbits that do not lie in the basin of the strange attractor. However, their methodology is not capable of controlling all chaotic systems or controlling to all periodic orbits [66]. One of the most popular approaches for controlling chaos is Ott-Grebogi-Yorke (OGY) method [67]. This method utilizes the Poincaré map of the system. The control scheme is restricted to the unstable periodic orbits that are embedded in the chaotic attractor and only those unstable periodic orbits can be stabilized whose largest Lyapunov exponent is small compared to the reciprocal of the time interval between which parameter changes [68]. In 1992, Pyragas [68] showed that unstable periodic orbits can be stabilized by delayed feedback controller and in contrast to the OGY method his approach was noise resistant. Jackson & Grosu [16] and Chen [69] independently suggested the use of an open loop (Hübler type) and a closed loop (feedback) actions. Unlike traditional OGY control and Pyragas delayed feedback control, Chen's dual control methodology allows control of chaotic systems to any desired motions. However, Chen incorrectly guaranteed the asymptotic stability of the controlled system by using the eigenvalues of time-varying Jacobian. In 2000, Sinha & Henrichs [70] used the concept of dual control and developed a general approach for local control of

chaotic systems to desired periodic orbits. In their approach, the control law was a combination of a nonlinear feedforward component and a linear feedback component. They designed the feedback controller using Sinha & Joseph method [9] and hence, the asymptotic stability cannot be guaranteed. Sinha *et al.* [71] circumvented this problem by utilizing the symbolic computational technique developed by Sinha & Butcher [17]. They computed the state transition matrix of the feedback system in terms of unknown control gains and guaranteed asymptotic stability by placing Floquet multipliers at desired locations inside the unit circle using a method similar to 'Pole placement' approach.

Although control of chaos has been under detailed investigation for almost last three decades, however, to the authors' best knowledge none of these researches considered the control of chaos to quasi-periodic motions. There are several physical systems that inherent quasi-periodic behaviors, such as motion of a heart & motion of the basilar membrane in the cochlea of the inner ear. The chaotic motion of heart during cardiac arrhythmia could be fatal and hence, a control system is required to drive this irregular behavior to the regular quasi-periodic motion of the heart.

In the present work, a combination of feedforward and feedback controllers is utilized to control chaotic systems to desired periodic or quasi-periodic motions. The design of linear feedback controllers may require a guarantee of stability of ordinary linear differential equations with quasi-periodic coefficients (quasi-periodic systems). An approximate approach proposed in this work is employed to analyze the stability of quasi-periodic systems. The linear feedback controllers are designed using the symbolic technique presented in Ref. [17].

Chapter 2

Stability Analysis of Quasi-Periodic Systems

2.1 Introduction

Parametrically excited linear systems with oscillatory coefficients have been generally modeled by Mathieu or Hill equations (periodic coefficients) because their stability and response can be determined by Floquét theory. However, in many cases the parametric excitation is not periodic but consists of frequencies that are incommensurate, making them quasi-periodic. Unfortunately, there is no complete theory for linear dynamic systems with quasi-periodic coefficients. Motivated by this fact, in this chapter, an approximate approach has been proposed to determine the stability and response of quasi-periodic systems. It is suggested here that a quasi-periodic system may be replaced by a periodic system with an appropriate large principal period and thus making it suitable for an application of the Floquét theory. Based on this premise, a systematic approach has been developed and applied to three typical quasi-periodic systems. In addition, state transition matrices are also computed symbolically in terms of system parameters using Chebyshev polynomials and Picard iteration method. The coefficients of parametric excitation terms are not necessarily small in all cases. First some basic results of Floquét theory are summarized in the following.

2.2 Some basic results of Floquet theory

Floquét theory predicts the stability and response of linear ordinary differential equations with periodic coefficients [72]. Consider

$$\dot{x} = A(t)x \qquad x(0) = x_0 \tag{2.1}$$

where, $x \in \mathbb{R}^n$, $t \in \mathbb{R}^+$, $A(t)$ is an $n \times n$ periodic matrix with the principal period T. Let $\Phi(t)$ be the state transition matrix (STM) such that it satisfies the above linear equation with $\Phi(0) = I$; then the solution of Eq. (2.1) can be written as

$$x(t) = \Phi(t)x_0 \qquad 0 \le t \le T \tag{2.2}$$

For $t \ge T$, it can be calculated by

$$x(t + sT) = \Phi(t)\Phi^s(T)x_0 \qquad 0 \le t \le T \qquad s = 1,2,3,\ldots \tag{2.3}$$

where, $\Phi(T)$ is the Floquét transition matrix (FTM) or the monodromy matrix. The stability criteria for periodic systems depends upon the eigenvalues of $\Phi(T)$, called the '*Floquét multipliers*' and the system is stable if all '*Floquét multipliers*' lie on or inside the unit circle, otherwise it is unstable.

According to the Lyapunov-Floquét theorem [73], STM can be expressed as

$$\Phi(t) = L(t)e^{Ct} \qquad L(t) \in \mathbb{C}^{n \times n},\ C \in \mathbb{C}^{n \times n} \quad \forall\ t \ge 0 \tag{2.4}$$

or , $$\Phi(t) = Q(t)e^{Rt} \qquad Q(t) \in \mathbb{R}^{n \times n},\ R \in \mathbb{R}^{n \times n} \quad \forall\ t \ge 0 \tag{2.5}$$

where, $L(t)$ is T periodic and $Q(t)$ is $2T$ periodic. $L(t)$ and $Q(t)$ are known as Lyapunov-Floquét (L-F) transformations. Using the transformations, $x = L(t)z$ or $x = Q(t)z$, Eq. (2.1) can be reduced to equations with constant coefficients

$$\dot{z} = Cz \text{ or } \dot{z} = Rz \text{ , respectively,} \tag{2.6}$$

where C and R are time-invariant matrices.

A specific form of Eq. (2.1) is the well-known Mathieu equation given by

$$\ddot{x} + \left(a + b\cos\omega_1 t\right)x = 0 \tag{2.7}$$

where, $\sqrt{a} = \omega_n$ is the natural frequency of the system (with $b = 0$) and ω_1 is the parametric excitation frequency. In $a \sim b$ plane, stability boundaries cross $b = 0$ line or originate from

$$a = \left(\frac{K\omega_1}{2}\right)^2 \qquad K = \begin{cases} 0,2,4,\ldots & T \text{ periodic} \\ 1,3,5,\ldots & 2T \text{ periodic} \end{cases} \tag{2.8}$$

2.3 Proposition and a General Methodology

The general linear ordinary differential equations with quasi-periodic coefficients may be represented by

$$\dot{x} = A(\theta,\lambda)\,x \quad ; \quad \frac{d\theta}{dt} = \omega \qquad x(0,\lambda) = x_0 \tag{2.9}$$

where, $x(\theta,\lambda) \in \mathbb{R}^n$, $A(\theta,\lambda)$ is an $n \times n$ matrix that is 2π periodic in $\theta = \{\theta_1, \theta_2, \ldots, \theta_m\}$ and is a continuous function of a set of control parameters λ; $\omega = \{\omega_1, \omega_2, \ldots, \omega_m\} \in \mathbb{R}^m$ is the frequency vector of $A(\theta,\lambda)$ and t is the time. When $A(\theta,\lambda)$ has finite ($m \geq 2$) incommensurate frequencies, then, $A(\theta,\lambda)$ is quasi-periodic.

A simple form of Eq. (2.9) is the damped QP Hill equation given by

$$\ddot{x} + d\,\dot{x} + \left(a + \sum_{i=1}^{m} b_i \cos\left(\omega_i t\right)\right)x = 0 \tag{2.10}$$

Equation (2.10) can be rewritten in the state space form as

$$\dot{x} = \begin{bmatrix} 0 & 1 \\ -\left(a + \sum_{i=1}^{m} b_i \cos(\omega_i t)\right) & -d \end{bmatrix} x \tag{2.11}$$

where, $x = \{x_1 \quad x_2\}^T$ and $\omega = \{\omega_1, \omega_2, \ldots, \omega_m\}$ is the frequency basis of the coefficient matrix.

The stability of Eq. (2.10) (or Eq. (2.11)) cannot be investigated by Floquét theory since the 'principal period' for such a system tends to infinity. However, an approximate period can always be defined such that for every $\varepsilon > 0$, there exists a length of time $T(\varepsilon)$ that contains a number, $T_a(\varepsilon)$ for which $|A(t + T_a(\varepsilon)) - A(t)| < \varepsilon$. For a given ε , $T_a(\varepsilon)$ can be determined by truncating the frequency module of $A(\omega t, \lambda)$ defined as $|k_1\omega_1 \pm k_2\omega_2 \pm \ldots \pm k_m\omega_m|$; $k_i = 0, 1, 2, \ldots$ and $k_1 = k_2 = \ldots = k_m \neq 0$. Frequency module can be truncated by fixing the upper limit on k_i. The '*minimum frequency*', $\omega_{\min}$ in the truncated frequency module can be chosen to define the approximate principal period, T_a of the parametric quasi-periodic term. Thus, the following parameters are defined as

$$\omega_{\min} = Min\left(|k_1\omega_1 \pm k_2\omega_2 \pm \ldots \pm k_m\omega_m|\right) \quad ; \quad \omega_{\min} \neq 0 \quad \text{and} \quad T_a = 2\pi/\omega_{\min} \tag{2.12}$$

$\omega_{\min}$ depends on a particular set of values of k_i used in Eq. (2.12). For example, if the coefficient matrix, $A(\omega t, \lambda)$ in Eq. (2.11) consists of two incommensurate frequencies $\omega_1 = \pi$ and $\omega_2 = 7.0$ in the frequency basis, then Eq. (2.12) can be written as $Min\left(|k_1\omega_1 \pm k_2\omega_2|\right)$. If k_1 and k_2 vary from 0 to 14, then $\omega_{\min} = 0.274334$ and $T_a = 22.9034$. This $\omega_{\min}$ is observed when $k_1 = 9$ and $k_2 = 4$ but is a minimum up to the

maximum value of $k_1, k_2 = 19$. Once $\omega_{\min}$ and T_a have been calculated, the original quasi-periodic system, Eq. (2.11) is replaced by the following periodic system.

$$\dot{x} = \begin{bmatrix} 0 & 1 \\ -\left(a + \sum_{i=1}^{m} b_i \cos\left(\bar{\omega}_i t\right) \right) & -d \end{bmatrix} x \tag{2.13}$$

where, ω_i in Eq. (2.11) has been approximated by $\bar{\omega}_i$ such that $\bar{\omega}_i$ are integral multiples of $\omega_{\min}$, the minimum frequency of the approximate system. From Eq. (2.12) this translates into the principal period $T_a = 2\pi/\omega_{\min}$. Due to the periodic nature of approximate system, its stability and response can be determined by the Floquét theory (*c.f.*, section 2.2) and it is expected that the solution of Eq. (2.13) is the approximate solution of the original quasi-periodic system, Eq. (2.11).

As the approximate system is a periodic system with the principal period T_a, T_a and $2T_a$ stability boundaries can be obtained like the Mathieu equation as described in section 2.2 and hence expressions for a when $b_i = 0$; $i = 1,...,m$ should be similar to Eq. (2.8). Thus, the stability boundaries in the approximate system would originate from

$$a = \left(\frac{K\omega_{\min}}{2} \right)^2 \quad ; \qquad K = \begin{cases} 0, 2, 4, \ldots & T_a \text{ periodic} \\ 1, 3, 5, \ldots & 2T_a \text{ periodic} \end{cases} \tag{2.14}$$

Using T_a as the principal period of the system, the STM of the approximate system can be computed and subsequently stability chart can be plotted using the following expressions [74]

$$Tr\left(\Phi(T_a, \lambda) \right) = \pm 2 \qquad \text{(Undamped system, } d = 0 \text{)} \tag{2.15}$$

and $$Det\left(\mathrm{I} \pm \Phi(T_a, \lambda) \right) = 0 \qquad \text{(Damped system, } d \neq 0 \text{)} \tag{2.16}$$

The development of such an approximate theory for quasi-periodic systems also allows one to construct Lyapunov-Perron (L-P) transformation matrices that reduce the linear quasi-periodic systems to systems with time-invariant coefficients.

2.4 Computational Details and Stability Charts for Some Typical Cases

Three cases are studied in this work. It includes two cases in which $A(\omega t, \lambda)$ in Eq. (2.11) consists of two frequencies and for the last case $A(\omega t, \lambda)$ contains three frequencies. The two frequency cases are the simplest examples of QP Hill equations. In the first case study, the two frequencies are selected as $\omega_1 = \pi$ and $\omega_2 = 7.0$. This set is chosen as a possible representative of systems where ω_1 and ω_2 are relatively apart. In such cases finding $\omega_{\min}$ could possibly involve a large number of k_1 and k_2 in Eq. (2.12) as compared to frequency pairs with smaller differences between them. Also, in the corresponding periodic cases with excitation frequencies ω_1 and ω_2, the main parametric resonance regions would be away from each other and the other unstable regions in between main parametric resonances (due to combination of frequencies), will also be apart making the stability chart possibly less complicated. For the second case study $\omega_1 = 1.0$ and $\omega_2 = \left(1+\sqrt{5}\right)/2$ (known as golden ratio), where the difference between the two frequencies is 0.618034, much smaller as compared to 3.85841 in Case Study 1. Existence of an '*instability loop*' in one of the main instability regions is the typical feature of this case. This case has also been investigated by Broer and Simó [31] using rotation number and maximal Lyapunov exponent. The results obtained from the proposed method have been compared with those given in reference in [31]. In the third case, the coefficient matrix, $A(\omega t, \lambda)$ in Eq. (2.11) contains three frequencies: $\omega_1 = 1.0$, $\omega_2 = \sqrt{3}$ and

$\omega_3 = \sqrt{11}$. The difference between the frequencies ($\omega_2 - \omega_1 = 0.732051$, $\omega_3 - \omega_2 = 1.58457$ and $\omega_3 - \omega_1 = 2.31662$) are relatively smaller than the Case Study 1. A number of instability loops are observed in the parametric space.

2.4.1 Case Study 1: $\omega_1 = \pi$ and $\omega_2 = 7.0$

The damped QP Hill equation, Eq. (2.10) reduces to Eq. (1.1) which can be represented in the state space form using Eq. (2.11) as

$$\dot{x} = \begin{bmatrix} 0 & 1 \\ -\left(a + b_1 \cos \pi t + b_2 \cos 7t\right) & -d \end{bmatrix} x \tag{2.17}$$

As a first step, a set of minimum frequencies ($\omega_{\min}$) are calculated using Eq. (2.12) over a range of values of k_1 and k_2 and is listed with their corresponding approximate periods (T_a) in Table 2.1. It should be observed that $\omega_{\min}$ is defined for a set of maximum values of k_1 and k_2. For example, as shown in Table 2.1, $\omega_{\min} = 0.168147$ is minimum in the range $k_1, k_2 = 0$ to 28 and it occurs for $k_1 = 20$ and $k_2 = 9$. As k_1 and k_2 are increased further, a frequency smaller than $\omega_{\min} = 0.168147$ is obtained for $k_1 = 29$ and $k_2 = 13$. This new $\omega_{\min}$ ($= 0.106187$) remains minimum up to $k_1, k_2 = 48$ as seen in Table 2.1.

Table 2.1: Minimum frequencies ($\omega_{\min}$) with their corresponding periods (T_a) and the frequencies of the approximate (periodic) system. (Case Study 1)

Entry Number (E. No.)	Range of k_1, k_2 values	$\omega_{\min}$ ($\omega_{\min} \neq 0$)	$T_a = 2\pi/\omega_{\min}$	Total number of frequencies	$\bar{\omega}_1$	$\bar{\omega}_2$
Col. 1	Col. 2	Col. 3	Col. 4	Col. 5	Col. 6	Col. 7
1	0 to 1	3.14159	2.0	4	3.14159000	6.28318000
2	0 to 8	0.716815	8.76542	144	2.86726000	6.45133500
3	0 to 19	0.274334	22.9034	760	3.01767400	7.13268400
4	0 to 28	0.168147	37.3672	1624	3.19479300	7.06217400
5	0 to 48	0.106187	59.1709	4704	3.07942300	7.00834200
6	0 to 77	0.061960	101.407	12012	3.15996000	7.00148000
7	0 to 126	0.0442270	142.067	32004	3.14011700	6.98786600
8	0 to 331	0.0177330	354.323	219784	3.13874100	7.00453500
9	0 to 790	0.00876099	717.178	1249780	3.14519541	7.00003101

In order to approximate the quasi-periodic system, Eq. (2.17) by a periodic system, the frequencies $\omega_1 = \pi$ and $\omega_2 = 7$ are replaced by $\bar{\omega}_1$ and $\bar{\omega}_2$, respectively, which are the integral multiples of $\omega_{\min}$. Equation (2.13) reduces to the form

$$\dot{x} = \begin{bmatrix} 0 & 1 \\ -\left(a + b_1 \cos \bar{\omega}_1 t + b_2 \cos \bar{\omega}_2 t\right) & -d \end{bmatrix} x \tag{2.18}$$

Columns 6 and 7 in Table 2.1 show $\bar{\omega}_1$ and $\bar{\omega}_2$ for various $\omega_{\min}$. For instance, when $\omega_{\min} = 0.168147$ (E. No. 4 in Table 2.1), $\omega_1/\omega_{\min} = 18.6836$ and $\omega_2/\omega_{\min} = 41.6302$. The nearest integers are 19 and 42 and therefore, $\bar{\omega}_1 = 19\omega_{\min} = 3.194793$ and $\bar{\omega}_2 = 42\omega_{\min} = 7.062174$. Since the greatest common divisor (GCD) of 19 and 42 is 1, the $\omega_{\min}$ remains as a minimum frequency in the approximate system. In case of $\omega_{\min} = 0.106187$ (E. No. 5 in Table 2.1), $\omega_1/\omega_{\min} = 29.5855$ and $\omega_2/\omega_{\min} = 65.9214$ and thus we can set $\bar{\omega}_1 = 30\omega_{\min} = 3.18561$ and $\bar{\omega}_2 = 66\omega_{\min} = 7.008342$. As the GCD of 30 and 66 is 6, the minimum frequency of the approximate system has changed to $6\omega_{\min}$ which implies that the period of the approximate system is not the same as the approximate period of the quasi-periodic system that is computed by truncating the frequency module of coefficient matrix. In order to avoid this situation, we can change one of the integers or both such that the GCD becomes 1. In this particular case, the frequencies of the approximate system could be represented by $\bar{\omega}_1 = 29\omega_{\min} = 3.079423$ and $\bar{\omega}_2 = 66\omega_{\min} = 7.008342$.

Once an approximate system has been defined (*c.f.*, Eq. (2.18)), the STM, $\Phi(t, \lambda)$ can be calculated numerically using Floquét theory. Setting $b_1 = b_2 = b$ (for convenience)

and using MATHEMATICA, $\Phi(t,a,b,d)$ of the approximate system was computed and stability charts were plotted in the $a \sim b$ plane utilizing Eqs. (2.15) and (2.16). All computations in this work were performed on a laptop computer with a 2.50 GHz i7-4710MQ 4-core processor and 24 GB of RAM.

A note of interest: As indicated in section 2.2, a linear periodic system can be reduced to a system with constant coefficients by using L-F transformations. A similar result, known as Lyapunov-Perron (L-P) transformations, exists for quasi-periodic systems that reduces the linear quasi-periodic systems to systems with constant coefficients. Denoting $P(\omega t,\lambda)$ as the L-P transformation, the change of variable $x = P(\omega t,\lambda)\, z$ reduces Eq. (2.9) to the following system [75, 76].

$$\dot{z} = A_0(\lambda)\, z \tag{2.19}$$

where $A_0(\lambda)$ is a time-invariant matrix. It should be noted that the frequency basis of L-P transformation, $P(\omega t,\lambda)$ is same as the coefficient matrix, $A(\omega t,\lambda)$. Since in the proposed methodology the minimum frequency $\omega_{\min}$ is computed by truncating the frequency module of $A(\omega t,\lambda)$, the frequency module of the $P(\omega t,\lambda)$ will be same as the truncated frequency module of $A(\omega t,\lambda)$. Column 5 in Table 2.1 shows the total number of frequencies that could be present in $P(\omega t,\lambda)$ for a particular $\omega_{\min}$ and it can be calculated using $\left((2j+1)^m - 1\right)\big/2$ where, m is the number of frequencies in the frequency basis and j is the largest value of k_i ; $i = 1,2,\ldots$.

2.4.1.1 The Undamped System ($d = 0$)

In this section, the undamped QP equation is investigated and stability charts are plotted for various values of minimum frequencies in order to ascertain the largest value of $\omega_{\min}$ that would yield stability boundaries up to a desired accuracy. As a guideline, it is to be noted that for the periodic case of $\omega_1 = \pi$, the stability boundaries of main parametric instability region arise from $a = \omega_1^2/4 = 2.46740$, while for $\omega_2 = 7.0$, these arise from $a = \omega_2^2/4 = 12.25$ and both are $2T$ periodic. This is easily verified by Eq. (2.8). For the QP Hill equation as well, Zounes and Rand [30] reported that stability boundaries of main instability regions arise from same values of a. A careful examination of stability charts (see Fig. 2.1 through Fig. 2.3) leads us to the following observations.

For a given $\omega_{\min}$, say $\omega_{\min} = 0.274334$, a number of T_a and $2T_a$ stability boundaries stem from the a axis in the $a \sim b$ plane, as anticipated (see Fig. 2.1). The T_a and $2T_a$ unstable regions are either due to primary frequencies ($\bar{\omega}_1$ and $\bar{\omega}_2$) or due to various combinations of $\bar{\omega}_1$ and $\bar{\omega}_2$. From Fig. 2.1 through 2.3, it could be observed that as $\omega_{\min}$ decreases, the number of unstable regions increases in the parametric space and the prominent regions of instability become clearly visible. The bifurcation points on a axis are T_a and $2T_a$ periodic and can be computed using Eq. (2.14). It is observed that the two main instability regions stem approximately from $a = 2.5$ and $a = 12.50$.

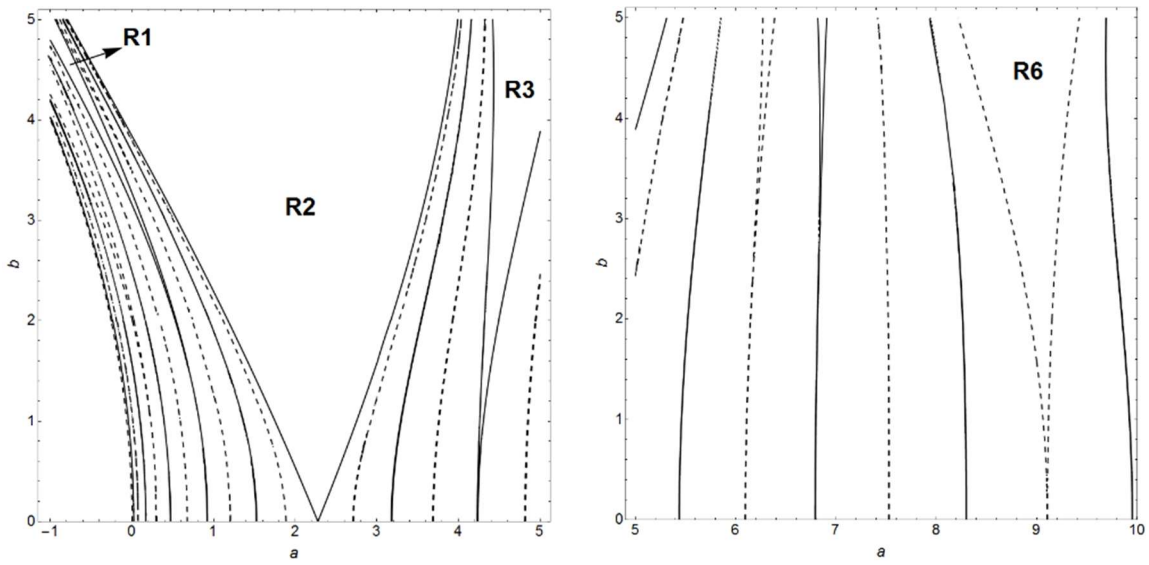

(i) (ii)

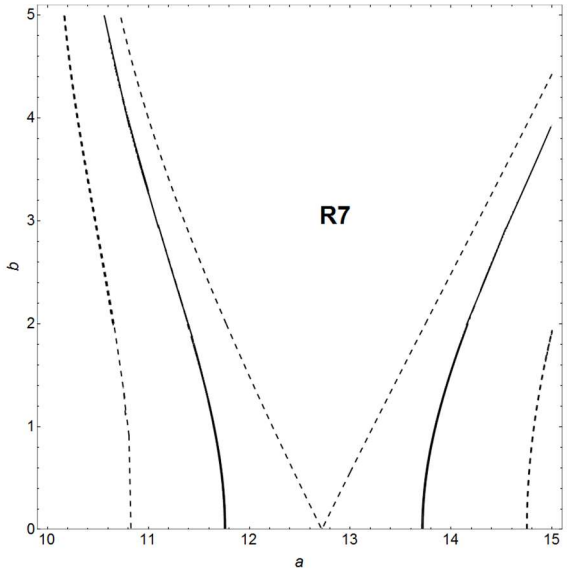

(iii)

Figure 2.1: Stability diagram of the QP Hill equation with $\omega_1 = \pi$ and $\omega_2 = 7.0$. $\omega_{\min} = 0.274334$; Solid: $2T_a$ periodic, Dashed: T_a periodic

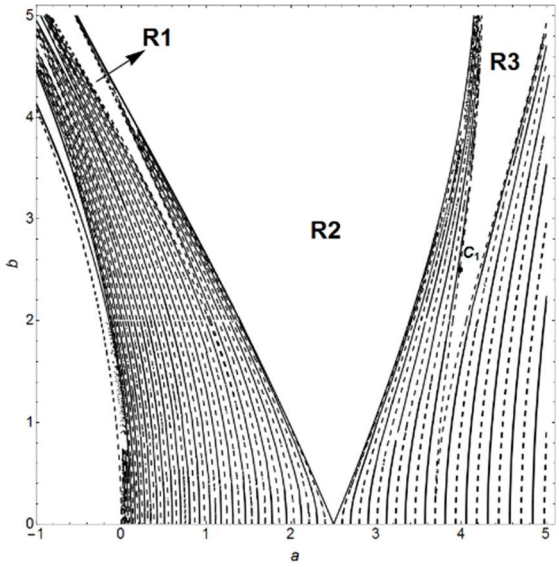

(i)

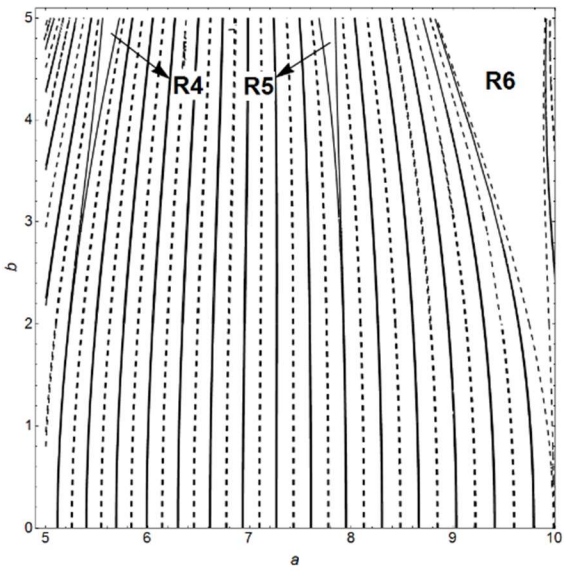

(ii)

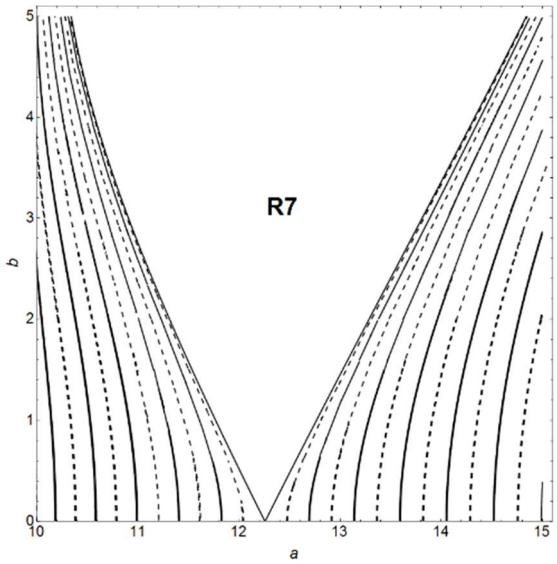

(iii)

Figure 2.2: Stability diagram of the QP Hill equation with $\omega_1 = \pi$ and $\omega_2 = 7.0$. $\omega_{\min} = 0.0619600$; Solid: $2T_a$ periodic, Dashed: T_a periodic

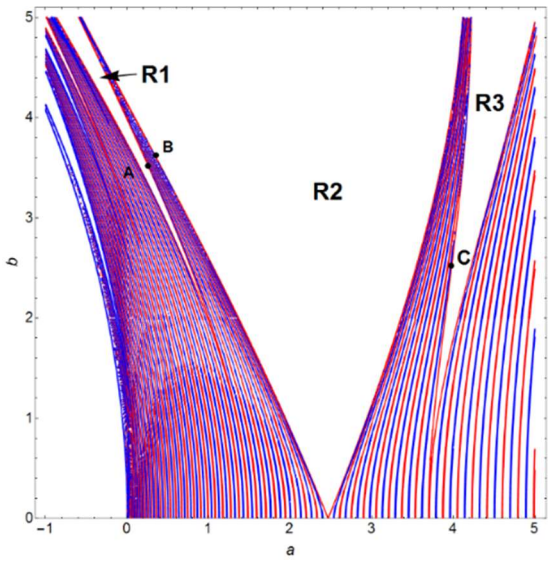

(i)

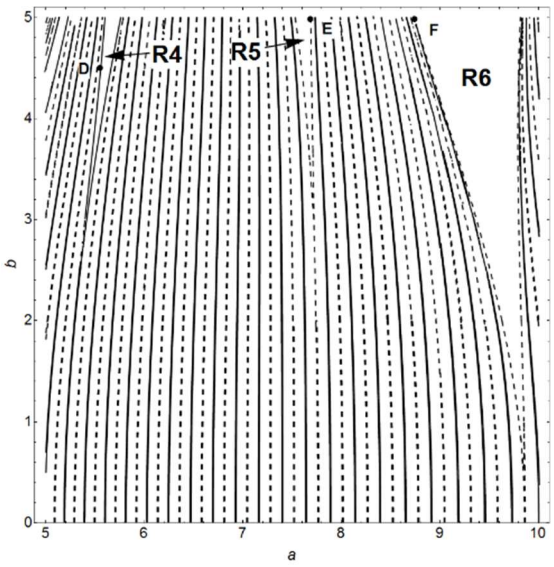

(ii)

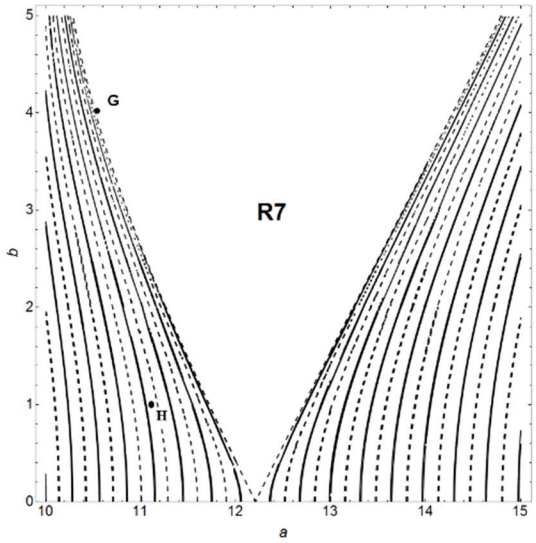

(iii)

Figure 2.3: Stability diagram of the QP Hill equation with $\omega_1 = \pi$ and $\omega_2 = 7.0$. $\omega_{\min} = 0.0442270$; Red/Solid: $2T_a$ periodic, Blue/Dashed: T_a periodic

For $\omega_{\min} = 0.0442270$, the main instability regions start from $a = 2.46508$ and $a = 12.2076$ and are $2T_a$ and T_a periodic, respectively. In periodic systems the main parametric resonance (2:1) is $2T$ periodic and occurs at $a = 2.46740$ for $\omega_1 = \pi$ and at $a = 12.25$ for $\omega_2 = 7.0$ (*c.f.,* Eq. (2.8)) which are close to the values obtained from Eq. (2.14). Using the concept of winding number, Zounes and Rand [30] reported that all stability boundaries arise from $a = \left(k_1\omega_1 \pm k_2\omega_2\right)^2 / 4$; $k = 0,1,2,\ldots$ and the main instability regions stem from $a = 2.46740$ ($k_1 = 1$ and $k_2 = 0$) and $a = 12.25$ ($k_1 = 0$ and $k_2 = 1$) which are identical to the Floquét theory. In fact, this expression is same as Eq. (2.14) if $K\omega_{\min}$ is replaced by $k_1\omega_1 \pm k_2\omega_2$. However, since k_1 and k_2 are finite by definition of $\omega_{\min}$, it is a subset of results given in [30]. A prominent instability region is also observed near the T periodic unstable region (1:1) of periodic system that emanates from $a = 9.86960$ for the excitation frequency $\omega_1 = \pi$ (see Fig. 2.3). For $\omega_{\min} = 0.0442270$ this instability region is T_a periodic and it stems from $a = 9.86033$ that is close to the exact bifurcation point $a = 9.86960$ calculated using Zounes and Rand [30] expression with $k_1 = 2$ and $k_2 = 0$.

The selection of $\omega_{\min}$ could involve a number of trials but this problem is circumvented by performing a convergence study of the bifurcation points. Since the main instability regions in the quasi-periodic system arise from $a = \omega_1^2/4$ and $a = \omega_2^2/4$, a convergence study of these bifurcation points is used as a guideline in the selection of $\omega_{\min}$. Figure 2.4 demonstrates the convergence of bifurcation points of the main instability regions as the approximate period, T_a increases ($\omega_{\min}$ decreases). The y axis denotes the

difference between the exact (a_e) and approximate (a_a) bifurcation points, $a_e - a_a$ and the x axis is represented by the expression, $\log_{10}\left(T_a/T_a^1\right)$ where T_a^1 is the smallest T_a in Table 2.1 *i.e.*, 2.0. A non-uniform convergence is observed. It is expected that with a decrease in $\omega_{\min}$, the accuracy of the proposed method would increase. However, as $\omega_{\min}$ is made smaller, T_a increases and hence it would require longer computation time. Keeping the computational time reasonable, $\omega_{\min} = 0.0442270$ is used in further investigations. This results in $T_a = 142.067$, $\bar{\omega}_1 = 71\omega_{\min} = 3.140117$ and $\bar{\omega}_2 = 158\omega_{\min} = 6.987866$.

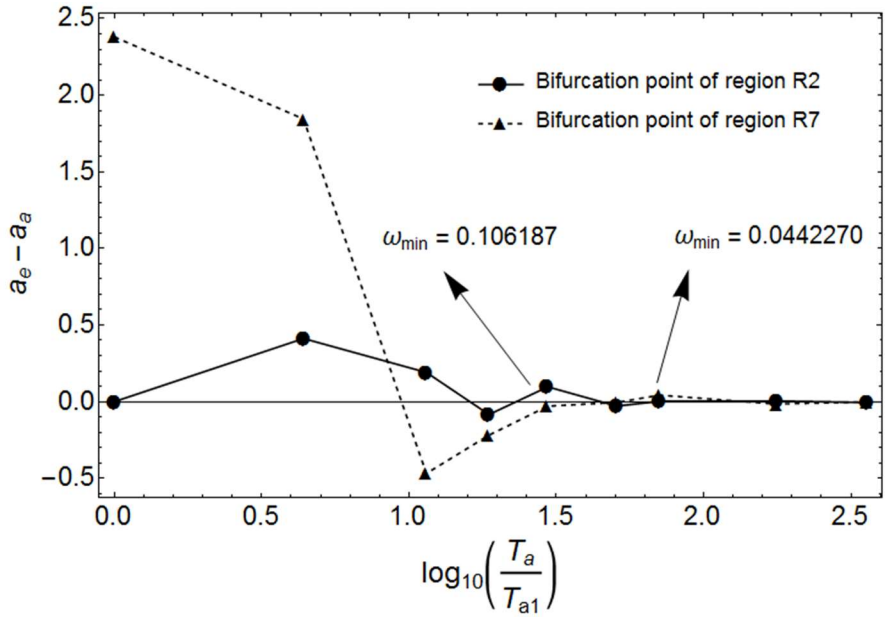

Figure 2.4: Convergence diagram of bifurcation points of the main instability regions of QP Hill equation with $\omega_1 = \pi$ and $\omega_2 = 7.0$.

2.4.1.1A Poincaré Maps and Spectral Analysis

In order to check the accuracy of the stability boundaries, Poincaré maps of approximate solutions (*c.f.*, Eq. (2.18)) constructed by Floquét theory using $T_a = 2\pi/\omega_{\min} = 142.067$ and numerical (so-called 'exact') solutions of the original system given by Eq. (2.17) are compared at some typical points close to the stability boundaries.

These points are denoted by A, B, C, D, F and G in Fig. 2.3. Approximate and exact (numerical) Poincaré maps constructed at these points are shown in Fig. 2.5. It is observed that the maps are qualitatively similar, however, there are significant differences between the amplitudes of approximate (left column) and exact (right column) solutions. The differences in amplitudes of approximate and exact solutions are due to slight discrepancies between the location of approximate and exact stability boundaries in the parametric space. For instance, if point B is assumed near the exact boundary by changing parameter 'a' from $a = 0.356044$ to $a = 0.358719$ keeping 'b' constant ($b = 3.6$), a stable exact solution of large amplitude is obtained (see Fig. 2.6) which is much closer to the approximate Poincaré map for point B (see Fig. 2.5(ii)). After all, the boundaries constitute the most sensitive portion of the stability chart. The 'exact' (a, b) values corresponding to the boundary near these points are determined by computing the maximal Lyapunov exponent via numerical integration. In Table 2.2, column 3 shows the 'b' values corresponding to these points, while columns 4 and 5 show the corresponding 'a' values obtained by the proposed approximate method and by computing the maximal Lyapunov exponents, respectively. Figure 2.5(vii) shows the Poincaré maps constructed at one of the typical stable points (point H in Fig. 2.3) and it could be observed that the exact and approximate maps match qualitatively and quantitively. Maps at other stable points also show similar patterns but are omitted for brevity.

To further ensure that T_a or $2T_a$ stability boundaries constructed using Floquét theory with $T_a = 2\pi/\omega_{\min} = 142.067$ are accurate representations of exact stability boundaries, spectral analysis using Discrete Fourier Transform (DFT) is performed on

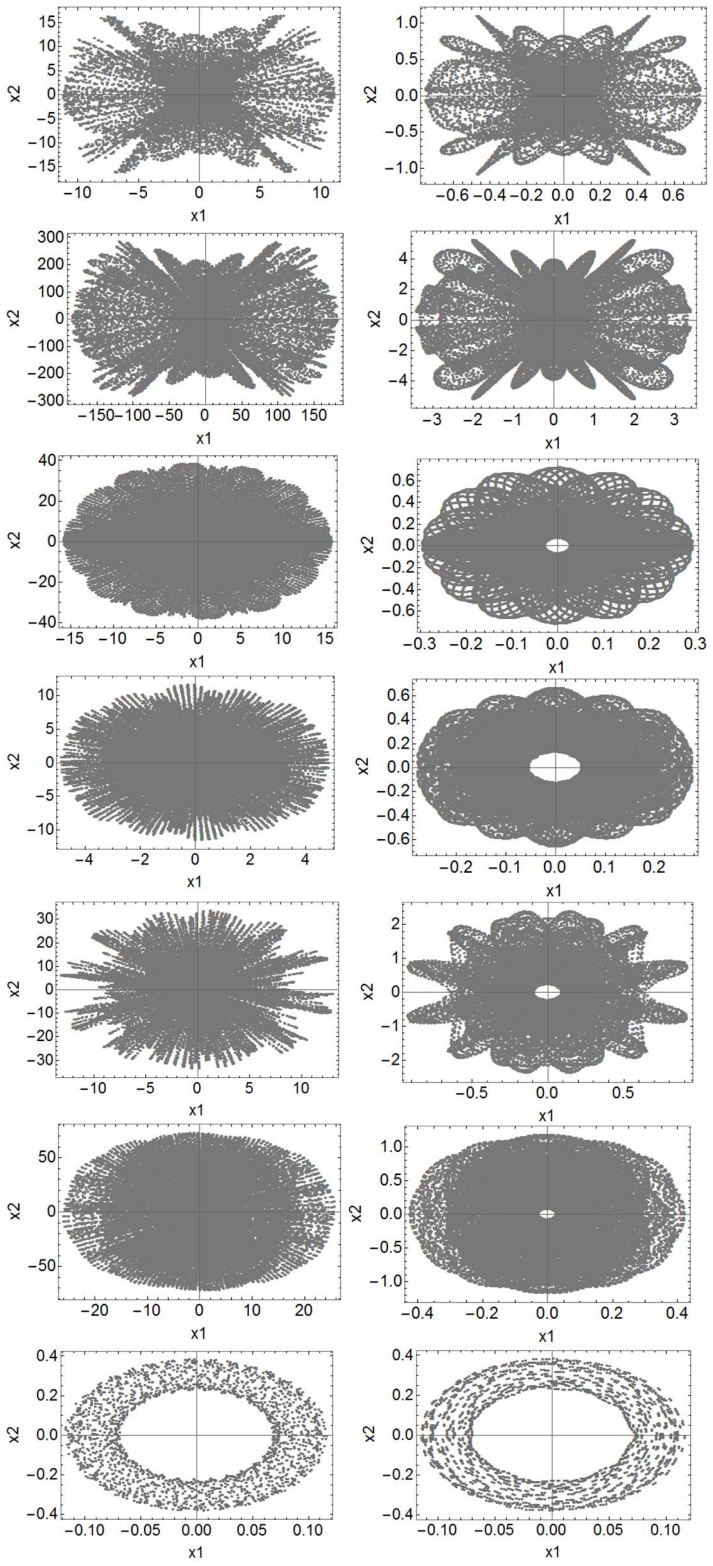

(i) Point A
$a_a = 0.268080$ $b = 3.5$ and $d = 0$

(ii) Point B
$a_a = 0.356044$ $b = 3.6$ and $d = 0$

(iii) Point C
$a_a = 3.976490$ $b = 2.5$ and $d = 0$

(iv) Point D
$a_a = 5.556$ $b = 4.5$ and $d = 0$

(v) Point F
$a_a = 8.730260$ $b = 5.0$ and $d = 0$

(vi) Point G
$a_a = 10.52374$ $b = 4.0$ and $d = 0$

(vii) Point H
$a_a = 11.1$ $b = 1.0$ and $d = 0$

Figure 2.5: Poincaré maps of approximate and exact solutions constructed at a few typical points in the stability diagram of QP Hill equation with $\omega_1 = \pi$ and $\omega_2 = 7.0$ ($\omega_{\min} = 0.0442270$; see Fig. 2.3). Left column: Approximate system (Eq. (2.18), Right Column: Original QP system, Eq. (2.17).

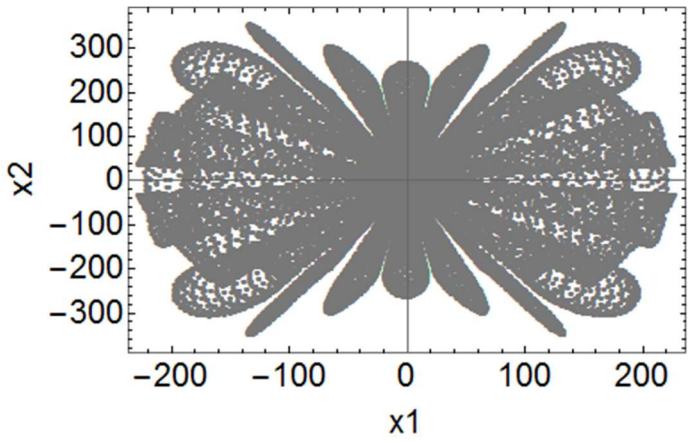

Figure 2.6: Poincaré map of an exact solution computed near the exact stability boundary ($a_e = 0.358719$ $b = 3.6$ and d=0) of QP system with $\omega_1 = \pi$ and $\omega_2 = 7.0$.

approximate and exact solutions. The solutions are generated for points marked A through G in Fig. 2.3. In Table 2.2, columns 3 and 4 specify the locations of these points in the parametric space. Columns 6 indicates the dominant frequency in the frequency spectrum of approximate solutions (f_{aa}) near the boundaries that are computed using Floquét theory. As an example consider point B ($a = 0.356044$ and $b = 3.6$) near the main instability region arising from $a = 2.46508$. At this point the approximate dominant frequency, $f_{aa} = 1.56934$. If point B is assumed near the exact stability boundary ($a = 0.358719$ and $b = 3.6$), the exact dominant frequency, $f_{oe} = 1.5708$ which is close to f_{aa}. Figure 2.7 shows the frequency spectrum of the solutions at/near point B. Other frequencies in the frequency spectrum are the integral multiples of $\omega_{\min}/2$ and they represent the influence of other harmonics on the stability boundaries. From columns 6 and 7, it is observed that $f_{aa} \approx f_{oe}$ which implies that the approximate stability boundaries constructed using Floquét theory with $T_a = 142.067$ are accurate representations of exact stability boundaries.

Table 2.2: DFT results. $\omega_1 = \pi$ and $\omega_2 = 7.0$. $\omega_{min} = 0.0442270$

Instability regions	Location selected for comparison	b	a Near approx. boundary)	a (Near exact boundary)	Dominant frequency in the frequency spectrum		Frequency content in terms of ω_1 and ω_2 (See Col. 6-7)	Frequency combination causing parametric resonance (See Col. 8)	Approx. bifurcation points ($b = 0$)	Exact bifurcation points [30] ($b = 0$)
					Approx. system (f_{aa})	Original system (f_{oe})				
Col.1	Col.2	Col. 3	Col. 4	Col. 5	Col. 6	Col. 7	Col. 8	Col. 9	Col. 10	Col. 11
R1	A	3.5	0.268080	0.265350	1.21624	1.21242	$(3\omega_1 - \omega_2)/2$	$3\omega_1 - \omega_2$	1.47925	1.46989
R2	B	3.6	0.356044	0.358719	1.56934	1.57080	$\omega_1/2$	ω_1	2.46508	2.46740
R3	C	2.5	3.976490	3.992400	1.92387	1.92855	$(\omega_2 - \omega_1)/2$	$\omega_2 - \omega_1$	3.70129	3.72183
R4	D	4.5	5.556000	5.593000	2.27769	2.28640	$(2\omega_2 - 3\omega_1)/2$	$2\omega_2 - 3\omega_1$	5.18787	5.23316
R5	E	5.0	7.688600	7.679700	2.78630	2.78270	$(4\omega_1 - \omega_2)/2$	$4\omega_1 - \omega_2$	7.76347	7.74612
R6	F	5.0	8.730260	8.747440	3.13944	3.14159	$2\omega_1/2$	$2\omega_1$	9.86033	9.86960
R7	G	4.0	10.52374	10.56381	3.49300	3.49905	$\omega_2/2$	ω_2	12.2076	12.2500

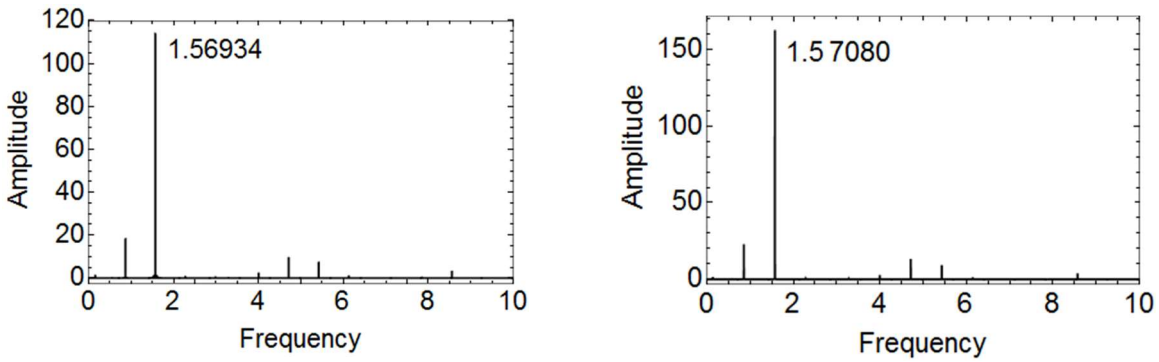

(i) (ii)

Figure 2.7: Frequency spectrum of solutions. (i) Approximate solution generated at Point B ($a_a = 0.356044$ $b = 3.6$ and d=0; see Fig. 2.3) using Floquét theory with $T_a = 142.067$. (ii) Exact solution generated near the exact boundary ($a_e = 0.358719$ $b = 3.6$ and d=0).

As the number of instability regions change with a change in $\omega_{\min}$, the characteristic nature of the stability boundaries (T_a periodic or $2T_a$ periodic) representing a particular unstable region in the parametric space can change as well. For instance, consider point C_1 ($a = 3.9792$ and $b = 2.5$) in the stability chart corresponding to $\omega_{\min} = 0.0619600$ (see Fig. 2.2). Point C_1 lies near the T_a periodic stability boundary of the prominent instability region that arises from $a = 3.68932$. As shown in Fig. 2.8(i) & 2.8(ii), the shape of the Poincaré maps constructed at this point for approximate and exact solutions are similar. The DFT of the solutions shows that $f_{aa} = 1.92076$ (see Fig. 2.8(iii)). If $\omega_{\min}$ is reduced further to 0.0442270, the same unstable region is bounded by $2T_a$ periodic boundaries and it arises from $a = 3.70129$. Point C ($a = 3.97649$ and $b = 2.5$; see Fig. 2.3), which is close to point C_1, is now near the $2T_a$ periodic stability boundary and the approximate dominant frequency, $f_{aa} = 1.92387$ while near the exact boundary $f_{oe} = 1.92855$. The f_{aa} of points C and C_1 are close to f_{oe} suggesting that both minimum

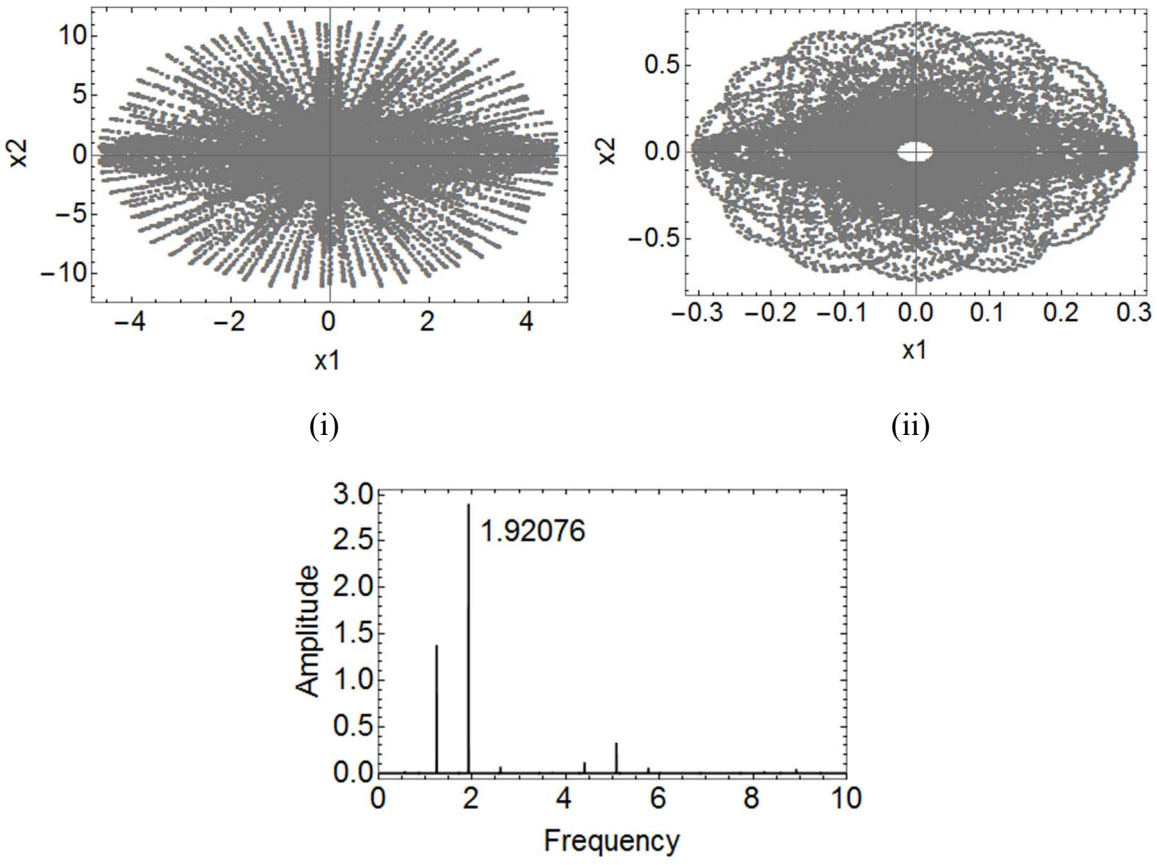

Figure 2.8: (i) and (ii) Poincaré maps of approximate and exact solutions, respectively constructed at point C_1 in Fig. 2.2 with $\omega_1 = \pi$ and $\omega_2 = 7.0 \,.\, \omega_{min} = 0.0619600$. (iii) Frequency spectrum of the approximate solution generated at Point C_1.

frequencies *i.e.*, $\omega_{min} = 0.0619600$ and 0.0442270 could be used in the proposed method.

DFT is also helpful in identifying the frequency combinations that cause the parametric resonances. Seven prominent instability regions, R1 through R7, as shown in Fig. 2.3, are investigated and the dominant frequencies at/near points A-G are identified and shown in columns 6 and 7 of Table 2.2. The error depends upon the proximity of a point to the exact boundary and the quality of the DFT software. For periodic systems the periodicity of the bifurcation points on the a axis in $a \sim b$ plane is same as the periodicity of the stability boundaries originating from them. In the case of quasi-periodic systems,

since the bifurcation points are given by [30] $a=\left(k_1\omega_1 \pm k_2\omega_2\right)^2/4$, the frequency content of the boundaries may be expressed as $\left(\pm k_1\omega_1 \pm k_2\omega_2\right)/2$. With this observation, the general forms of f_{aa} and f_{oe} listed in columns 6 and 7 (Table 2.2) may be expressed as

$$f_{aa} \approx f_{oe} \approx \frac{\left(\pm k_1\omega_1 \pm k_2\omega_2\right)}{2} \approx \frac{\left(\pm k_1\bar{\omega}_1 \pm k_2\bar{\omega}_2\right)}{2} \tag{2.20}$$

For instance, point D ($a=5.5560$ and $b=4.5$) near the stability boundary of R4 (see Fig. 2.3) has $f_{aa}=2.27769$ and $f_{oe}=2.28640$ (see Fig. 2.9). Then $f_{aa} \approx f_{oe} \approx \frac{\left(-3\omega_1+2\omega_2\right)}{2}$ $=2.2876$ suggests that unstable region, R4 is formed due to frequency combination $\left(-3\omega_1+2\omega_2\right)$. The parametric resonances due to combination of excitation frequencies as shown in Table 2.2 are different from combination resonances in periodic systems with multiple degrees of freedom where they occur when the excitation frequency is a combination of natural frequencies of different modes of the system.

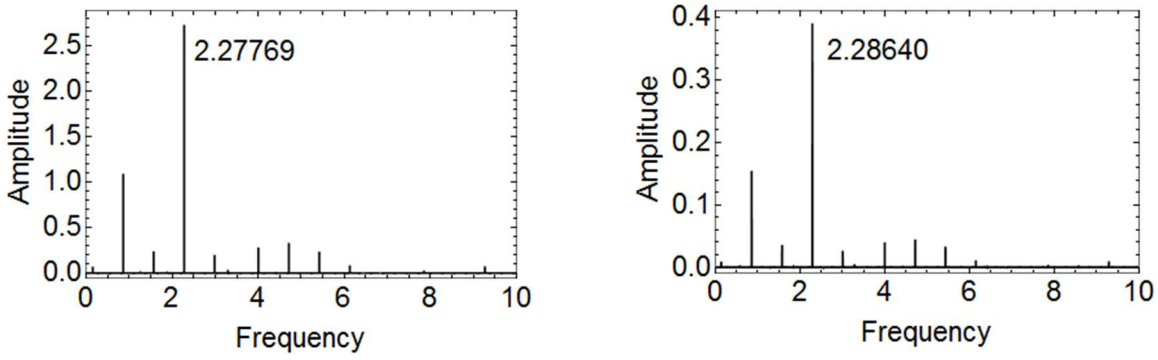

(i) (ii)

Figure 2.9: Frequency spectrum of solutions. (i) Approximate solution generated at Point D ($a_a=5.556$ $b=4.5$ and $d=0.0$; see Fig. 2.3) using Floquét theory with $T_a=142.067$. (ii) Exact solution generated near the exact boundary ($a_e=5.593$ $b=4.5$ and d=0).

In between the prominent instability regions, a bunch of narrow strips of unstable regions are observed between R2 and R3 in Fig. 2.3. These instability regions arise due to various combinations of frequencies $\bar{\omega}_1$ and $\bar{\omega}_2$ and their number increases with smaller and smaller $\omega_{\min}$ (*c.f.*, Eq. (2.14)). The order of resonance $|k_1|+|k_2|$ of prominent instability regions may be calculated using column 9 of Table 2.2. From Fig. 2.3, it is observed that the width of prominent instability regions decreases with an increase in the order of resonance. These narrow strips of unstable regions are of higher order as compared to the prominent regions of instability. The bifurcation points of these narrow strips may not be close to the exact bifurcation points as opposed to the prominent regions of instability that move closer to exact locations and correct widths with a decrease in $\omega_{\min}$. It may be conjectured that with further reduction in '*minimum frequency*,' these narrow strips of unstable regions will also attain appropriate widths and locations in the parametric space. In section 2.4.1.2, it is shown that in presence of damping, these instability regions disappear for smaller values of b.

In Fig. 2.10, instability regions of quasi-periodic system are compared with periodic systems with excitation frequencies, π and 7.0. Although, the main instability regions in the quasi-periodic system originate from same bifurcation points on the a axis as in the periodic systems (*c.f.*, section 2.4.1.1), the extensions of the boundaries are a bit different from the periodic systems. For smaller values of b ($b<1$), the boundaries of main instability regions are close to each other, however, quasi-periodic boundaries start deviating as b increases. For the quasi-periodic system, in Fig. 2.3(ii), instability region R6 starts near $a=10.0$ which is similar for periodic case with excitation π as shown in Fig. 2.10(i). The deviation of quasi-periodic boundaries from periodic boundaries could

possibly be the influence of other harmonics on a particular instability region. In the following, a technique similar to the Hill's method of infinite determinants is used to investigate the influence of harmonics on the stability boundaries.

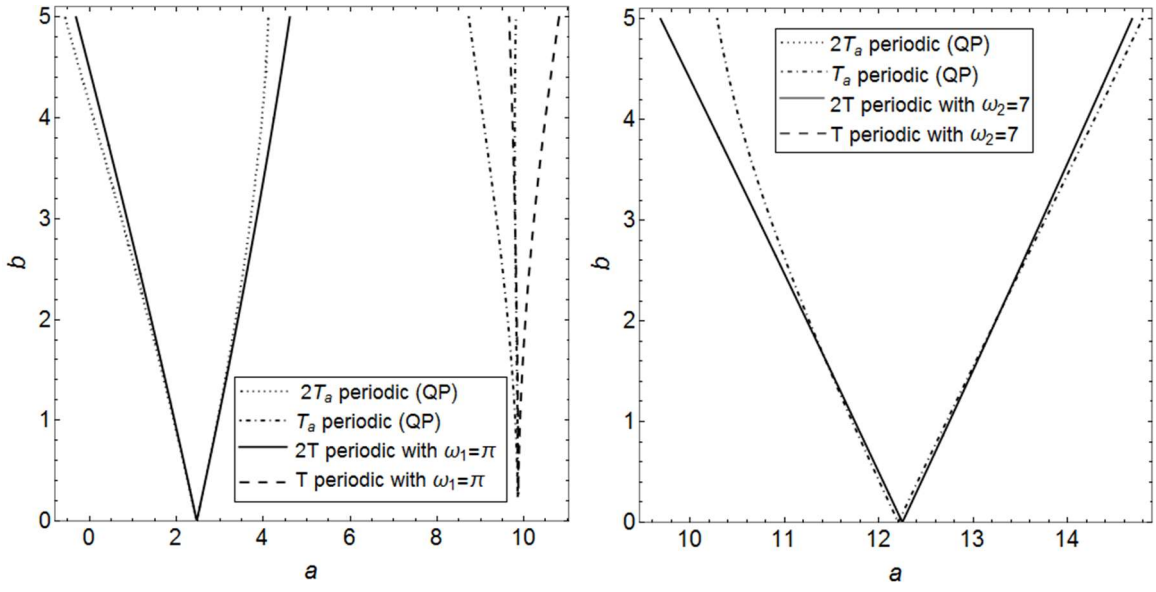

(i) (ii)

Figure 2.10: Comparison of instability regions of the QP system ($\omega_1 = \pi$ and $\omega_2 = 7.0$, $\omega_{\min} = 0.0442270$) with periodic systems. (i) QP system versus periodic system with $\omega_1 = \pi$ (ii) QP system versus periodic system $\omega_2 = 7.0$

2.4.1.1B Generalized Hill's Infinite Determinants Method

As discussed earlier, the frequency contents of the stability boundaries can be expressed as $\left(\pm k_1\omega_1 \pm k_2\omega_2\right)/2$ (*c.f.*, Eq. (2.20)) implying that the corresponding solution may be written in the form of a generalized Fourier series as

$$x(t) = \sum_{k_1,k_2=0}^{+j} \left[H_{k_1k_2} \cos\left(\frac{k_1\omega_1 \pm k_2\omega_2}{2} \right) t + L_{k_1k_2} \sin\left(\frac{k_1\omega_1 \pm k_2\omega_2}{2} \right) t \right] \tag{2.21}$$

Thus, an approach similar to the Hill's method of infinite determinants may be applied to compute the stability boundaries for quasi-periodic systems. Substituting Eq. (2.21) in

Eq. (2.17) for the undamped case and equating the coefficients of $\sin(\bullet)$ and $\cos(\bullet)$ leads to a set of linear homogenous algebraic equations in terms of $H_{k_1k_2}$ and $L_{k_1k_2}$. Approximate analytical expressions for stability boundaries can be computed by setting the determinants of coefficient matrices to zero for a finite value of j in Eq. (2.21). Zounes and Rand [30] used the same approach to plot the stability diagram of a QP Hill equation. However, in their investigation the amplitude of parametric forcing term was kept rather small ($b = 0.1$). In Fig. 2.11, the stability boundaries of main instability regions obtained from the proposed method using Floquét theory with $T_a = 142.067$ are compared with the stability boundaries computed using the Hill's approach. It is observed that with an increase in the number of terms in the generalized Fourier series (*i.e.*, j), the stability boundaries obtained from Hill's type approach move towards the boundaries obtained from the proposed method.

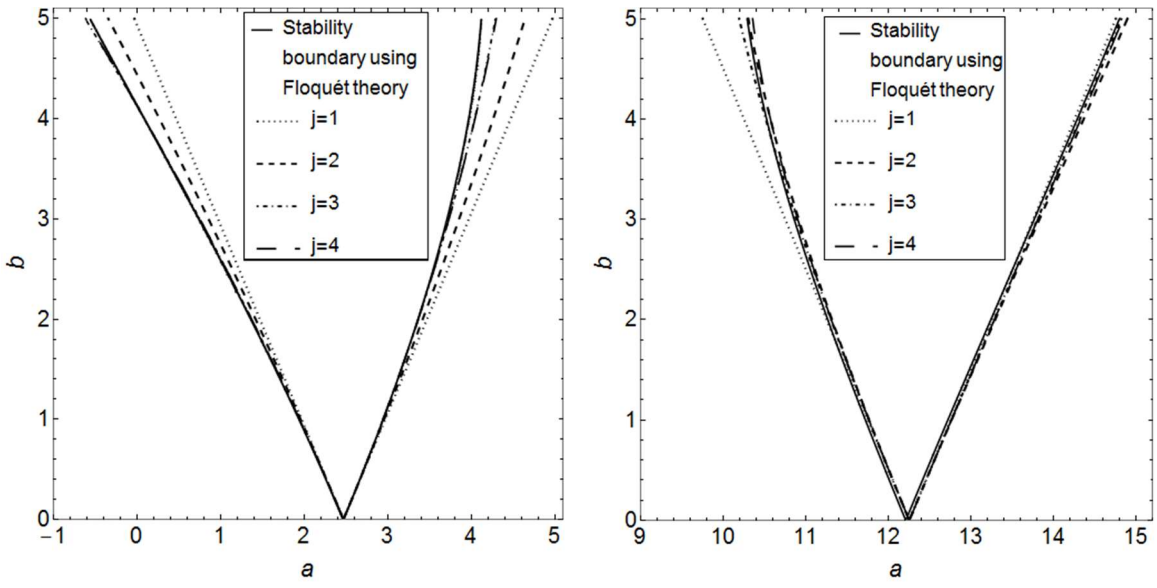

Figure 2.11: Comparison between the stability boundaries of the main instability regions computed using Floquét theory ($T_a = 142.067$) and Hill's type approach.

Although, the Hill's type approach provides analytical expressions for the stability boundaries, for larger values of j, the dimensions of coefficient matrices increase making this approach computationally inefficient. For example, when $j = 4$, the dimension of the coefficient matrix is 41×41 and in addition, the convergence of this method cannot always be guaranteed [1, 33]. In order to overcome these shortcomings, a symbolic technique for the computation of STM is presented in section 2.5 and stability diagrams are obtained.

Nevertheless, the Hill's approach clearly shows the influence of harmonics on the stability boundaries, which in turn explains the presence of a number of peaks in the frequency spectrum of solutions. For example, Fig. 2.7 shows the frequency spectrum of solutions generated at point B (Fig. 2.3(i)) near the stability boundary of instability region R2. A number of peaks corresponding to frequencies 0.853538, 1.5708, 4.71239, and 5.42965 are observed in the DFT of the original equation near the exact boundary (see Fig. 2.7(ii)) and these frequencies can be expressed as $\left(5\omega_1 - 2\omega_2\right)/2$, $\omega_1/2$, $3\omega_1/2$ and $\left(2\omega_2 - \omega_1\right)/2$, respectively. As the original quasi-periodic system is approximated by a periodic system with excitation frequencies $\bar{\omega}_1 = 3.140117$ and $\bar{\omega}_2 = 6.987866$, the exact peaks in the frequency spectrum are approximately represented by the frequencies 0.863138, 1.56934, 4.71088 and 5.41851 (see Fig. 2.7(i)). Since the stability boundaries are $2T_a$ periodic, these frequencies are integral multiples of $\omega_{\min}/2$. Using Eq. (2.20) these frequencies may also be expressed as $\left(5\omega_1 - 2\omega_2\right)/2$, $\omega_1/2$, $3\omega_1/2$ and $\left(2\omega_2 - \omega_1\right)/2$, respectively. These are identical to the frequency combinations obtained for the original quasi-periodic system.

2.4.1.2 The Damped system ($d \neq 0$)

In this section, influence of damping (d) on the stability diagram of QP Hill equation (Eq. (2.17)) is studied. Following the procedure described in section 2.4.1 stability charts are plotted for the damped system using Eq. (2.16). Figure 2.12 shows the stability chart for $\omega_{\min} = 0.0442270$ and $d = 0.1$. It is observed that only some of the prominent instability regions persist in the parametric region defined by $a = 0$ to 15 and $b = 0$ to 4.

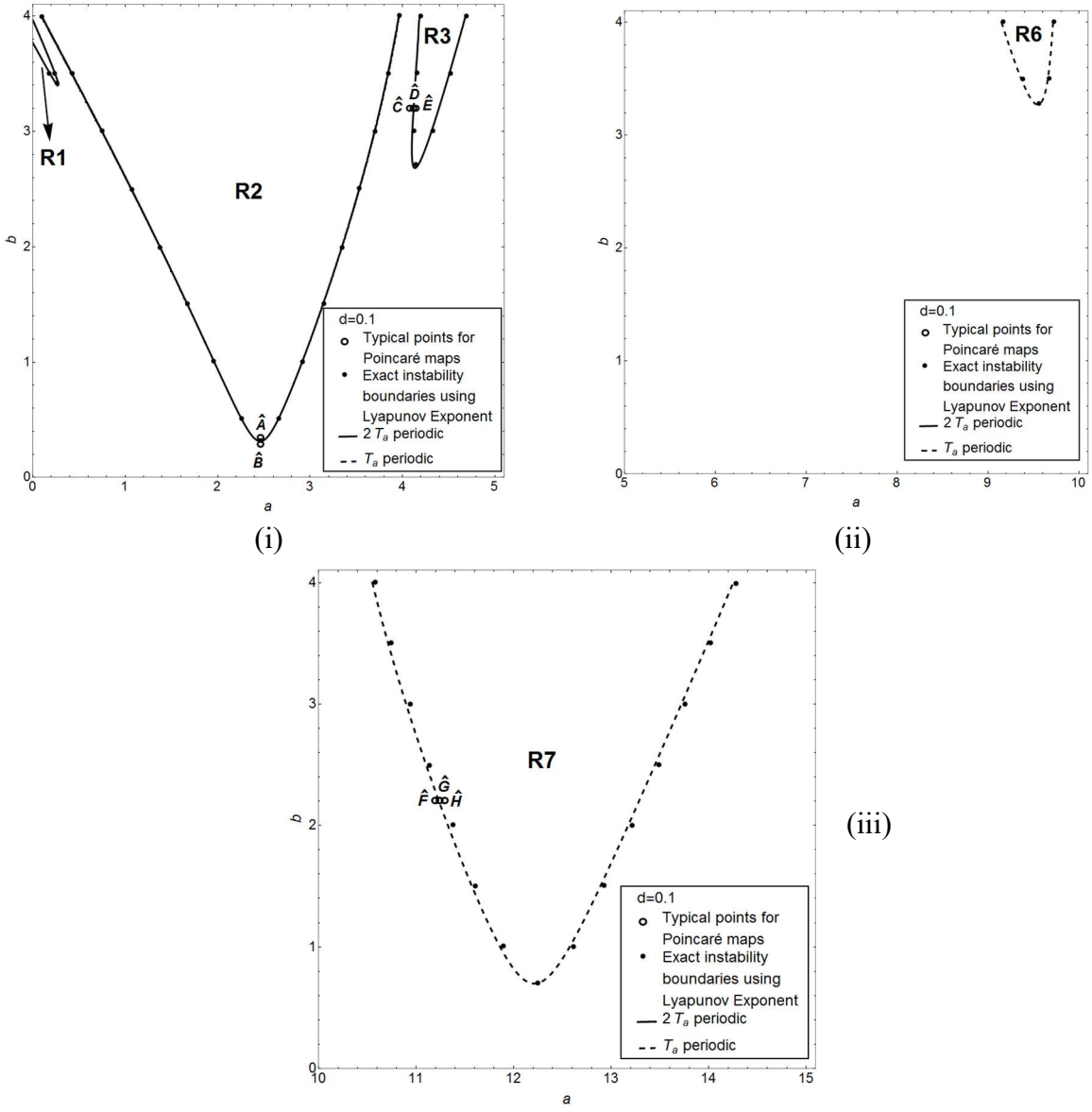

Figure 2.12: Stability diagram of the damped QP Hill equation with $\omega_1 = \pi$ and $\omega_2 = 7.0$. $\omega_{\min} = 0.0442270$ and $d = 0.1$.

Stability boundaries from the proposed method are compared with the exact boundaries obtained using Lyapunov exponents and Poincaré maps. Since maximal Lyapunov exponent is negative for a stable damped system and positive for an unstable system, the exact stability boundaries can be plotted by detecting the critical values of system parameters where the maximal Lyapunov exponent changes from positive to negative or vice versa. For the unstable region R2, the exact stability boundaries obtained from maximal Lyapunov exponent lie on the approximate boundaries computed using Floquét theory with $T_a = 142.067$ ($\omega_{\min} = 0.0442270$). A slight variation between approximate and exact boundaries can be observed in case of other prominent instability regions. Poincaré maps at some typical points viz., $\hat{A}$ through $\hat{H}$ (Fig. 2.12) are constructed and shown in Figs. 2.13(i)-(viii). For the unstable region R2, the Poincaré maps of approximate and exact solutions at point $\hat{A}$ ($a = 2.467$ $b = 0.315$ and $d = 0.1$) and point $\hat{B}$ ($a = 2.467$ $b = 0.313$ and $d = 0.1$) agree with each other. The solutions (approximate and exact) are unstable and stable at points $\hat{A}$ and $\hat{B}$, respectively. It is important to note that there is a very small difference between these points and the stability boundary lies in between them. Now, consider Poincaré maps constructed at points $\hat{F}$ ($a = 11.230$ $b = 2.2$ and $d = 0.1$), $\hat{G}$ ($a = 11.250$ $b = 2.2$ and $d = 0.1$) and $\hat{H}$ ($a = 11.280$ $b = 2.2$ and $d = 0.1$). Although the growth/decay rate of solutions are not the same, the qualitative behaviors of exact and approximate solutions match at points $\hat{F}$ and $\hat{H}$. However, a disagreement is observed at point $\hat{G}$ since the exact solution is found to be stable while the approximate solution is unstable. This discrepancy is expected as the approximate bifurcation point, $a_a = 12.2076$ lies before the exact point, $a_e = 12.25$ on the a axis. A

disagreement at point $\hat{D}$ ($a = 4.130$ $b = 3.2$ and $d = 0.1$) can also be explained similarly. The general behavior of solutions is similar to each other at points $\hat{C}$ ($a = 4.120$ $b = 3.2$ and $d = 0.1$) and $\hat{E}$ ($a = 4.140$ $b = 3.2$ and $d = 0.1$).

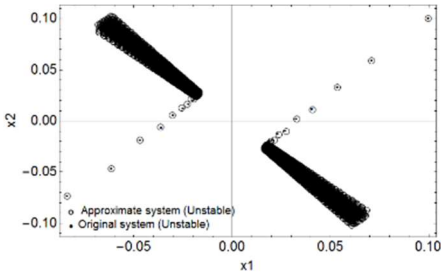

(i) Point $\hat{A}$: $a = 2.467$, $b = 0.315$ and $d = 0.1$

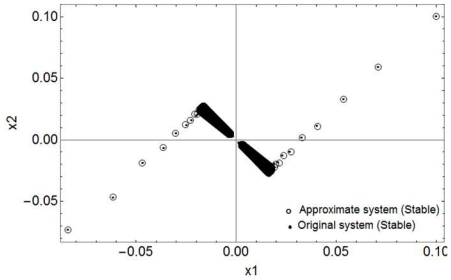

(ii) Point $\hat{B}$: $a = 2.467$, $b = 0.313$ and $d = 0.1$

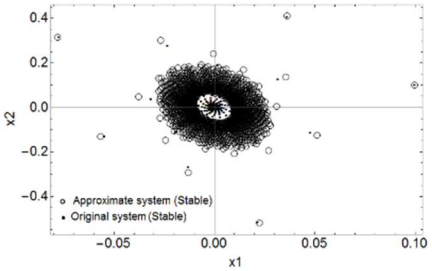

(iii) Point $\hat{C}$: $a = 4.120$, $b = 3.2$ and

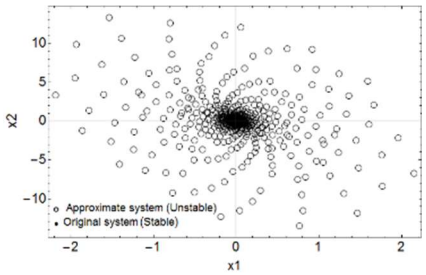

(iv) Point $\hat{D}$: $a = 4.130$, $b = 3.2$ and $d = 0.1$

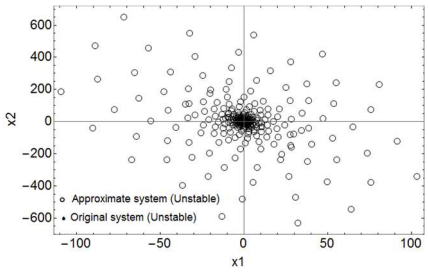

(v) Point $\hat{E}$: $a = 4.140$, $b = 3.2$ and $d = 0.1$

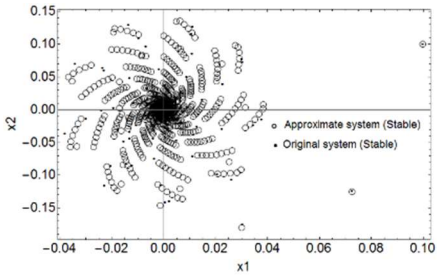

(vi) Point $\hat{F}$: $a = 11.230$, $b = 2.2$ and $d = 0.1$

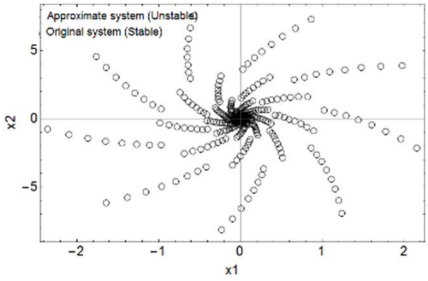

(vii) Point $\hat{G}$: $a = 11.250$, $b = 2.2$ and $d = 0.1$

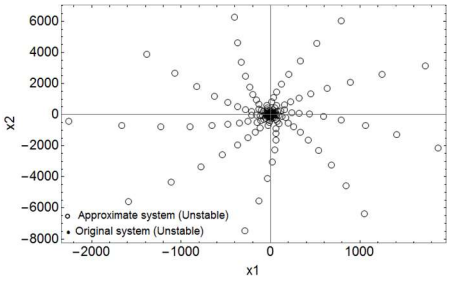

(viii) Point $\hat{H}$: $a = 11.280$, $b = 2.2$ and $d = 0.1$

Figure 2.13: Poincaré maps of the approximate and the exact solutions of the damped QP Hill equation with $\omega_1 = \pi$ and $\omega_2 = 7.0$. $\omega_{\min} = 0.0442270$ (see Fig. 2.12).

In Fig. 2.14, stability boundaries of main instability regions are plotted using three approaches: maximal Lyapunov exponent, proposed method using Floquét theory with $T_a = 142.067$ and Hill's type approach with $j = 1$ in Eq. (2.21). A good agreement among all three approaches is observed near b_{cr}, the minimum amplitude of parametric forcing term required for instability. In Hill's type approach, a better approximation can be achieved by including more terms in the generalized Fourier series (*c.f.*, Eq. (2.21)). However, no such attempts were made.

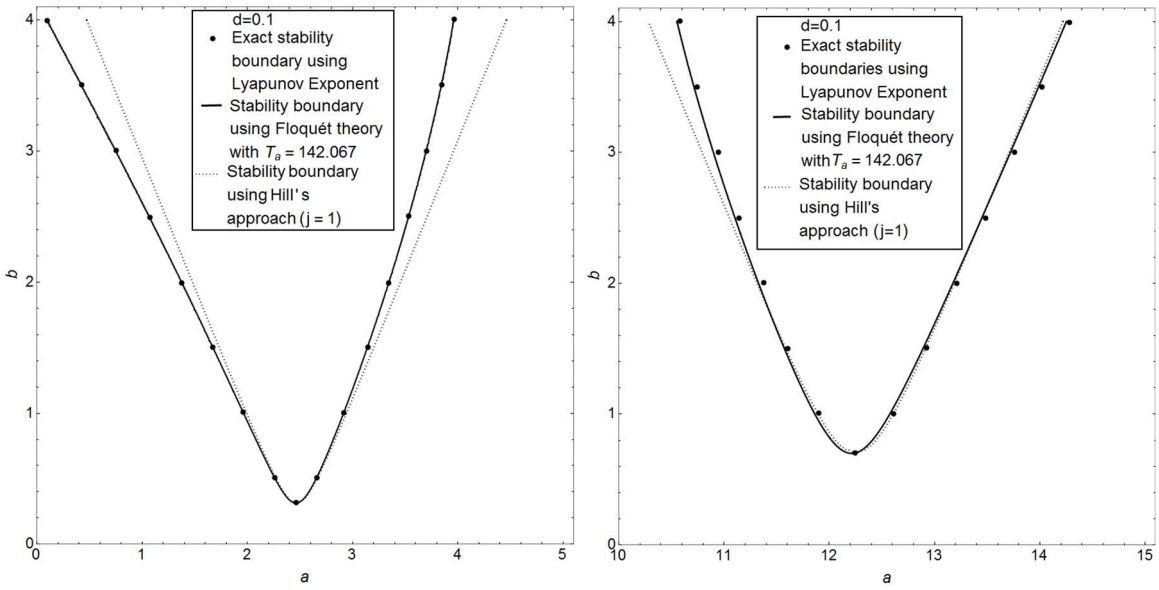

(i) (ii)

Figure 2.14: Comparison between the stability boundaries of the main instability regions of the damped QP Hill equation ($\omega_1 = \pi$ and $\omega_2 = 7.0$) computed using three approaches: maximal Lyapunov exponent, proposed method using Floquét theory ($T_a = 142.067$) and Hill's type approach.

Thus far, b_1 and b_2 in Eq. (2.17) have been assumed to have the same values for the sake of convenience. Figure 2.15 shows the effect of b_2 on the main instability region, R2 (see Fig. 2.3). When $b_2 = 0$, the approximate stability boundary constructed using

Floquét theory with $T_a = 142.067$ (or $\omega_{\min} = 0.0442270 \Rightarrow \bar{\omega}_1 = 3.140117 \approx \pi$) lies almost on the stability boundary of the main instability region of periodic system with excitation frequency $\omega_1 = \pi$, as anticipated. As the value of b_2 increases, the instability region R2 moves toward the vertical axis, $a = 0$ implying that with the increase in b_2 more unstable regions are squeezed into the parametric space. It should be noted that by changing the value of b_2 an unstable point can be stabilized and the bifurcation point can also be moved.

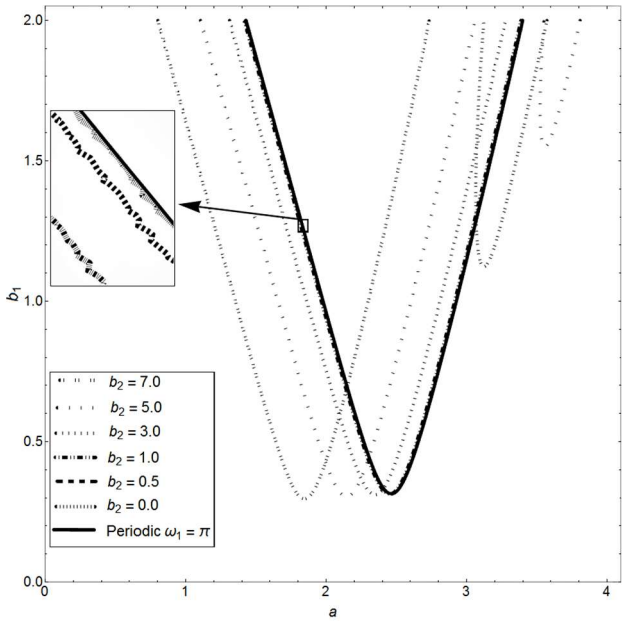

Figure 2.15: Effect of b_2 on the main instability region corresponding to $\omega_1 = \pi$ *i.e.,* R1 in the damped QP Hill equation with $\omega_1 = \pi$ and $\omega_2 = 7.0$. $\omega_{\min} = 0.0442270$.

2.4.2 CASE STUDY 2: $\omega_1 = 1.0$ and $\omega_2 = \left(1+\sqrt{5}\right)/2$

In this case, the frequencies form the 'golden ratio' that is well known for its interesting history and irrationality. In contrast to the previous case study, the frequencies

Table 2.3: Minimum frequencies ($\omega_{\min}$) with their corresponding periods (T_a) and the frequencies of the approximate (periodic) system. (Case Study 2)

Entry Number (E. No.)	Range of k_1, k_2 values	$\omega_{\min}$ ($\omega_{\min} \neq 0$)	$T_a = 2\pi/\omega_{\min}$	Total number of frequencies	$\bar{\omega}_1$	$\bar{\omega}_2$
Col. 1	Col. 2	Col. 3	Col. 4	Col. 5	Col. 6	Col. 7
1	0 to 1	0.618034	10.1664	4	1.23606800	1.85410200
2	0 to 2	0.381966	16.4496	12	1.14589800	1.52786400
3	0 to 4	0.236068	26.616	40	0.94427200	1.65247600
4	0 to 7	0.145898	43.0656	112	1.02128600	1.60487800
5	0 to 12	0.0901699	69.6816	312	0.99186890	1.62305820
6	0 to 20	0.0557281	112.747	840	1.00310580	1.61611490
7	0 to 33	0.0344419	182.429	2244	0.99881510	1.61876930
8	0 to 54	0.0212862	295.176	5940	1.00045140	1.61775120

ω_1 and ω_2 are smaller in magnitudes and also the difference between them is relatively small *i.e.*, 0.618034 instead of 3.85841 in Case Study 1. Due to the proximity of the frequencies, it is anticipated that more instability regions will be squeezed into a smaller region, and thus the stability chart could be quite intricate.

The damped QP Hill equation is similar to Eq. (2.17) with excitation frequencies 1.0 and $\left(1+\sqrt{5}\right)\Big/2$. Following the procedure discussed in section 2.4.1, $\omega_{\min}$ is computed over a range of k_1 and k_2 and are tabulated in Table 2.3 along-with their corresponding periods, T_a. It is important to note that $\omega_{\min} = 0.0212862$ (E. No. 8 in Table 2.3) is almost one half of the $\omega_{\min} = 0.0442270$ (minimum frequency used in Case Study 1, see E. No. 7 in Table 2.1) but it is obtained for relatively smaller value of k_1 and k_2 ($k_1 = 34$ and $k_2 = 21$). This occurs due to the smaller difference between the frequencies.

Once $\omega_{\min}$ has been fixed, the approximate system can be defined using columns 6 and 7 of Table 2.3. The selection of $\omega_{\min}$ was based on a convergence study of the bifurcation points of the main instability regions stemming from a axis corresponding to

$\omega_1 = 1.0$ and $\omega_2 = \left(1+\sqrt{5}\right)/2$. Figure 2.16 shows the convergence study of two bifurcation points and it can be observed that for $\omega_{\min} < 0.0901699$, the difference between the exact (a_e) and approximate (a_a) bifurcation points of main instability regions (*i.e.*, $a_e - a_a$) are relatively small. For $\omega_{\min} = 0.0557281$, $a_e - a_a$ is -0.001555 and +0.001552 for regions R1 and R2 (see Fig. 2.17), respectively. The difference $a_e - a_a$ decreases with a decrease in $\omega_{\min}$; however, this causes T_a to increase and as a compromise, $\omega_{\min} = 0.0557281$ ($T_a = 112.747$) was selected as the minimum frequency for further investigations (see Table 2.3).

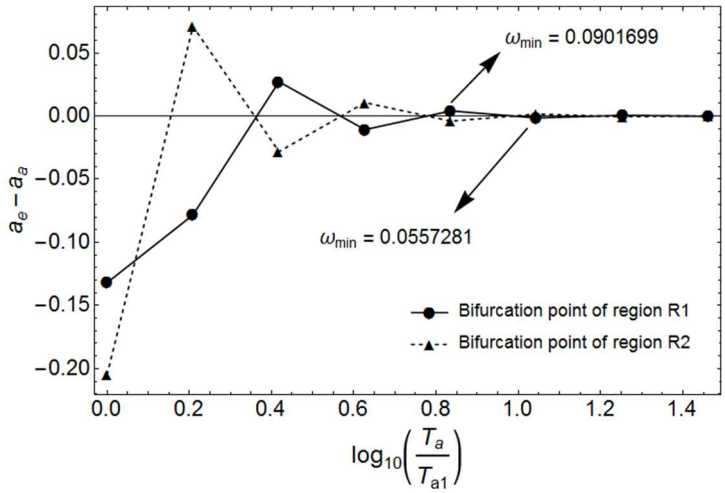

Figure 2.16: Convergence diagram of bifurcation points of the main instability regions of QP Hill equation with $\omega_1 = 1 \text{and} \omega_2 = \left(1+\sqrt{5}\right)/2$.

For this value of $\omega_{\min}$, the approximate system can be defined by replacing $\omega_1 = 1.0$ and $\omega_2 = \left(1+\sqrt{5}\right)/2$ by $\bar{\omega}_1 = 1.00310580$ and $\bar{\omega}_2 = 1.61611490$ (*c.f.*, Table 2.3) and thus it takes the form

$$\dot{x} = \begin{bmatrix} 0 & 1 \\ -\left(a + b_1 \cos 1.00310580\, t + b_2 \cos 1.61611490\, t\right) & -d \end{bmatrix} x \qquad (2.22)$$

In the following, the STM is computed numerically using Floquét theory with $T_a = 112.747$ for undamped and damped systems and stability charts are plotted. For the sake of convenience, all computations are performed by setting $b_1 = b_2 = b$.

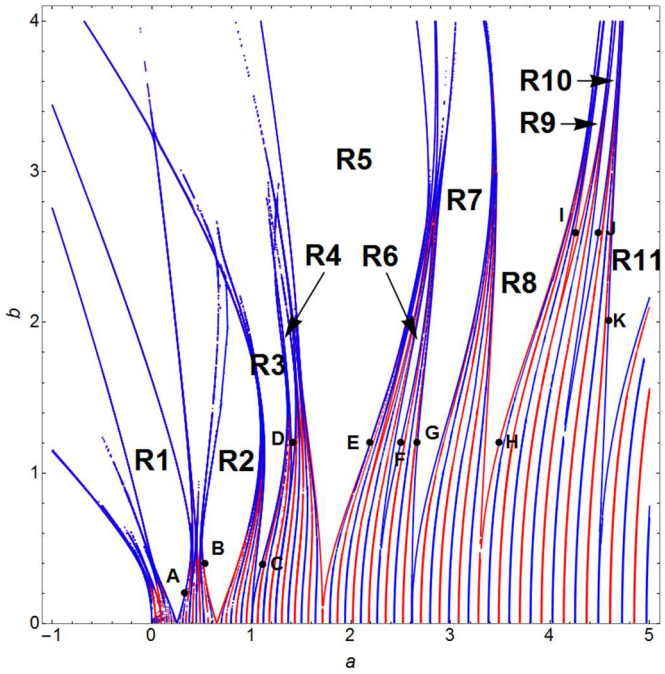

Figure 2.17: Stability diagram of the QP Hill equation with $\omega_1 = 1 \text{and} \, \omega_2 = \left(1+\sqrt{5}\right)\Big/2$. $\omega_{\min} = 0.0557281$; Red: $2T_a$ periodic, Blue: T_a periodic

2.4.2.1 The Undamped System ($d = 0$)

Figure 2.17 shows the stability diagram for the undamped system corresponding to $\omega_{\min} = 0.0557281$ (or $T_a = 112.747$). As anticipated, the stability chart is quite complicated as compared to the Case Study 1. The investigation is restricted to the parametric space of $-1.0 \le a \le 5.0$ and $0.0 \le b \le 4.0$ and prominent instability regions are marked as R1 through R11.

The main instability regions R1 and R2 stem from $a = 0.251555$ and $a = 0.652957$ in the $a \sim b$ plane and are T_a and $2T_a$ periodic, respectively. According to reference [30],

the main instability regions arise from $a = 0.25$ ($k_1 = 1$ and $k_2 = 0$) and $a = 0.654508$ ($k_1 = 0$ and $k_2 = 1$). It is to be noted that the approximate bifurcation points calculated using Floquét theory with $T_a = 112.747$ are extremely close to the exact bifurcations that are computed using the concept of winding number. In case of periodic system with excitation frequency ω_1 (ω_2), the main instability region arises from $a = 0.25$ ($a = 0.654508$) and is $2T$ periodic where T the is the period corresponding to excitation frequency ω_1 (ω_2). The Approximate and exact bifurcation points of other prominent instability regions, marked as R3 through R11 in Fig. 2.17 are listed in the last two rows of Tables 2.4a and 2.4b and a good agreement between them can be observed.

This case has also been studied by Broer and Simó [31] using rotation number and maximal Lyapunov exponent. They numerically plotted the stability diagram in the $a \sim b$ plane defined by $a = 0.25$ to 1.0 and $b = 0.0$ to 1.0. In Fig. 2.18, the approximate stability boundaries computed using the Floquét theory with $T_a = 112.747$ are compared with the numerically computed boundaries reported in reference [31]. The comparison is made at some typical points (marked as black dots) and it is clear that there is an excellent agreement between the two results in the main instability regions.

One of the special features of this case is the presence of an '*instability loop*' in the main instability region, R2 (see Fig. 2.17). The '*instability loops*' or '*instability pockets*' [43, 44] are known to appear in periodic cases where the parametric forcing term has two or more commensurate frequencies. These pockets also exist in Meissner's equation [77]. Broer and Simó [31] were unable to capture this feature since their investigation was restricted

Table 2.4a: DFT results. $\omega_1 = 1 \text{and} \, \omega_2 = \left(1+\sqrt{5}\right)/2$. $\omega_{\min} = 0.0557281$.

Instability regions		R1	R2	R3	R4	R5	R6
Location selected for comparison		A	B	C	D	E	F
b		0.2	0.4	0.4	1.2	1.2	1.2
a (Near approx. boundary)		0.334122	0.515954	1.1046	1.39915	2.19418	2.49952
a (Near exact boundary)		0.332638	0.517030	1.0994	1.40099	2.19314	2.48982
Dominant frequency in the frequency spectrum	Approx. system (f_{aa})	0.501554	0.807570	1.00395	1.11456	1.30961	1.50513
	Original system (f_{oe})	0.500140	0.808620	0.99977	1.11840	1.30882	1.49998
Frequency content in terms of ω_1 and ω_2		$\omega_1/2$	$\omega_2/2$	$2\omega_1/2$	$(2\omega_2-\omega_1)/2$	$(\omega_1+\omega_2)/2$	$3\omega_1/2$
Freq. combinations causing parametric resonance		ω_1	ω_2	$2\omega_1$	$2\omega_2-\omega_1$	$\omega_1+\omega_2$	$3\omega_1$
Approx. bifurcation points ($b=0$)		0.251555	0.652957	1.00622	1.24225	1.71508	2.264
Exact bifurcation points [30] ($b=0$)		0.25	0.654508	1.0	1.25	1.71353	2.25

Table 2.4b: DFT results. $\omega_1 = 1 \text{and} \, \omega_2 = \left(1+\sqrt{5}\right)/2$. $\omega_{\min} = 0.0557281$.

Instability regions		R7	R8	R9	R10	R11
Location selected for comparison		G	H	I	J	K
b		1.2	1.2	2.6	2.6	2.0
a (Near approx. boundary)		2.6687	3.4898	4.2496	4.49000	4.58476
a (Near exact boundary)		2.6743	3.4830	4.2558	4.47710	4.58619
Dominant frequency in the frequency spectrum	Approx. system (f_{aa})	1.61555	1.81117	1.92262	2.00655	2.11767
	Original system (f_{oe})	1.61657	1.80972	1.92564	2.00117	2.11854
Frequency content in terms of ω_1 and ω_2		$2\omega_2/2$	$(2\omega_1+\omega_2)/2$	$(3\omega_2-\omega_1)/2$	$4\omega_1/2$	$(\omega_1+2\omega_2)/2$
Freq. combinations causing parametric resonance		$2\omega_2$	$2\omega_1+\omega_2$	$3\omega_2-\omega_1$	$4\omega_1$	$\omega_1+2\omega_2$
Approx. bifurcation points ($b=0$)		2.61183	3.28031	3.69647	4.02488	4.48452
Exact bifurcation points [30] ($b=0$)		2.61803	3.27254	3.71353	4.0	4.48607

to a smaller parametric region. These loops also exist in other unstable regions (for instance, R6 in Fig. 2.17).

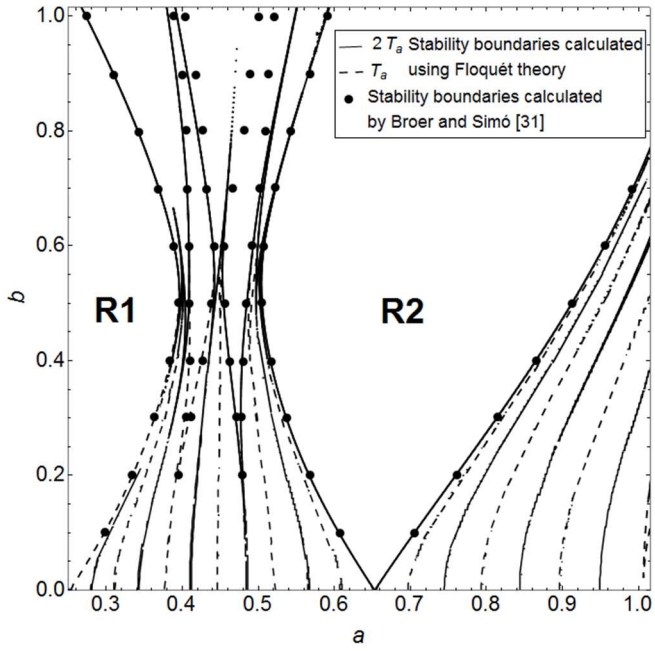

Figure 2.18: Comparison between the stability boundaries computed using Floquét theory ($\omega_{\min} = 0.0557281$) and those computed by Broer and Simo [31].

The accuracies of the stability boundaries were also checked by constructing Poincaré maps of the approximate and exact (numerical solution of Eq. (2.11) with $\omega_1 = 1.0$, $\omega_2 = \left(1+\sqrt{5}\right)\Big/2$ and $d = 0$) solutions at some typical points (marked A through K in Fig. 2.17) in the stability chart. The exact and approximate maps were found to be qualitatively similar at all these points. For the sake of brevity, these maps are not shown here.

In order to check the frequency contents of approximate and exact boundaries, DFT analyses were performed at points A through K. The results are listed in Tables 2.4a & 2.4b and it can be observed that $f_{aa} \approx f_{oe}$ at all points implying that the boundaries computed using the Floquét theory are accurate representations of the exact boundaries. The dominant frequencies in approximate solutions are further used to identify the frequency

combinations causing parametric resonances and the results are also listed in Tables 2.4a & 2.4b.

2.4.2.2 The Damped System ($d \neq 0$)

The approximate stability chart obtained from Eq. (2.22) with $d = 0.1$ is shown in Fig. 2.19. Only a few prominent instability regions remain in the parametric space defined by $a = 0$ to 5 and $b = 0$ to 1. The approximate boundaries are compared with the exact boundaries computed using the maximal Lyapunov exponent and an excellent agreement is observed. Further, no instability boundaries were detected in the range of $2.5 \le a \le 5.0$ and $0.0 \le b \le 1.0$ .The qualitative behaviors of solutions near the approximate boundaries are also studied by constructing the Poincaré maps and found to be similar. Once again, these are not included.

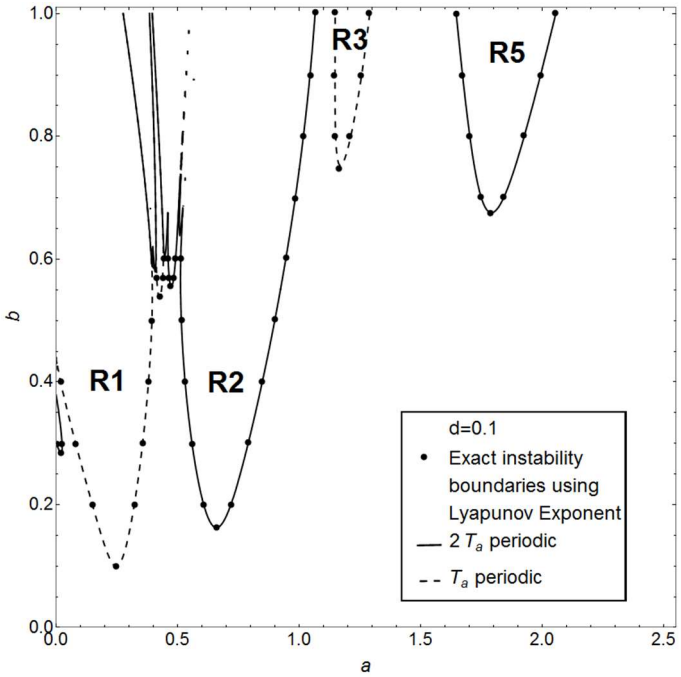

Figure 2.19: Stability diagram of the damped QP Hill equation with $\omega_1 = 1$ and $\omega_2 = \left(1+\sqrt{5}\right)/2$. ($\omega_{\min} = 0.0557281$ and $d = 0.1$.)

2.4.3 CASE STUDY 3: $\omega_1 = 1.0$, $\omega_2 = \sqrt{3}$ and $\omega_3 = \sqrt{11}$

This case is included to demonstrate the viability of the proposed methodology when the frequency basis of the coefficient matrix, $A(\omega t, \lambda)$ has more than two frequencies. The differences between the frequencies ($\omega_2 - \omega_1 = 0.732051$, $\omega_3 - \omega_2 = 1.58457$ and $\omega_3 - \omega_1 = 2.31662$) are relatively small and thus a complicated structure of the stability chart should be expected.

The damped QP Hill equation for this case can be written in the state space form using Eq. (2.11). In order to fix $\omega_{\min}$, a convergence study was once again performed on the bifurcation points of the main instability regions and the diagram is shown in Fig. 2.20. Using $\omega_{\min} = 0.0216711$, the approximate system is defined by replacing the frequencies of the original quasi-periodic system with new frequencies $\bar{\omega}_1 = 0.99687060$, $\bar{\omega}_2 = 1.73368800$ and $\bar{\omega}_3 = 3.31567830$ and the approximate system takes the form.

$$\dot{x} = \begin{bmatrix} 0 & 1 \\ -\left(a + b_1 \cos 0.99687060t + b_2 \cos 1.73368800t + b_3 \cos 3.31567830t\right) & -d \end{bmatrix} x \quad (2.23)$$

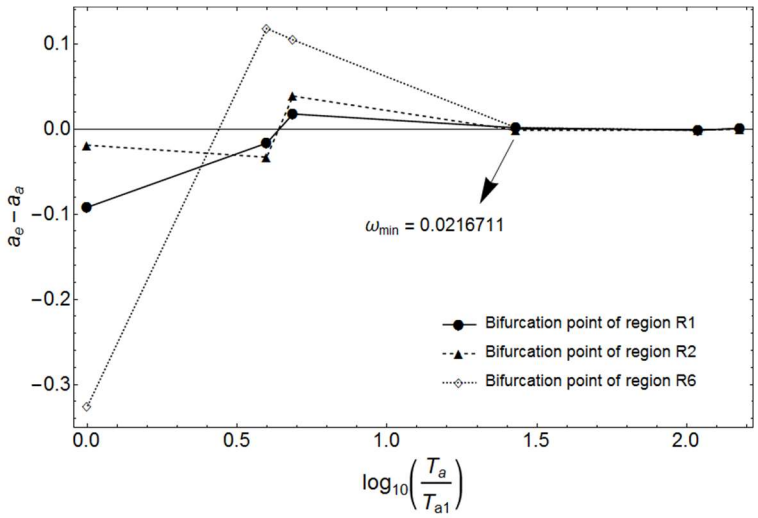

Figure 2.20: Convergence diagram of bifurcation points of the main instability regions of QP Hill equation with $\omega_1 = 1, \omega_2 = \sqrt{3}$ and $\omega_3 = \sqrt{11}$ (See Fig. 2.21).

This is a periodic system with $T_a = 289.934$ and the stability diagram for the undamped case is plotted in the following section using Floquét theory. Once again, for the sake of convenience all computations are performed assuming $b_1 = b_2 = b_3 = b$.

2.4.3.1 The Undamped System ($d = 0$)

The stability diagram for this case is plotted for $-1.0 \le a \le 5.0$ and $0.0 \le b \le 2.2$ using Floquét theory with $T_a = 289.934$ and is shown in Fig. 2.21. Due to the presence of three frequencies and relatively smaller $\omega_{\min}$, the stability diagram is quite complicated as compared to the previous cases. Ten prominent instability regions are observed and are marked as R1 through R10 in Fig. 2.21, where R1, R2 and R6 are the main parametric resonance regions corresponding to frequencies $\omega_1 = 1.0, \omega_2 = \sqrt{3}$ and $\omega_3 = \sqrt{11}$, respectively.

The main instability regions R1, R2 and R6 stem from $a = 0.248438, 0.751419$ and 2.74843, respectively and are T_a, T_a and $2T_a$ periodic, respectively. Using the expression given in reference [30], the main instability regions R1, R2 and R6 arise from $a = 0.25 (k_1 = 1$ and $k_2 = k_3 = 0)$, $a = 0.75 (k_2 = 1$ and $k_1 = k_3 = 0)$ and $a = 2.75 (k_3 = 1$ and $k_1 = k_2 = 0)$, respectively. Once again, it should be noted that these points are identical to those predicted by Floquét theory for Mathieu equations with parametric excitation frequencies of $\omega_1 = 1.0, \omega_2 = \sqrt{3}$ and $\omega_3 = \sqrt{11}$, respectively. Approximate and exact bifurcation points corresponding to all prominent instability regions (R1- R10) are tabulated in Tables 2.5a & 2.5b and an excellent agreement can be observed. A number of instability loops can also be seen in the stability diagram (Fig 2.21). In the following section, a symbolic technique has been presented and found to be very

useful in obtaining a more detailed picture of the stability chart in the region $-1.0 \le a \le 1.0$ and $0.0 \le b \le 2.2$ (see Fig. 2.24) since it is not very clear in Fig. 2.21.

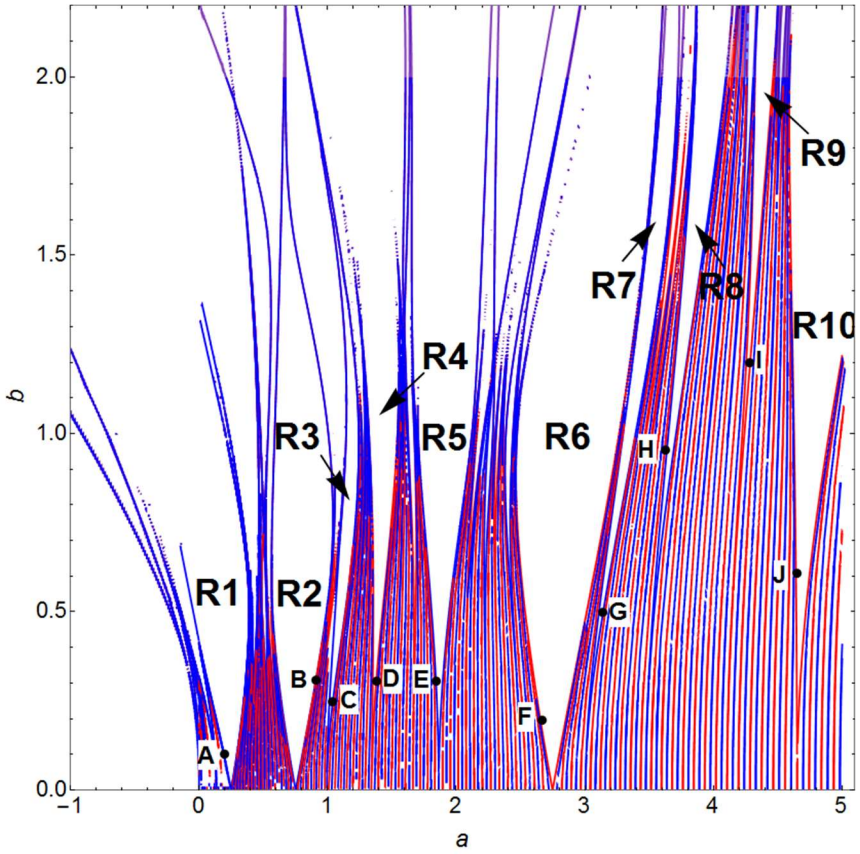

Figure 2.21: Stability diagram of the QP Hill equation with $\omega_1 = 1$, $\omega_2 = \sqrt{3}$ and $\omega_3 = \sqrt{11}$. $\omega_{\min} = 0.0216711$; Red: $2T_a$ periodic, Blue: T_a periodic

Similar to previous case studies, Poincaré maps of approximate and exact solutions were constructed at points A-J (marked in Fig. 2.21) near the stability boundaries and they were found to be qualitatively similar (not shown). Results of DFT performed at these points are tabulated in Tables 2.5a & 2.5b and it can be observed that for all prominent instability regions $f_{aa} \approx f_{oe}$ implying that the approximate boundaries are accurate representations of the exact boundaries. As before, the DFT is also used to identify the frequency combinations that cause parametric resonances as listed in these tables. The actual DFT diagrams have been omitted for brevity.

Table 2.5a: DFT results. $\omega_1 = 1.0$, $\omega_2 = \sqrt{3}$ and $\omega_2 = \sqrt{11}$. $\omega_{\min} = 0.0216711$.

Instability regions		R1	R2	R3	R4	R5
Location selected for comparison		A	B	C	D	E
b		0.1	0.3	0.25	0.3	0.3
a (Near approx. boundary)		0.194335	0.903717	1.01434	1.37711	1.84289
a (Near exact boundary)		0.195890	0.902442	1.01977	1.37465	1.84495
Dominant frequency in the frequency spectrum	Approx. system (f_{aa})	0.498435	0.866844	0.996664	1.1594	1.36528
	Original system (f_{oe})	0.500102	0.865808	1.00001	1.15837	1.36595
Frequency content in terms of ω_1, ω_2 and ω_3		$\omega_1/2$	$\omega_2/2$	$2\omega_1/2$	$(\omega_3 - \omega_1)/2$	$(\omega_1 + \omega_2)/2$
Freq. combinations causing parametric resonance		ω_1	ω_2	$2\omega_1$	$\omega_3 - \omega_1$	$\omega_1 + \omega_2$
Approx. bifurcation points ($b = 0$)		0.248438	0.751419	0.993751	1.34422	1.86399
Exact bifurcation points 30] ($b = 0$)		0.25	0.75	1.0	1.34169	1.86603

Table 2.5b: DFT results. $\omega_1 = 1.0$, $\omega_2 = \sqrt{3}$ and $\omega_2 = \sqrt{11}$. $\omega_{\min} = 0.0216711$.

Instability regions		R6	R7	R8	R9	R10
Location selected for comparison		F	G	H	I	J
b		0.2	0.5	0.95	1.2	0.6
a (Near approx. boundary)		2.65317	3.14206	3.6361	4.2847	4.64064
a (Near exact boundary)		2.65473	3.13834	3.6437	4.2788	4.64948
Dominant frequency in the frequency spectrum	Approx. system (f_{aa})	1.65784	1.7339	1.86371	2.02662	2.15627
	Original system (f_{oe})	1.65823	1.73207	1.86609	2.0244	2.15883
Frequency content in terms of ω_1, ω_2 and ω_3		$\omega_3/2$	$2\omega_2/2$	$(2\omega_1 + \omega_2)/2$	$(\omega_2 + \omega_3 - \omega_1)/2$	$(\omega_1 + \omega_3)/2$
Freq. combinations causing parametric resonance		ω_3	$2\omega_2$	$2\omega_1 + \omega_2$	$\omega_2 + \omega_3 - \omega_1$	$\omega_1 + \omega_3$
Approx. bifurcation points ($b = 0$)		2.74843	3.00567	3.47343	4.10568	4.64952
Exact bifurcation points [30] ($b = 0$)		2.75	3.0	3.48205	4.09794	4.65831

2.5 Symbolic Computation of STM

In section 2.4, the stability charts for the quasi-periodic systems were numerically studied using the Floquét theory. However, once a quasi-periodic system has been approximated by a periodic system, it is possible to obtain the state transition matrix (STM) in a symbolic form. In 1997, Sinha and Butcher [17] developed a symbolic technique for computing the STM of a linear time-periodic system of arbitrary dimension via Picard iterations and shifted Chebyshev polynomials. In the following their technique is briefly outlined for completeness.

2.5.1 A Brief Outline of the Symbolic Technique [17]

Consider a linear time periodic system

$$\dot{x}(t,\lambda) = A(t,\lambda)x(t,\lambda) \qquad x(0,\lambda) = x_0 \tag{2.24}$$

where, $x(t,\lambda) \in \mathbb{R}^n$, $t \in \mathbb{R}^+$, λ is a set of system parameters and $A(t,\lambda)$ is an $n \times n$ periodic matrix that can be written as $A(t,\lambda) = A_1(\lambda)f_1(t) + A_2(\lambda)f_2(t) + \cdots + A_r(\lambda)f_r(t)$. $A_i(\lambda)$; $i = 1,...,r$ contain coefficients of periodic functions $f_i(t)$ with period γ_i *i.e.*, $f_i(t) = f_i(t+\gamma_i)$. In case of commensurate frequencies, the principal period, T of the system matrix $A(t,\lambda)$ is the lowest positive number such that $p_i\gamma_i = T$ where $p_i \in \mathbb{Z}^+$. If $\Phi(t,\lambda)$ is the STM of Eq. (2.24), then

$$x(t,\lambda) = \Phi(t,\lambda)x_0 \qquad 0 \le t \le T \tag{2.25}$$

Note that the Eq. (2.24) is equivalent to the integral equation

$$x(t,\lambda) = x_0 + \int_0^t A(\tau,\lambda)x(\tau,\lambda)d\tau \tag{2.26}$$

Assuming the zeroth approximation of Eq. (2.26) as $x(0,\lambda)=x_0$, the first approximation can be written as

$$x_1(t,\lambda)=x_0+\int_0^t A(\tau_0,\lambda)x_0(\tau_0,\lambda)d\tau_0=\left[I+\int_0^t A(\tau_0,\lambda)d\tau_0\right]x_0 \tag{2.27}$$

where τ_0 is a dummy variable. With each iteration, a better approximation is achieved and the $(p+1)^{th}$ approximation is given by

$$\begin{aligned} x_{p+1}(t,\lambda) &= x_0+\int_0^t A(\tau_p,\lambda)x_p(\tau_p,\lambda)d\tau_p \\ &= \left[I+\int_0^t A(\tau_p,\lambda)d\tau_p+\int_0^t A(\tau_p,\lambda)\int_0^{\tau_p} A(\tau_{p-1},\lambda)d\tau_{p-1}d\tau_p+\cdots\right. \\ &\quad \left.+\int_0^t A(\tau_p,\lambda)\ldots\int_0^{\tau_1} A(\tau_0,\lambda)d\tau_0\ldots d\tau_p\right]x_0 \end{aligned} \tag{2.28}$$

where $\tau_0,\ldots,\tau_p$ are the dummy variables. A truncated version of this series of integrals yields an approximation to $\Phi(t,\lambda)$. In general, the symbolic computation of $\Phi(t,\lambda)$ via Eq. (2.28) leads to a complicated expression and is inefficient when $r>1$ due to repeated integration by parts.

Following Sinha and Butcher [17], first, the transformation $t=T\tau$ is applied to Eq. (2.24) which normalizes the system's principal period to 1. Thus, Eq. (2.24) takes the form

$$x'(\tau,\lambda)=\bar{A}(\tau,\lambda)x(\tau,\lambda) \qquad x(0,\lambda)=x_0 \tag{2.29}$$

where $x'(\tau,\lambda)=\frac{dx}{d\tau},\tau\in[0,1]$ and $\bar{A}(\tau,\lambda)=\bar{A}(\tau+1,\lambda)$. The $\bar{A}(\tau,\lambda)$ is expressed as $\bar{A}(\tau,\lambda)=\bar{A}_1(\lambda)f_1(\tau)+\bar{A}_2(\lambda)f_2(\tau)+\cdots+\bar{A}_r(\lambda)f_r(\tau)$ where $f_i(\tau)=f_i(\tau+1)$ and $\bar{A}_i(\lambda)=TA_i(\lambda)$.

The normalized system matrix is expanded in m_c shifted Chebyshev polynomials of first kind and can be written as

$$\bar{A}(\tau,\lambda)=\hat{T}^T(\tau)D(\lambda) \tag{2.30}$$

where $\hat{T}(\tau)$ and $D(\lambda)$ are $nm_c\times n$ matrices defined as

$$\hat{T}(\tau)=I_n\otimes T^*(\tau) \qquad D(\lambda)=\sum_{i=1}^{r}\bar{A}_i(\lambda)\otimes d_i \tag{2.31}$$

In the above equation, d_i are the $m_c\times 1$ column vectors that contain known coefficients of the Chebyshev expansions of the one-periodic functions, $T^*(\tau)$ are the shifted Chebyshev polynomials of first kind and $\otimes$ represents the Kronecker product.

Using the integration operational matrix (G) and product operational matrix (Q_{d_i}), an expression for the STM can be obtained as [17]

$$\Phi^{(p,m_c)}(\tau,\lambda)=\hat{T}^T(\tau)\left[\hat{I}+\sum_{s=1}^{p}\left(\left[L(\lambda)\right]^{s-1}\right)P(\lambda)\right]=\hat{T}^T(\tau)B(\lambda) \tag{2.32}$$

where $\hat{I}=I_n\otimes\underbrace{\{1\ 0\ 0\ \ldots\ 0\}}_{m_c}^{T}$. $B(\lambda)$ contains the Chebyshev coefficients of the elements of $\Phi(\tau,\lambda)$ and is expressed in terms of $L(\lambda)$ and $P(\lambda)$. The $L(\lambda)$ and $P(\lambda)$ are $nm_c\times nm_c$ and $nm_c\times n$ matrices defined as

$$L(\lambda)=\sum_{i=1}^{r}\bar{A}_i(\lambda)\otimes\left(G^TQ_{d_i}\right) \qquad P(\lambda)=\sum_{i=1}^{r}\bar{A}_i(\lambda)\otimes\left(G^Td_i\right) \tag{2.33}$$

Equation (2.32) is valid only in the interval $0 \le \tau \le 1$ and solution for $\tau > 1$ can be computed using Eq. (2.3). The expression for $\Phi(\tau, \lambda)$ is in normalized time and could be transformed to real time by the substitution $\tau = t / T$.

The computation of STM via Eq. (2.32) is very efficient and approximation to a desired degree of accuracy can be obtained by selecting the number of Picard iterations, p and the number of Chebyshev polynomials, m_c. The number of Chebyshev polynomials required for convergence can be reduced by dividing the principal period into a number of sub-intervals. Following the methodology described above, the STM for each sub-interval can be computed and combined, using the semigroup property of the transition matrix [78], to determine the STM valid over the principal period and is given by

$$\Phi(t_N, t_0, \lambda) = \prod_{si=1}^{N} \Phi(t_{N+1-si}, t_{N-si}, \lambda) \tag{2.34}$$

where N represents the number of sub-intervals (si).

2.5.2 Symbolic Computation of STM for Case Study 2

In order to demonstrate the applicability of this approach, the STM for Case Study 2 ($\omega_1 = 1.0$ and $\omega_2 = \left(1+\sqrt{5}\right)\Big/2$) is computed in terms of system parameters a, b and time t. This particular case is more convenient since $T_a = 112.747$ is the smallest among the three case studies requiring relatively lower number of Chebyshev polynomials and sub-intervals.

As shown in section 2.4.2, the original QP system is approximated by the periodic system, Eq. (2.22) with $T_a = 112.747$ ($\omega_{\min} = 0.0557281$), and thus the periodic matrix $A(t, \lambda)$ can be represented as $A(t,\lambda) = A_1(\lambda) f_1(t) + A_2(\lambda) f_2(t) + A_3(\lambda) f_3(t)$

where $A_1(\lambda)=\begin{bmatrix} 0 & 1 \\ -a & -d \end{bmatrix}$; $A_2(\lambda)=\begin{bmatrix} 0 & 0 \\ -b_1 & 0 \end{bmatrix}$; $A_3(\lambda)=\begin{bmatrix} 0 & 0 \\ -b_2 & 0 \end{bmatrix}$; (2.35)

$$f_1(t)=1 \quad ; \quad f_2(t)=\cos 1.0031058t \quad ; \quad f_3(t)=\cos 1.6161149t \tag{2.36}$$

To reduce the number of Chebyshev polynomials, the principal period, T_a was divided into 30 equal sub-intervals such that the length of each sub-interval, $\Delta T_a = T_a/30$. Next, the transformation $t=(si-1)\Delta T_a+\Delta T_a\tau$; $si=1$ *to* $30, \tau\in[0,1]$ was applied to Eq. (2.22) to normalize the period of the system matrix to 1 in each sub-interval. The initial condition in each sub-interval was set to $\Phi(0)=I$ and system parameters were selected as $b_1=b_2=b$ and $d=0.0$ for convenience.

Using the methodology described in section 2.5.1, STM for each subinterval was calculated with varying number of m_c (Chebyshev polynomials) and p (Picard iterations) and the STM over the principal period, T_a was obtained using Eq. (2.34). For conciseness, only one element of FTM for one of the subintervals; the third subinterval ($si=3$), in terms of system parameters is shown in the Appendix A. Using the symbolic FTM and Eq. (2.15), the stability chart can be plotted in the $a\sim b$ plane. Two charts are presented here to show the influence of m_c (number of Chebyshev polynomials) and p (number of Picard iterations) on the accuracy and convergence of this technique. Figure 2.22 shows the stability chart obtained with $m_c=15$ and $p=20$, whereas $m_c=20$ and $p=30$ were used for the chart in Fig. 2.23. It is seen from Fig. 2.22 that for $a>2.5$, the diagram is incomplete/inaccurate reflecting the lower number of m_c and p used in the computation. However, Fig. 2.23 is identical to Fig. 2.17 demonstrating the capability of the symbolic approach. Plotting the stability diagram requires a large amount of memory due to very

long expression of $Tr\left(\Phi(T_a,a,b)\right)$. This problem was circumvented by calculating the $Tr\left(\Phi(T_a,a,b)\right)$ at a grid of equally spaced sampling points. 'ListContourPlot' command in MATHEMATICA was used for plotting the stability diagrams.

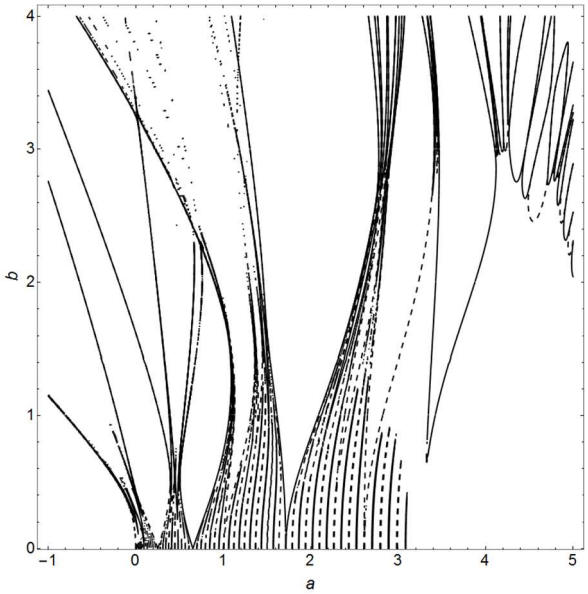

Figure 2.22: Stability diagram of the QP Hill equation with $\omega_1 = 1$ and $\omega_2 = \left(1+\sqrt{5}\right)/2$ using symbolic FTM ($\omega_{\min} = 0.0557281$, $m_c = 15$ and $p = 20$) . Solid: $2T_a$ periodic, Dashed: T_a periodic

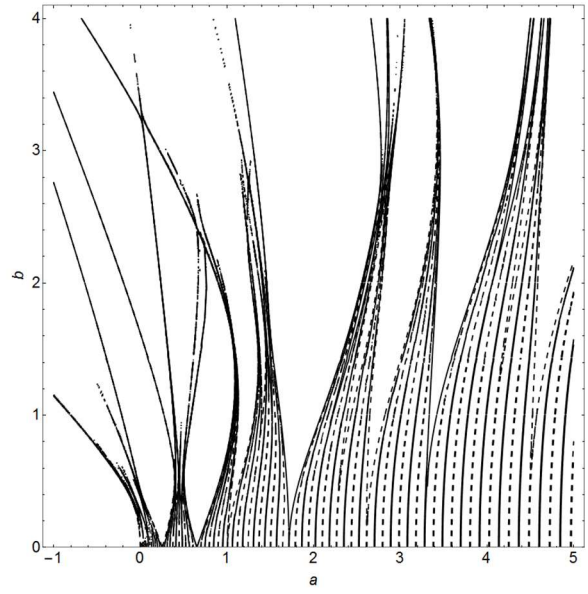

Figure 2.23: Stability diagram of the QP Hill equation with $\omega_1 = 1$ and $\omega_2 = \left(1+\sqrt{5}\right)/2$ using symbolic FTM ($\omega_{\min} = 0.0557281$, $m_c = 20$ and $p = 30$) . Solid: $2T_a$ periodic, Dashed: T_a periodic

It is important to note that unlike perturbation and averaging methods, this symbolic technique does not require existence of a small parameter or a generating solution. All system parameters are treated equally in the symbolic technique. Existence of an instability loop in one of the main instability regions, R2, is an important feature of the stability diagram for this case (see Fig. 2.23) and it could easily be missed if techniques such as perturbation and averaging are used.

The symbolic technique is also employed for Case Study 3 ($\omega_1 = 1.0$, $\omega_2 = \sqrt{3}$ and $\omega_3 = \sqrt{11}$) in order to show the details of the stability diagram in the parametric region defined by $-1.0 \le a \le 1.0$ and $0.0 \le b \le 2.2$ since it is not very clear in Fig. 2.21. Figure 2.24 shows the stability diagram plotted using $si = 40$, $m_c = 25$ and $p = 35$. The successful application of symbolic technique to the three-frequency case also demonstrates its viability for multi-frequency systems.

Chapter 3

Instability Pockets and Influence of Damping in Parametrically Excited Systems

3.1 Introduction

In most parametrically excited systems stability boundaries cross each other at several points to form closed unstable sub-regions commonly known as '*Instability Pockets*'. The first aspect of this study explores some general characteristics of these instability pockets and their structural modifications in the parametric space as damping is induced in the system. Secondly, the possible destabilization of undamped systems due to addition of damping in parametrically excited systems has been investigated. The study is restricted to SDF systems that can be modeled by Hill and Quasi-Periodic Hill equations. Three typical cases of Hill equation, e.g., Mathieu, Meissner and three-frequency Hill equations are analyzed. Locations of the intersections of stability boundaries (commonly known as coexistence points), are determined using the property that two linearly independent solutions coexist at these intersections. In the second part of the study, the symbolic/analytic forms of state transition matrices are used to compute the minimum values of damping coefficients required for instability pockets to vanish from the parametric space. The phenomenon of destabilization due to damping, previously observed in systems with two degrees of freedom or higher, is also demonstrated in systems with one degree of freedom.

3.2 Results

The study covers two types of parametrically excited systems that can be modeled by Hill and QP Hill equations. To investigate these systems, the following form is considered.

$$\ddot{x} + d\,\dot{x} + \left(a + b\,p(t)\right)x = 0 \tag{3.1}$$

where, $p(t)$ is the parametric excitation, a, b & d are the system parameters and t is the time.

Three typical cases of Hill equation are examined in the present study. It includes Mathieu, Meissner and three-frequency Hill equations. Since these equations have periodic coefficients, Floquet theory can be applied to analyze them. The QP Hill equation is explored using the approximate method proposed in chapter 2. The approach utilizes Floquet theory to determine an approximate response and stability of the original quasi-periodic system. Instability pockets are seen in the stability diagrams of Meissner, three-frequency Hill and QP Hill equations. These pockets are observed for relatively larger amplitudes (b) of parametric excitations. In the case of Meissner equation with a square wave coefficient, simple expressions for the number and locations of instability pockets in parametric space are developed. Destabilization effect of damping is also investigated in the stability diagrams of all four equations.

3.2.1 Mathieu Equation

The damped Mathieu equation (Eq. (3.1) with $p(t) = \cos\omega t$) can be represented in the state space form as

$$\dot{x} = \begin{bmatrix} 0 & 1 \\ -\left(a + b\cos\omega t\right) & -d \end{bmatrix} x \tag{3.2}$$

where, ω is the parametric frequency and $T = 2\pi/\omega$ is the principal period of the system. The initial condition was set to $\Phi(0) = I$ & $\omega = 1$. Following the procedure described in Sec. 2.5, the STM of Eq. (3.2) was computed in symbolic form as a function of system parameters (a, b & d) and time, t. Utilizing the symbolic FTM & the following expression [72], stability charts were plotted in $a \sim b$ plane for a set of damping values, d.

$$Tr\left(\Phi(T,\lambda)\right) = \pm(1+e^{-Td}) \tag{3.3}$$

Figure 3.1 shows the stability diagram of Eq. (3.2) for $d = 0$ and 0.5 as obtained with 28 Chebyshev expansion terms and 40 Picard iterations. A numerical computation produced an identical diagram. Regions of stability and instability are separated by periodic boundaries that are either T or $2T$ periodic and the unstable regions lie in between the boundaries of same period. For $d = 0$, the boundaries of an unstable region do not intersect to form instability pockets in the parametric space as stated in Ref. [42].

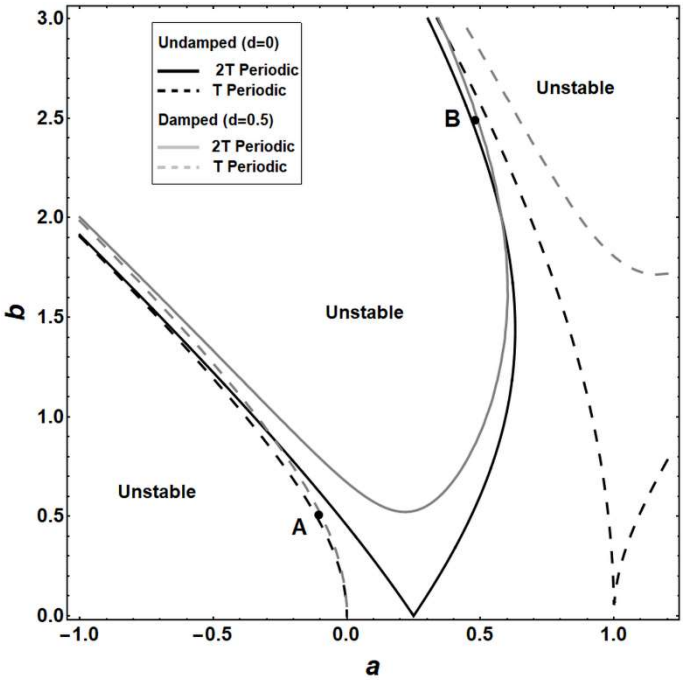

Figure 3.1: Stability diagram of damped Mathieu equation (3.2) with $d = 0$ and 0.5.

From Fig. 3.1, it is observed that, due to damping both unstable regions (except the first T periodic boundary that stems from $a = 0$) are lifted up from the a axis in the parametric space and hence, parametric resonances for small amplitudes of excitation (b) is almost impossible. For $b < 1.9$ (approximately), the $2T$ periodic region of instability of the damped Mathieu equation ($d = 0.5$) lies inside the instability region of the undamped equation ($d = 0$) implying that stability is unchanged below this value of b by the addition of damping. However, it is seen that the first T periodic boundary of the damped system that arises from $a = 0$ encloses the boundary of the undamped system thereby expanding the unstable area, and thus it can be concluded that the system becomes unstable due to the presence of damping. Equation (3.2) can also be analyzed in $a \sim d$ plane keeping 'b' constant and the stability diagram is shown in Fig. 3.2 for $b = 0.5$. It is observed that only the width of the first unstable region is increasing with an increase in damping which

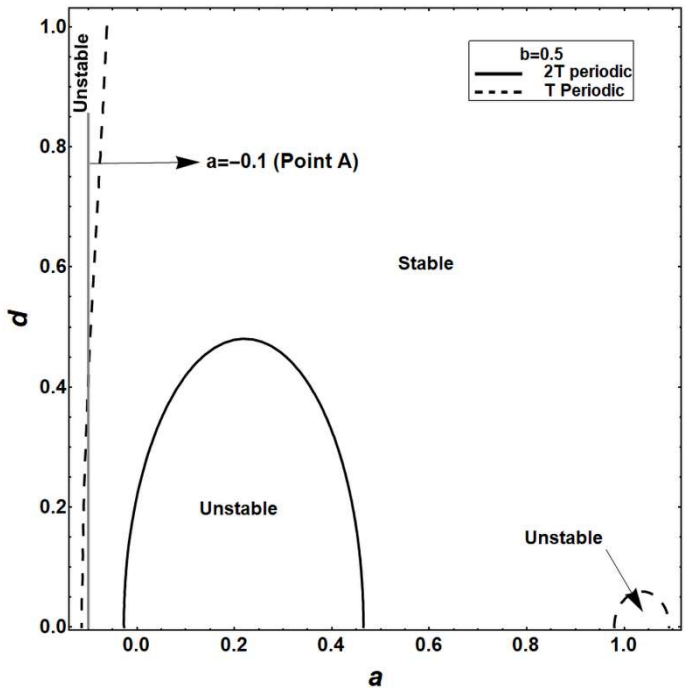

Figure 3.2: Stability diagram of damped Mathieu equation (9) in $a \sim d$ plane ($b = 0.5$).

implies that for $b = 0.5$ a damped system could become unstable if system parameters are close to the first T periodic boundary. For instance, when $a = -0.1$ & $b = 0.5$ (point A in Figs. 3.1 and 3.2) the system becomes unstable if the value of 'd' is beyond a critical damping value. Widths of the other two unstable regions in Fig. 3.2 are decreasing with an increase in damping implying that of destabilization due to damping is not possible near these regions for $b = 0.5$. However, these unstable regions depict destabilization phenomenon for large amplitudes of parametric excitation (see point B in Fig. 3.1 and point C in Fig. 3.3) and it could easily be missed if techniques such as perturbation and averaging are used (for instance, see Fig. 2 in Ref. [79]). Damping causes unstable regions to move to the right from the b axis, thereby causing a cross over between undamped and damped instability boundaries which leads to destabilization. The movement of unstable regions

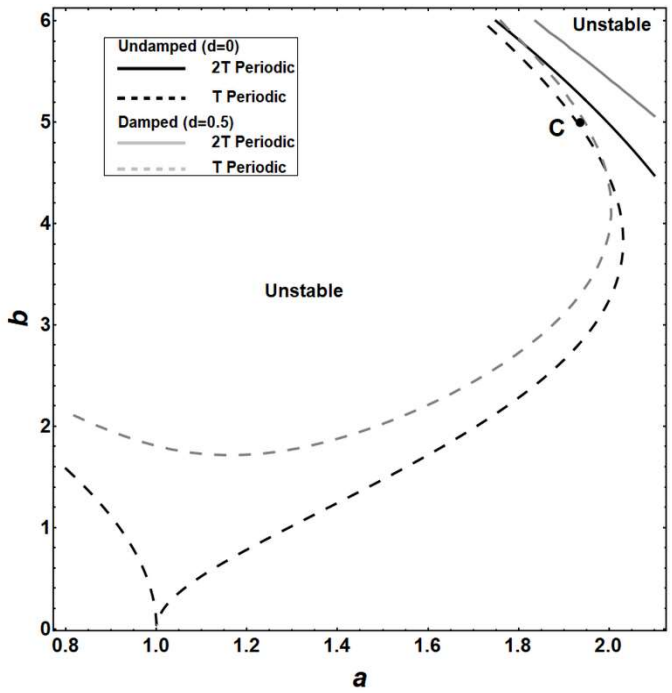

Figure 3.3: Stability diagram of damped Mathieu equation (9) with $d = 0$ & 0.5.

towards the right is expected and can be demonstrated by applying the transformation, $y = x e^{-d\,t/2}$ to Eq. (3.1) (with $p(t) = \cos \omega t$). The transformed equation takes the form

$$\ddot{y} + \left(\overline{a} + b \cos \omega t\right) y = 0 \qquad ; \qquad \overline{a} = \left(a - d^2/4\right) \tag{3.4}$$

which is similar to a Mathieu equation (Eq. (3.1) with $p(t) = \cos \omega t$ and $d = 0$) except the constant stiffness parameter, a has been modified to $\overline{a}$. Due to this change, the bifurcation points of the transformed equation have moved to larger values of a on the a axis which explains the movement of unstable regions to the right in the damped system. It should be noted that for a given d the unstable regions of Eq. (3.2) in $a \sim b$ plane lie inside the unstable regions of Eq. (3.4) drawn in $\overline{a} \sim b$ plane [1].

Equation (3.3) can also be used to determine d_{cr}, the critical value of damping at which a cross over between damped and undamped boundaries occurs. In Fig. 3.4, Eq. (3.3) is plotted as a function of d for points B ($a = 0.47$ and $b = 2.5$; see Fig. 1) and C ($a = 1.937$ and $b = 5.0$; see Fig. 3.3). The dual functions $\pm(1 + e^{-Td})$ are represented by the black curves while the gray curves (solid and dashed) represent $Tr\left(\Phi(T, a, b, d)\right)$. Equation (3.2) exhibits stable behavior if the system parameters are such that the $Tr\left(\Phi(T, a, b, d)\right)$ of Eq. (3.2) lies in-between the black curves. The intersections of curves are denoted by d_{cr} and due to the symbolic form of $Tr\left(\Phi(T, a, b, d)\right)$, Eq. (3.3) can be numerically solved for d_{cr} if a and b are given. For instance, $d_{cr} = 0.22315$ & 1.18059 for point B and destabilization occurs if d lies between these critical values as shown in Fig. 3.4.

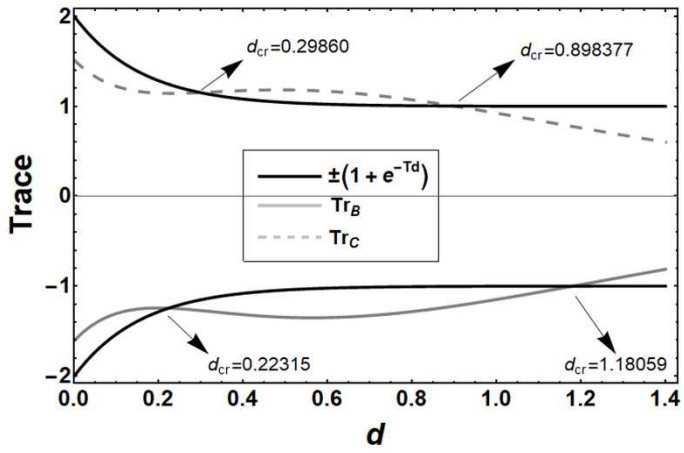

Figure 3.4: Critical values of damping for points B and C.

3.2.2 Meissner Equation

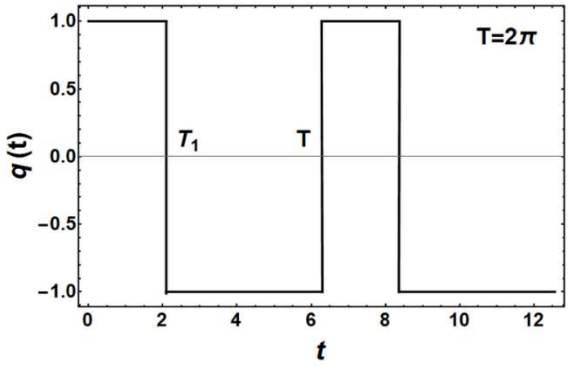

Figure 3.5: Unit rectangular waveform coefficient in the damped Meissner equation.

Meissner equation is a time-periodic parametrically excited system with a rectangular waveform coefficient. An example of such a waveform is shown in Fig. 3.5 where T_1 is the length of the positive segment. For $T_1 \neq 0.5\,T$, the average value of $q(t) \neq 0$; however, $q(t)$ can always be normalized to have a zero average. Then, Eq. (3.1) takes the following form

$$\ddot{x} + d\dot{x} + \big(a + b\,p(t)\big)x = 0 \quad ; \quad p(t) = \begin{cases} +2\left(1 - T_1/T\right) & 0 \le t < T_1 \\ -2\,T_1/T & T_1 \le t < T \end{cases} \quad \text{and} \quad \int_0^T p(t) = 0 \quad (3.5)$$

Since $p(t)$ is piecewise constant, Eq. (3.5) can be viewed as a system of equations with constant coefficients whose exact STM can be computed in terms of trigonometric/hyperbolic functions. For positive coefficients, an exact expression for STM is obtained and the FTM may be written as

$$\Phi(T,a,b,d)=\begin{bmatrix} y_{11}e^{-0.5Td} & y_{12}e^{-0.5Td} \\ y_{21}e^{-0.5Td}-0.5dy_{11}e^{-0.5Td} & y_{22}e^{-0.5Td}-0.5dy_{12}e^{-0.5Td} \end{bmatrix} \tag{3.6}$$

where,

$$y_{11}=\left[\cos\alpha T_1\cos\beta(T-T_1)-(\alpha/\beta)\sin\alpha T_1\sin\beta(T-T_1)\right]+ 0.5d\left[(1/\alpha)\sin\alpha T_1\cos\beta(T-T_1)+(1/\beta)\cos\alpha T_1\sin\beta(T-T_1)\right]$$

$$y_{12}=\left[(1/\alpha)\sin\alpha T_1\cos\beta(T-T_1)+(1/\beta)\cos\alpha T_1\sin\beta(T-T_1)\right]$$

$$y_{21}=\left[-\alpha\sin\alpha T_1\cos\beta(T-T_1)-\beta\cos\alpha T_1\sin\beta(T-T_1)\right]+ 0.5d\left[\cos\alpha T_1\cos\beta(T-T_1)-(\beta/\alpha)\sin\alpha T_1\sin\beta(T-T_1)\right]$$

$$y_{22}=\left[\cos\alpha T_1\cos\beta(T-T_1)-(\beta/\alpha)\sin\alpha T_1\sin\beta(T-T_1)\right]$$

$\alpha=\sqrt{a+2b\left(1-T_1/T\right)}$ and $\beta=\sqrt{a-2bT_1/T}$

Since the stability of the Meissner equation depends on T_1 (*c.f.* Eq. (3.6)), stability diagrams are constructed using Eqs. (3.3) and (3.6) for two typical values of 'c' as shown in Fig. 3.6 where, $T_1=cT$, $T=2\pi$ and $0<c<1$. From these figures, it can be observed that symmetry of the stability diagram about the a axis is affected by T_1. The diagram is symmetric if stability condition (see Eq. (3.3)) is not affected by the substitution $b=-b$ (for example, in the case of $c=0.5$). It should also be noted that instability boundaries in Fig. 3.6 intersect to form closed sub-regions known as '*Instability pockets*' or '*Instability loops*' and their location and number in the parametric space are affected by the parameter T_1 (see Fig. 3.6 and Ref. [45]).

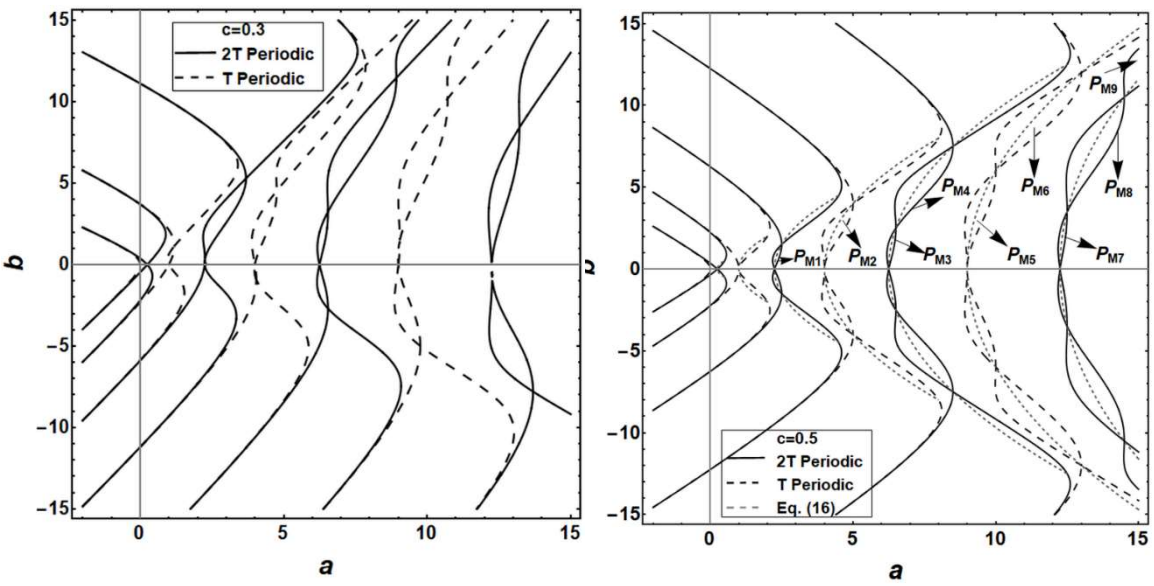

(i) (ii)

Figure 3.6: Stability diagrams of Meissner equation for $c = 0.3$ and 0.5.

3.2.2.1 Analysis of Instability pockets

At the intersections of stability boundaries, two linearly independent solutions of period T or $2T$ coexist and thus named as *coexistence points* [80]. For example, in Fig. 3.6(ii) the T periodic unstable region that arises from a=4 (on the a axis) has two instability pockets whose coexistence points are a=4 & b = 0 , a=5 & b = 4 and a=5 & b = -4. Since solutions are linearly independent and Floquet multipliers are +1 (T periodic) or -1 ($2T$ periodic) on stability boundaries, *i.e.*, $\Phi(T,\lambda)=+I$ or $-I$, respectively, at these points. Therefore, at these points, the off-diagonal elements of symbolic $\Phi(T,\lambda)$ can be set to zero to obtain a pair of nonlinear algebraic equations containing system's parameters. These equations can be simultaneously solved using numerical techniques to produce coexistence points. For the case of undamped Meissner equation $\Phi_{12}(T)$, $\Phi_{21}(T)$ and d are set to zero in Eq. (3.6) to yield

$$\Phi_{12}(T,a,b,0)=\left[(1/\alpha)\sin\alpha T_1\cos\beta(T-T_1)+(1/\beta)\cos\alpha T_1\sin\beta(T-T_1)\right]=0$$
$$\Phi_{21}(T,a,b,0)=\left[-\alpha\sin\alpha T_1\cos\beta(T-T_1)-\beta\cos\alpha T_1\sin\beta(T-T_1)\right]=0 \quad (3.7)$$

In this case, the expressions for $\Phi_{12}(T,a,b,0)$ and $\Phi_{21}(T,a,b,0)$ are simple and can be simultaneously solved to derive the following algebraic relation.

$$\left(k^4/16\right)+\left(X^2-Y^2\right)^2-\left(k^2/2\right)\left(X^2+Y^2\right)=0 \quad ; \quad k, \text{ an integer.} \quad (3.8)$$

where, $X^2=\left[a+2b(1-c)\right]c^2$, $Y^2=\left[a-2bc\right](1-c)^2$ and $k\,(\geq 1)$ is the k^{th} unstable region. The curve traced by Eq. (3.8) passes through all coexistence points. For the special case of square wave coefficient, $c=0.5$, and Eq. (3.8) reduces to the following simpler form

$$ak^2=b^2+k^4/4 \quad (3.9)$$

The above equation is drawn in Fig. 3.6(ii) for $k=1$ to 7 and it can be observed that it passes through all coexistence points. Franco and Collado [46] used a concept of maximum growth rate of solution and developed an approximate analytical expression for maximum energy lines in unstable regions of Meissner equation. First, they set $\partial Tr\left(\Phi(T,a,b,0)\right)/\partial a=0$ and using the assumption $\alpha/\beta+\beta/\alpha\approx 2$ they derived the expression $ak^2\approx b^2+k^4/4$ for the maximum energy lines that pass-through coexistence points. However, using α and β from Eq. (3.6), it can easily be checked that $\alpha/\beta+\beta/\alpha=2$ is only true when $b=0$! Further, it can be easily shown that $\partial Tr\left(\Phi(T,a,b,0)\right)/\partial a=0$ and Eq. (3.9) represent two different curves in the parametric space. Coexistence points in parametric space can be located by substituting Eq. (3.9) in $Tr\left(\Phi(T,a,b,0)\right)=\pm 2$ (Eq. 3.3 with $d=0$). The substitution leads to the following values of b.

$$b = 0 \quad \text{and} \quad b = \pm\frac{km}{2} \quad (b \neq 0) \quad \begin{cases} m < k \text{ and } \begin{matrix} m = 1,3,...,k-2 & \text{if k is odd} \\ m = 2,4,...,k-2 & \text{if k is even} \end{matrix} \end{cases} \tag{3.10}$$

Once b is known a can be calculated using Eq. (3.9). Table 3.1 shows the location of coexistence points in the stability diagram of Meissner equation ($c = 0.5$). The total number of coexistence points depends upon the parameter 'k' and the number of pockets in the k^{th} unstable region of Meissner equation with a square wave coefficient can be calculated by using the following expression.

$$\text{Number of instability pockets} = \begin{cases} k-1 & \text{if } k \text{ is odd} \\ k-2 & \text{if } k \text{ is even} \end{cases} \tag{3.11}$$

The same expression has also been computed by Gan and Zhang [45] using the rotation number approach. Equations (3.9) - (3.11) can be useful as the number of instability pockets and their locations in the parametric space can be determined a priori without plotting the stability diagram. For the general case of rectangular waveform ($c \neq 0.5$), an

Table 3.1: Location of coexistence points in the stability diagram of Meissner equation ($c = 0.5$).

k	System parameters	Location of coexistence points in parametric space					
		$b = 0$	$b \neq 0$				
			$m = 1$	$m = 2$	$m = 3$	$m = 4$	$m = 5$
1	b	0	-	-	-	-	-
	a	0.25	-	-	-	-	-
2	b	0	-	-	-	-	-
	a	1.0	-	-	-	-	-
3	b	0	± 1.5	-	-	-	-
	a	2.25	2.5	-	-	-	-
4	b	0	-	± 4	-	-	-
	a	4.0	-	5	-	-	-
5	b	0	± 2.5	-	± 7.5	-	-
	a	6.25	6.5	-	8.5	-	-
6	b	0	-	± 6	-	± 12	-
	a	9	-	10	-	13	-
7	b	0	± 3.5	-	± 10.5	-	± 17.5
	a	12.25	12.5	-	14.5	-	18.5

algebraic relation for the coexistence of solutions is not as simple and, in these situations, $Tr\left(\Phi(T,a,b,0)\right)=\pm 2$ and Eq. (3.8) can be simultaneously solved using numerical techniques to obtain the coexistence points.

3.2.2.2 Influence of damping

In this section, the influence of damping on instability pockets and stability diagram, in general, is investigated. Figure 3.7 shows the effect of damping on the instability pockets of Meissner equation with a square wave coefficient. It is observed that with an increase in damping the 'instability pockets' start turning into 'instability islands'. An instability pocket does disappear if a certain minimum amount of damping is added to the system. In time-periodic systems the growth rate of a solution depends on Floquet multipliers (or characteristic exponents) which in turn depend on damping 'd' and the trace of FTM. Since the trace of FTM is known in terms of system parameters, an expression relating the trace of FTM and damping coefficient 'd' is established in order to determine the minimum amount of damping required for an instability pocket to vanish.

Applying the transformation $y = x e^{-d\,t/2}$ to Eq. (3.5) yields an equation similar to Eq. (3.4) that has solutions of the form

$$y_n(t) = \Psi_n(t) e^{\frac{t}{T}\ln\rho_n} \qquad n = 1,2 \tag{3.12}$$

where, $\Psi_n(t) = \Psi_n(t+T)$ and ρ_n is the n^{th} Floquet multiplier. Then, the solution of Eq. (3.4) is given by

$$x_n(t) = \mathrm{X}_n(t) e^{\left(\frac{1}{T}\ln|\rho_n| - \frac{d}{2}\right)t} \quad ; \quad \mathrm{X}_n(t) = \Psi_n(t) e^{i\frac{t}{T}\arg\rho_n} \tag{3.13}$$

The solution $x_n(t)$ is bounded if $d/2 \geq (1/T)\ln|\rho_n|$ and can be rewritten in terms of $Tr\left(\Phi(T,a,b)\right)$ as

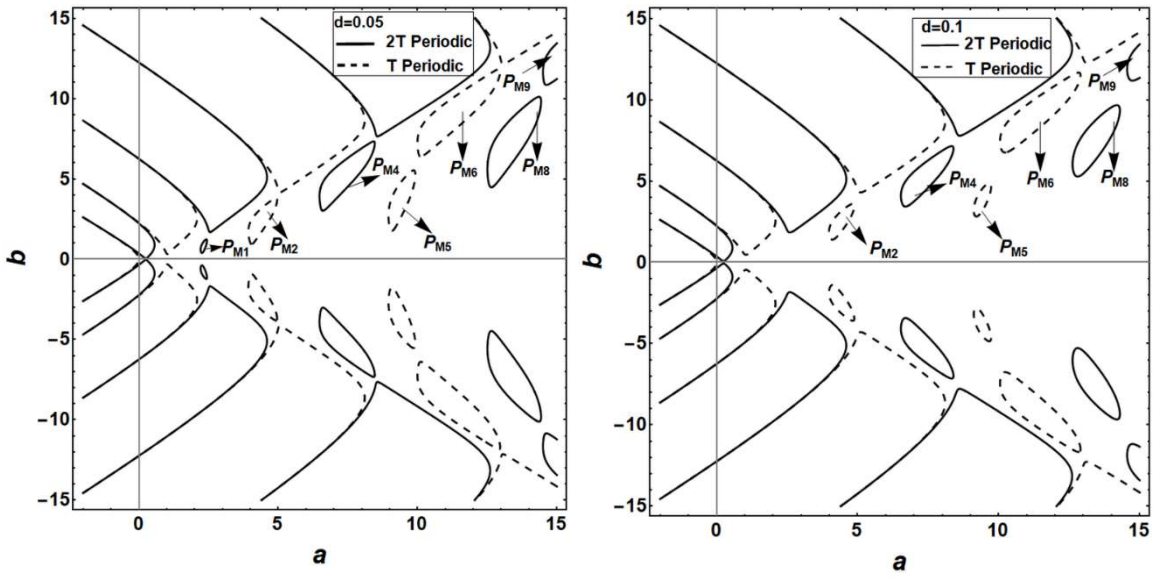

(i)

(ii)

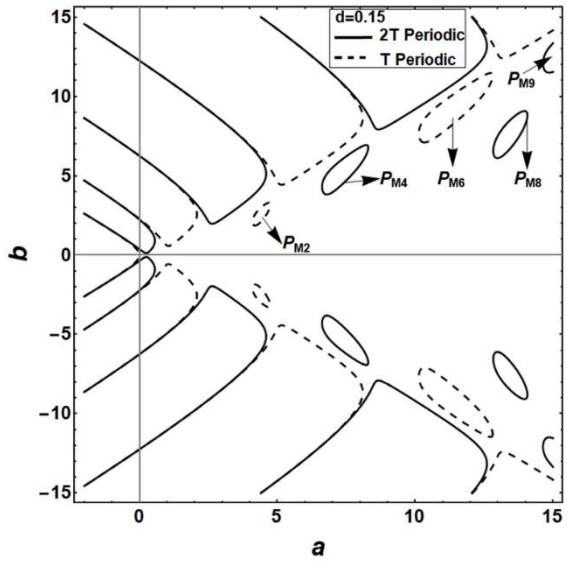

(iii)

Figure 3.7: Effect of damping on instability pockets of Meissner equation with a square wave coefficient.

$$\cosh\frac{dT}{2} \geq \frac{1}{2}\left|Tr\left(\Phi(T,a,b)\right)\right| \tag{3.14}$$

which is a transcendental inequality.

Due to the analytical form of $Tr\left(\Phi(T,a,b,0)\right)$, it's maximum/ minimum value can be easily calculated using 'Maximize' / 'Minimize' command available in MATHEMATICA

software. Once the maximum/ minimum value of $Tr\left(\Phi(T,a,b,0)\right)$ inside a pocket is known, Inequality (3.14) can be numerically solved to determine the minimum damping required for the pocket to vanish. For instance, in instability pocket P_{M5} the maximum value of $\left|Tr\left(\Phi(T,a,b,0)\right)\right| = 2.15649$ and it corresponds to $a = 9.41577$ and $b = 3.90382$. Using this value of the $\left|Tr\left(\Phi(T,a,b,0)\right)\right|$ in Inequality (3.14), a numerical solution yields $d = 0.125114$. Figure 3.8 shows the stability diagram of damped Meissner equation for $d = 0.125114$ and clearly the instability pocket P_{M5} (as seen Fig. 3.6(ii)) has disappeared. Even if the damping is reduced by a very small amount, say $d = 0.125113$, a small unstable region corresponding to the pocket P_{M5} reappears in the parametric space (see Fig. 3.8(ii)). For other instability pockets, minimum damping can be calculated in a similar manner and are tabulated in Table 3.2.

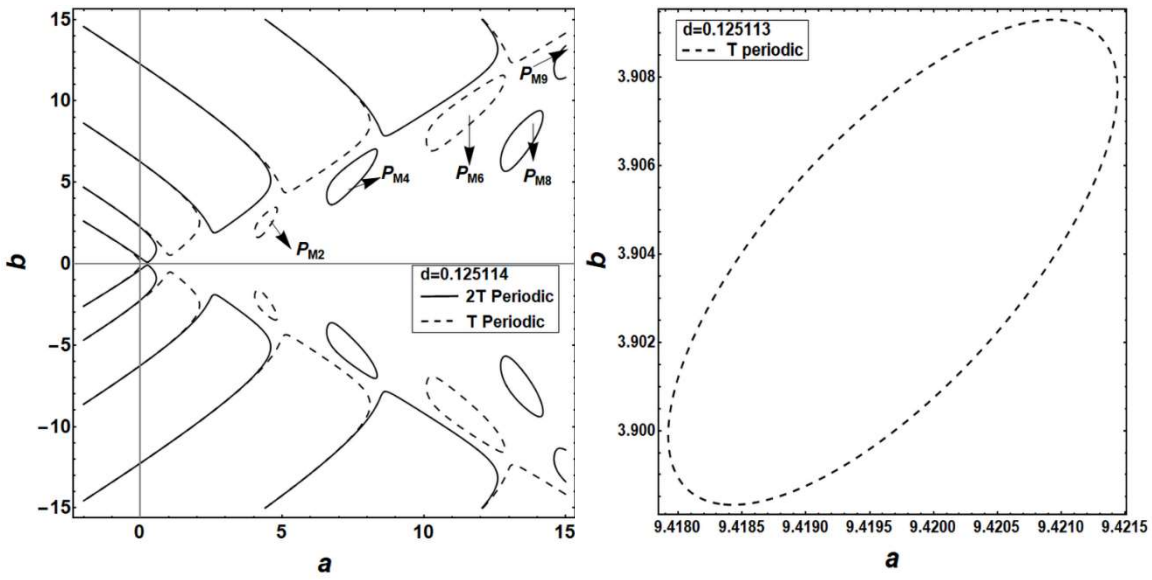

(i) (ii)

Figure 3.8: Effect of damping on instability pocket P_{M5}.

Table 3.2: Minimum damping required for instability pockets to vanish from the stability diagram of Meissner equation with a square wave coefficient (shown in Fig. 3.6(ii)).

Entry No.	Instability pocket	Maximum $\left\|Tr\left(\Phi(T,a,b,0)\right)\right\|$	a corresponding to maximum $\left\|Tr\left(\Phi(T,a,b,0)\right)\right\|$	b corresponding to maximum $\left\|Tr\left(\Phi(T,a,b,0)\right)\right\|$	Minimum damping coefficient (Inequality (3.14))
1	P_{M1}	2.05873	2.32394	0.831455	0.076953
2	P_{M2}	2.37641	4.41411	2.62657	0.192350
3	P_{M3}	2.02067	6.32462	1.37524	0.045720
4	P_{M4}	2.87334	7.43608	5.52681	0.287587
5	P_{M5}	2.15649	9.41577	3.90382	0.125114
6	P_{M6}	3.44933	11.4433	9.48040	0.363184
7	P_{M7}	2.01048	12.3248	1.92124	0.032573
8	P_{M8}	2.39691	13.4376	7.68648	0.197361
9	P_{M9}	4.06340	16.4465	14.4561	0.424966

The phenomenon of destabilization due to damping found in Mathieu equation (see Sec. 3.2.1) is also observed in Meissner equation. Figure 3.9 shows the destabilizing effect of damping in Meissner equation ($c = 0.5$).

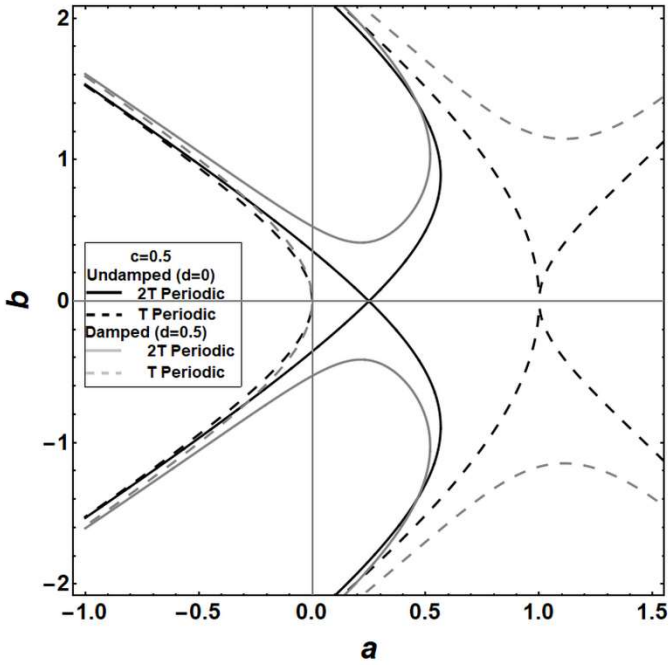

Figure 3.9: Destabilizing effect of damping in Meissner equation ($c = 0.5$).

3.2.3 Three-Frequency Hill Equation

In this section, the following form of damped Hill equation is studied.

$$\ddot{x} + d\,\dot{x} + \left(a + b\left(\cos t + \delta\cos 2t + \delta\cos 3t\right)\right)x = 0 \tag{3.15}$$

Equation (3.15) is similar to Eq. (3.1) with $p(t) = \cos t + \delta\cos 2t + \delta\cos 3t$ and for convenience, the coefficients of $\cos 2t$ and $\cos 3t$ are assumed to be identical and represented by δ .

The symbolic technique described in Sec. 2.5 was employed to compute the FTM of Eq. (3.15) in terms of system parameters a, b, d and δ using 40 Chebyshev polynomials and 58 Picard iterations. Utilizing the symbolic FTM and Eq. (3.3), a stability chart was plotted in the $a \sim b$ plane for $d = 0$ and $\delta = 1$ as shown in Fig. 3.10 and it is observed that this diagram is asymmetrical about the a axis. Instability pockets observed in the case of Meissner equation are also observed in the unstable regions R1 and R2. Once again, the coexistence points for these unstable regions can be calculated by setting the off-diagonal terms of the symbolic FTM to zero (see Sec. 3.2.2.1). The resulting nonlinear algebraic equations are simultaneously solved using numerical techniques to determine the coordinates $\left(\hat{a}, \hat{b}\right)$ of coexistence points. It is found that $\{(1,0),(1.71522, 2.93723)\}$ and $\{(2.25,0),(2.57748, 2.43895)\}$ are the coexistence points in regions R1 and R2, respectively.

Figure 3.11 shows the stability diagrams for two typical values of $\delta = 0.53$ and $\delta = 0.6$. A comparison of Fig. 3.10 with Fig. 3.11 reveals that the number of instability pockets in region R1 remains unchanged for all three values of δ . However, the instability pocket in

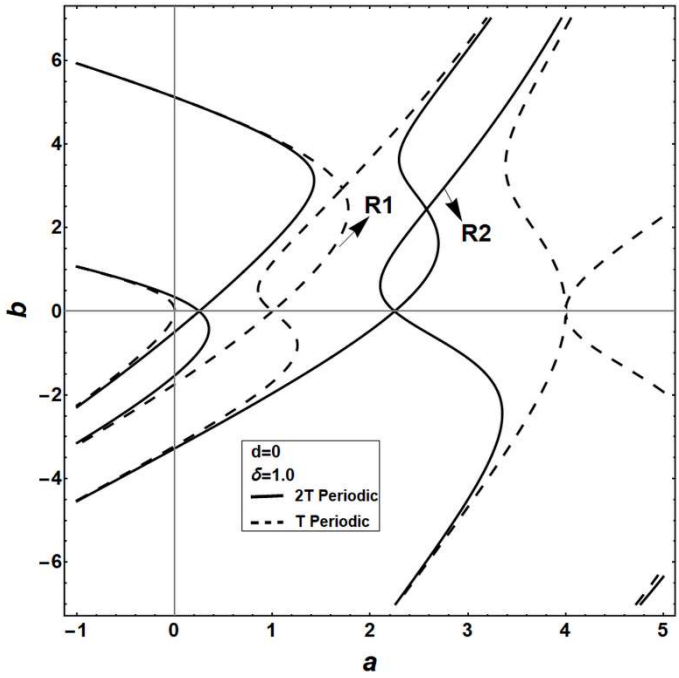

Figure 3.10: Stability diagram of three-frequency Hill equation (3.15) with $\delta = 1$.

region R2 opens up when δ is changed from 1 to 0.53 and another pocket is formed for $\delta = 0.6$ (see Fig. 3.11(ii)). The coexistence points corresponding to region R2 ($\delta = 0.6$) are found to be $(2.25, 0)$, $(2.66909, 2.94640)$ and $(3.69754, 6.2884)$. Using the symbolic form of $Tr\left(\Phi(T, a, b, 0, \delta)\right)$ in Inequality (3.14), the minimum values of damping d were calculated for instability pockets to vanish in Fig. 3.11(ii) which corresponds to $\delta = 0.6$. From the results shown in Table 3.3, it should be noted that $Max\left(\left|Tr\left(\Phi(T, a, b, 0, 0.6)\right)\right|\right)$ of P_{H3} is less than P_{H2} implying that P_{H3} vanishes before P_{H2} which is not true for the Meissner equation. Similar to Mathieu and Meissner's equations, the phenomenon of destabilization due to damping is also observed in three-frequency Hill equation. For the sake of brevity, it is not presented here.

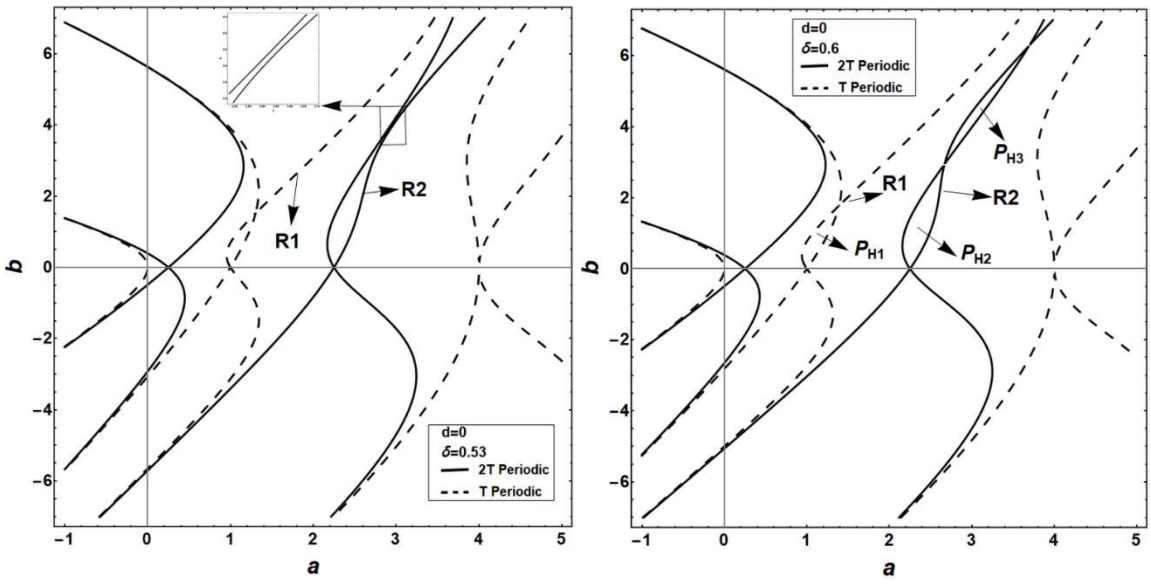

(i) (ii)

Figure 3.11: Stability diagram of three-frequency Hill equation (3.15) with $\delta = 0.53$ and $\delta = 0.6$.

Table 3.3: Minimum damping required for instability pockets to vanish from the stability diagram of three-frequency Hill equation (3.15) with $\delta = 0.6$.

E. No.	Instability pocket	Maximum $\lvert Tr(\Phi(T,a,b,0,0.6))\rvert$	a corresponding to maximum $\lvert Tr(\Phi(T,a,b,0,0.6))\rvert$	b corresponding to maximum $\lvert Tr(\Phi(T,a,b,0,0.6))\rvert$	Minimum damping coefficient (Inequality (3.14))
1	P_{H1}	2.14515	1.10937	0.809069	0.120548
2	P_{H2}	2.11975	2.36155	1.20602	0.109607
3	P_{H3}	2.05820	3.12859	4.60363	0.076608

3.2.4 Quasi-Periodic Hill Equation

One of the simplest forms of damped QP Hill equation can be represented by

$$\ddot{x} + d\,\dot{x} + \left(a + b_1 \cos\omega_1 t + b_2 \cos\omega_2 t\right) x = 0 \tag{3.16}$$

where, ω_1 and ω_2 are the two parametric excitation frequencies such that ω_1/ω_2 is an irrational number. Generally speaking, Floquet theory cannot be applied as the principal period of these systems tends to infinity. Nevertheless, Chapter 2 proposed a general approximate method based on Floquet theory to analyze quasi-periodic systems. In this

method, the quasi-periodic system is replaced by a periodic system with an appropriate large principal period to which Floquet theory can be applied to determine approximate stability and response of the original quasi-periodic system. In the following, one of the case studies is used to explore instability pockets and influence of damping in quasi-periodic systems.

Consider a damped quasi-periodic system with excitation frequencies $\omega_1 = 1.0$ & $\omega_2 = \left(1+\sqrt{5}\right)\big/2$ and thus Eq. (3.16) can be rewritten in the state space form as

$$\dot{x} = \begin{bmatrix} 0 & 1 \\ -\left(a + b_1 \cos t + b_2 \cos\left(1+\sqrt{5}\right)\big/2\right)t & -d \end{bmatrix} x \tag{3.17}$$

In order to determine approximate stability and response, Eq. (3.17) is replaced by the following approximate system (see Chapter 2 for details).

$$\dot{x} = \begin{bmatrix} 0 & 1 \\ -\left(a + b_1 \cos 1.00310580\ t + b_2 \cos 1.61611490\ t\right) & -d \end{bmatrix} x \tag{3.18}$$

Equation (3.18) is periodic with principal period, $T = 112.747$ and it can be analyzed using Floquet theory. For convenience, all computations are performed by setting $b_1 = b_2 = b$ and $d = 0$.

The symbolic technique described in Sec. 2.5 was employed to compute the FTM of Eq. (3.18) using 30 subintervals with 20 Chebyshev terms and 30 Picard iterations in each interval (see Chapter 2 for details). Figure 3.12 shows the stability chart where two instability pockets are identified in unstable regions R1 and R2 for analysis purposes. The coexistence points for unstable regions R1 and R2 are found to be {(0.6529570,0), (0.7284645, 2.3208767)} and {(2.2639978, 0), (2.8279853, 2.6537764)}, respectively (truncated at seven decimals). These coordinates represent approximate locations of

coexistence points of the original quasi-periodic system represented by Eq. (3.17). Since the bottommost coexistence points are the bifurcation points of unstable regions R1 and R2 on the a axis, their exact locations can be computed and are given by (0.6545085,0) and (2.25,0), respectively. At the top coexistence point of R1 ($a = 0.7284645$ and $b = 2.3208767$), the off-diagonal terms of the FTM are zero but, the diagonal terms are not exactly equal to -1. A large variation in FTM for a very small change in system parameters is observed in region R1 and it could be the main source of error in the computation of FTM and the coexistence point. Minimum values of damping required for the pockets in regions R1 and R2 to vanish were computed to be $d = 0.613229$ and 0.0623459, respectively. The phenomenon of destabilization due to damping is also observed in QP Hill equation, however, for conciseness, figure depicting this phenomenon is not shown.

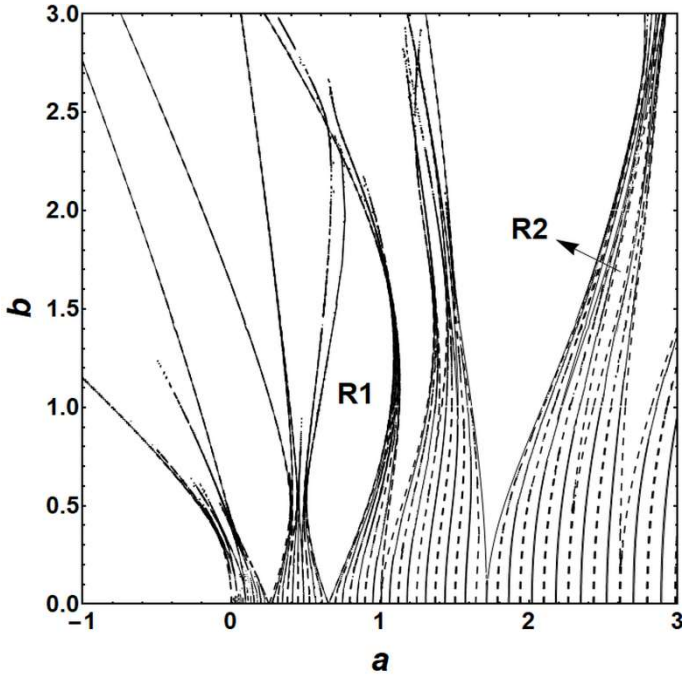

Figure 3.12: Stability diagram of QP Hill equation with $\omega_1 = 1.0$ and $\omega_2 = \left(1+\sqrt{5}\right)/2$. Solid: $2T$ periodic, Dashed: T Periodic

Chapter 4

Control of Nonlinear Systems to Desired Periodic or Quasi-Periodic Motions

4.1 Introduction

A novel method in the design of controllers to drive general nonlinear systems to desired periodic or quasi-periodic motions is presented in this chapter. The viability of the approach is demonstrated by controlling chaotic systems to desired motions. The proposed control system consists of a combination of a nonlinear feedforward controller and a linear feedback controller. The control gains for the feedback controller are determined by performing the stability analysis of the closed-loop systems that contain periodic or quasi-periodic coefficients. For the case of periodic coefficients, stability is determined using the well-known Floquet theory. Since there is no rigorous mathematical theory for the analysis of quasi-periodic systems, the approximate technique proposed in chapter 2 has been applied to determine the stability where the coefficients turned out to be quasi-periodic. In this approach, a quasi-periodic system is replaced by an approximate periodic system with an appropriate large principal period such that Floquet theory can be applied. Stability diagrams are used to select control gains to guarantee asymptotic stability of the feedback systems. Three examples of chaotic systems are studied in order to show applicability to a diverse class of problems. In the first case, the chaotic motion of a forced Duffing oscillator is driven to a two-frequency quasi-periodic square wave and a fixed point. In the control

to a fixed point, the system is constrained to follow a logarithmic spiral trajectory. The second case involves the control of the chaotic attractor of a parametrically forced Lorenz system to a periodic orbit whose frequency is irrationally related to the parametric excitation frequency. In the last case, the chaotic behavior of a Mathieu-Duffing oscillator is successfully driven to a two-frequency quasi-periodic motion.

4.2 Controller Design for Nonlinear Systems Exhibiting Undesirable Behavior

Consider a general nonlinear system,

$$\dot{\mathbf{x}} = \mathbf{f}(\mathbf{x}, t) \tag{4.1}$$

which has a chaotic (or an undesirable) response, $\mathbf{x}(t)$ for a given set of parameter values. Here, $\mathbf{x}$ is a $n \times 1$ state vector, $\mathbf{f}(\bullet)$ is a $n \times 1$ nonlinear vector function and t is the time. With the control law, $\mathbf{u}(t)$ Eq. (4.1) can be rewritten as

$$\dot{\mathbf{x}} = \mathbf{f}(\mathbf{x}, t) + \mathbf{u}(t) \tag{4.2}$$

In order to drive the chaotic response to the desired orbit, $\mathbf{y}(t)$, consider the control law,

$$\mathbf{u}(t) = \mathbf{u}_{\mathbf{f}} + \mathbf{u}_{\mathbf{t}} \tag{4.3}$$

where, $\mathbf{u}_{\mathbf{f}}$ is a nonlinear feedforward control and $\mathbf{u}_{\mathbf{t}}$ is a linear time-varying feedback control. $\mathbf{u}_{\mathbf{f}}$ and $\mathbf{u}_{\mathbf{t}}$ are defined as

$$\mathbf{u}_{\mathbf{f}} = \dot{\mathbf{y}} - \mathbf{f}(\mathbf{y}, t) \quad ; \quad \mathbf{u}_{\mathbf{t}} = \mathbf{K}(t)(\mathbf{x} - \mathbf{y}) \tag{4.4}$$

where, $\mathbf{K}(t)$ is a time-varying state feedback matrix. If the error between the actual (chaotic) and the desired trajectory is defined as $\mathbf{e} = \mathbf{x} - \mathbf{y}$, Eq. (4.2) can be rewritten in the following form using Eq. (4.3).

$$\dot{\mathbf{e}} = \mathbf{g}(\mathbf{e}, t) + \mathbf{u}_{\mathbf{t}} \tag{4.5}$$

It should be noted that the new dynamical system with $\mathbf{e}$ as the state vector and $\mathbf{g}$ as the nonlinear vector function has an equilibrium state at ($\mathbf{e} = \mathbf{0}$, $\mathbf{u}_t = \mathbf{0}$) and this is true regardless $\mathbf{y}(t)$ is a solution of Eq. (4.1). In the case when $\mathbf{y}(t)$ is a solution of Eq. (4.1), the feedforward control, $\mathbf{u}_f = \mathbf{0}$. It is noteworthy that the incorporation of feedforward control has reduced the tracking problem to the stabilization problem.

It is known that under certain conditions a nonlinear system behaves very similarly to its linearized approximation. Let $\mathbf{g}(\mathbf{0},t) = \mathbf{0} \quad \forall\, t \geq 0$ where $\mathbf{g}(\bullet)$ is a C^1 function. A Taylor series expansion of Eq. (4.5) around the equilibrium point ($\mathbf{e} = \mathbf{0}$, $\mathbf{u}_t = \mathbf{0}$) leads to

$$\dot{\mathbf{e}} = \mathbf{A}(t)\mathbf{e} + \mathbf{h}(\mathbf{e},t) + \mathbf{u}_t \tag{4.6}$$

where, $\mathbf{h}(\mathbf{e},t) = \mathbf{g}(\mathbf{e},t) - \mathbf{A}(t)\mathbf{e}$ and $\mathbf{A}(t) = \left[\frac{\partial \mathbf{g}(\mathbf{e},t)}{\partial t}\right]_{\substack{\mathbf{e}=\mathbf{0} \\ \mathbf{u}_t=\mathbf{0}}}$. If the condition,

$$\lim_{\|\mathbf{e}\|\to 0} sup_{t\geq 0}\left\{\frac{\|\mathbf{h}(\mathbf{e},t)\|}{\|\mathbf{e}\|}\right\} = 0 \tag{4.7}$$

is met, the system

$$\dot{\mathbf{e}} = \mathbf{A}(t)\mathbf{e} + \mathbf{u}_t \tag{4.8}$$

is the linearization of Eq. (4.5) around the equilibrium ($\mathbf{e} = \mathbf{0}$, $\mathbf{u}_t = \mathbf{0}$) [81]. Through the selection of an appropriate $\mathbf{u}_t$, the error dynamics, $\mathbf{e}$ in Eq. (4.8) may be driven to zero and the global asymptotic stability of Eq. (4.8) guarantees the local stability of the nonlinear system *i.e.*, Eq. (4.5).

In Eq. (4.8), $\mathbf{A}(t)$ could be a constant or a time-varying matrix and it depends upon the original nonlinear system, Eq. (4.1) and the desired motion, $\mathbf{y}(t)$. For instance, if the

original system is autonomous and $\mathbf{y}(t)$ is a fixed point, $\mathbf{A}(t)$ is a constant matrix. However, in the case when $\mathbf{y}(t)$ is a function of time, $\mathbf{A}(t)$ is a time-varying matrix. In this paper, the investigation is restricted to the cases where $\mathbf{A}(t)$ is a constant, a periodic or a quasi-periodic function of time.

When $\mathbf{A}(t)$ is time-invariant, stability can be easily guaranteed by several well-known methods. If $\mathbf{A}(t)$ is periodic, Floquet theory [9, 72] can be used to predict the stability and response of the system. According to Floquet theory, the stability of periodic systems depends upon the eigenvalues of the Floquet transition matrix (FTM), commonly known as 'Floquet multipliers'. The FTM is the state transition matrix (STM) computed at the end of the principal period. The periodic system is stable if all Floquet multipliers lie on or inside the unit circle, otherwise it is unstable. Unlike time-periodic systems, there is no complete mathematical theory for the analysis of linear ordinary differential equations with quasi-periodic coefficients (quasi-periodic systems). Floquet theory cannot be directly applied to quasi-periodic systems as their principal period tends to infinity. However, the approximate approach proposed in Chapter 2 can be employed to analyze quasi-periodic systems. In this approach, the quasi-periodic system is replaced by an approximate periodic system with an appropriate large principal period to which Floquet theory can be applied to determine approximate stability and response of the quasi-periodic system.

4.3 Applications to Chaotic Systems

In the following, the effectiveness of the control strategy is demonstrated by investigating three typical chaotic systems. In these examples, the chaotic systems and the desired motions are selected such that each example represents a distinct class of problems. In the

first example, chaos in a forced Duffing oscillator is controlled to a two-frequency quasi-periodic square wave with frequencies, $\omega_1 = 1$ and $\omega_2 = \left(1+\sqrt{5}\right)/2$. Linearization of the feedforward controlled system around the desired square wave yields a quasi-periodic system with ω_1 and ω_2 in its frequency basis. The chaotic attractor of forced Duffing oscillator is also driven to a fixed point through a logarithmic spiral trajectory. In this case, a time-varying equation is obtained after linearization. The second example concerns a parametrically forced Lorenz system that is used to model convective cooling for heat removal in various engineering systems [82]. The chaotic behavior of the system is driven to a periodic orbit whose frequency, $\omega_2 = \pi\left(1+\sqrt{5}\right)$ is irrationally related to the parametric excitation frequency, $\omega_1 = 2\pi$. Due to the incommensurate ratio between these frequencies, the linearization around the desired periodic orbit leads to a two-frequency quasi-periodic system. Sinha *et al.* [71] also studied the control of chaos in parametrically forced Lorenz system to a periodic orbit. However, in their investigation frequencies were commensurate ($\omega_1 = \omega_2 = 2\pi$). In the last example, a Mathieu-Duffing oscillator is successfully driven to a two-frequency quasi-periodic motion. Frequencies of the quasi-periodic motion, $\omega_2 = \sqrt{2}$ and $\omega_3 = \sqrt{7}$ are irrationally related to the parametric excitation frequency, $\omega_1 = 2$ of the Mathieu-Duffing equation. Contrary to other two examples, linearization of the feedforward controlled system around the quasi-periodic motion resulted in a three-frequency quasi-periodic system whose frequency basis consists of ω_1, $\left(\omega_3 - \omega_2\right)$ and $\left(\omega_2 + \omega_3\right)$.

4.3.1 Forced Duffing Oscillator: Control to a quasi-periodic square wave & a fixed point

A forced Duffing oscillator with linear damping is described by the equation

$$\ddot{x} + \xi\dot{x} + \alpha x + \beta x^3 = F\sin\omega t \tag{4.9}$$

where, ξ is the viscous damping coefficient, α is the stiffness parameter, β is the coefficient of nonlinear restoring force, F and ω are the amplitude and the frequency of the external input. For $\alpha = -1$, $\beta = 1$, $\xi = 0.4$, $F = 0.4$ and $\omega = 1$, Eq. (4.9) possesses a chaotic attractor as shown in Fig. 4.1.

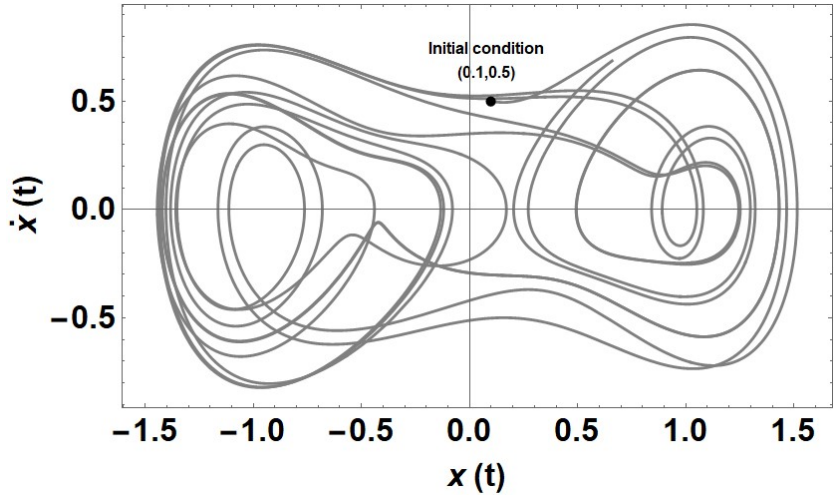

Fig. 4.1: Chaotic behavior of the uncontrolled forced Duffing oscillator in the phase plane.

4.3.1A Control to a quasi-periodic square wave

In order to control the chaotic response, the system is subject to the control $u(t)$ and is represented by

$$\ddot{x} + 0.4\dot{x} - x + x^3 = 0.4\sin t + u(t) \tag{4.10}$$

where, $u(t)$ is defined by Eq. (4.3). Let the desired motion be a quasi-periodic square wave, $y(t) = 0.1 + 0.25\,sgn[\cos\omega_1 t + 0.8\cos\omega_2 t]$ where, $\omega_1 = 1$ and $\omega_2 = \left(1+\sqrt{5}\right)/2$ as shown in Fig. 4.2. Here, $sgn[p(t)] = 1$ for $p(t) \geq 0$ and $sgn[p(t)] = -1$ for $p(t) < 0$.

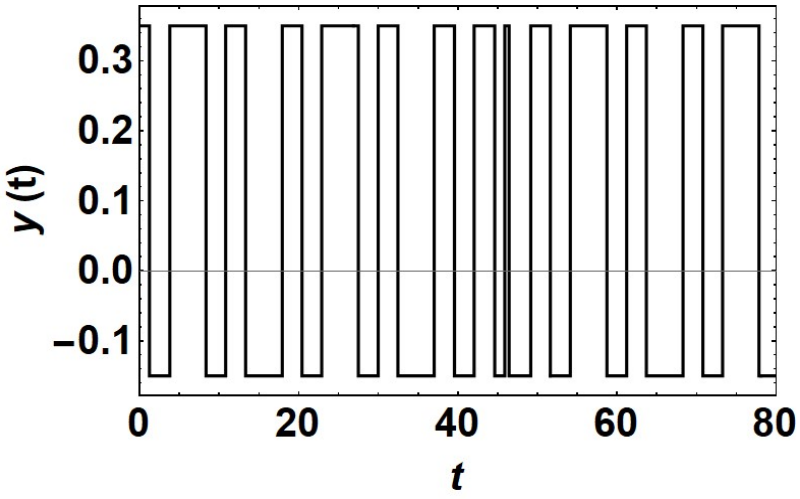

Fig. 4.2: Quasi-periodic square wave, $y(t)=0.1+0.25sgn\left[\cos\omega_1 t+0.8\cos\omega_2 t\right]$ where $\omega_1=1$ and $\omega_2=\left(1+\sqrt{5}\right)/2$.

Using Eq. (4.4), the feedforward control can be written as

$$u_f = \ddot{y} + 0.4\dot{y} - y + y^3 - 0.4\sin t \tag{4.11}$$

Defining $e=x-y$, the linearized equation of the feedforward controlled system is given by

$$\ddot{e} + 0.25\dot{e} + \left(3y^2 - 1\right)e = u_t \tag{4.12}$$

where,

$$y^2 = 0.01 + 0.0625sgn\left[0.82 + 0.5\cos 2\omega_1 t + 0.32\cos 2\omega_2 t + 0.8\cos\left(\omega_1+\omega_2\right)t + 0.8\cos\left(\omega_1-\omega_2\right)t\right] + 0.05sgn\left[\cos\omega_1 t + 0.8\cos\omega_2 t\right]$$

and $u_t = -k_1 e - k_2\dot{e}$; k_1 and k_2 being the unknown control gains. The damping term may be removed by applying the change of variable, $e = z\mathrm{Exp}\left[-\left(0.4+k_2\right)t\right]$ to yield

$$\ddot{z} + \left(a - 0.25d^2 + 3y^2\right)z = 0 \tag{4.13}$$

where, $a = k_1 - 1$ and $d = 0.4 + k_2$.

Table 4.1: Minimum frequencies ($\omega_{\min}$) with their corresponding periods (T_a) and the frequencies of the approximate system (periodic system).

Entry Number (E. No.)	Range of j_1, j_2 values	$\omega_{\min}$ ($\omega_{\min} \neq 0$)	$T_a = 2\pi/\omega_{\min}$	$\bar{\omega}_1$	$\bar{\omega}_2$
Col. 1	Col. 2	Col. 3	Col. 4	Col. 5	Col. 6
1	0 to 1	0.618034	10.1664	1.23606800	1.85410200
2	0 to 2	0.381966	16.4496	1.14589800	1.52786400
3	0 to 4	0.236068	26.616	0.94427200	1.65247600
4	0 to 7	0.145898	43.0656	1.02128600	1.60487800
5	0 to 12	0.0901699	69.6816	0.99186890	1.62305820
6	0 to 20	0.0557281	112.747	1.00310580	1.61611490
7	0 to 33	0.0344419	182.429	0.99881510	1.61876930
8	0 to 54	0.0212862	295.176	1.00045140	1.61775120

In Eq. (4.13), the frequency basis of the coefficient consists of incommensurate frequencies, $\omega_1 = 1$ and $\omega_2 = \left(1+\sqrt{5}\right)\big/2$. Thus, the approximate approach presented in Chapter 2 is utilized to analyze the stability of Eq. (4.13) such that k_1 and k_2 can be determined. As a first step, minimum frequencies ($\omega_{\min}$) and their corresponding approximate principal periods (T_a) are calculated over the range of j_1 & j_2 and are listed in Table 4.1. In order to construct the approximate system (periodic system) , the frequencies, $\omega_1 = 1$ and $\omega_2 = \left(1+\sqrt{5}\right)\big/2$ in Eq. (4.13) are replaced with $\bar{\omega}_1$ and $\bar{\omega}_2$, respectively, which are integral multiples of $\omega_{\min}$. Cols. 5 and 6 in Table 4.1 show $\bar{\omega}_1$ and $\bar{\omega}_2$ for various $\omega_{\min}$. For example, when $\omega_{\min} = 0.145898$ (E. No. 4 in Table 4.1), $\omega_1/\omega_{\min} = 6.85410$ and $\omega_2/\omega_{\min} = 11.0902$. The nearest integers are 7 & 11 and hence, $\bar{\omega}_1 = 7\omega_{\min} = 1.021286$ and $\bar{\omega}_2 = 11\omega_{\min} = 1.604878$. There are two main instability regions for Eq. (4.13). These two instability regions correspond to frequencies ω_1 & ω_2 and originate from the bifurcation points $\bar{a} = \omega_1^2/4$ & $\bar{a} = \omega_2^2/4$, respectively where, $\bar{a} = a - 0.25d^2 + 0.03$. It should be noted that in a periodic system with excitation

frequency, ω_1 or ω_2 the main instability region also arise from the same bifurcation point, $\bar{a} = \omega_1^2/4$ or $\bar{a} = \omega_2^2/4$. Since the main instability regions in quasi-periodic and periodic systems arise from same bifurcation points, the minimum frequency can be selected by performing the convergence study for these bifurcation points. Figure 4.3 depicts the convergence of bifurcation points of main instability regions as T_a increases (or $\omega_{\min}$ decreases). The $y-$axis represents the difference between exact, $\left(\bar{a}_e = \omega_1^2/4 \; and \; \omega_2^2/4\right)$ and approximate $\left(\bar{a}_a = \bar{\omega}_1^2/4 \text{ and } \bar{\omega}_2^2/4\right)$ bifurcation points, $\left(\bar{a}_e - \bar{a}_a\right)$ while the $x-$axis is denoted by the expression, $\log_{10}\left(T_a/T_a^1\right)$ where, T_a^1 is the smallest T_a in Table 4.1 *i.e.*, 10.1664. From Fig. 4.3 it can be observed that as T_a increases or $\omega_{\min}$ decreases, the difference between the bifurcation points converges to zero. Larger T_a increases the computation time and therefore, as a compromise, $\omega_{\min} = 0.0557281$ is selected for further investigation.

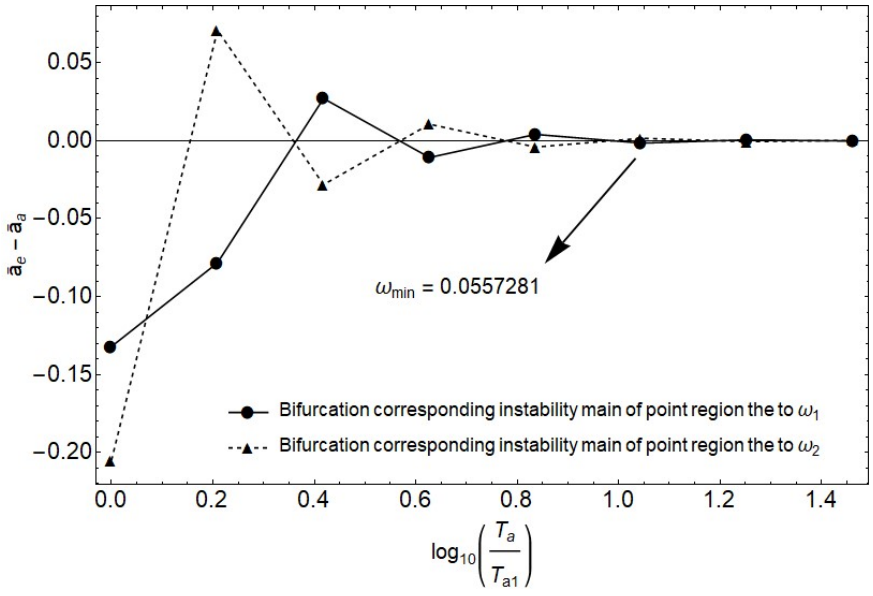

Fig. 4.3: Convergence diagram of bifurcation points of main instability regions of linearized error equation (4.13).

For $\omega_{\min} = 0.0557281$, the approximate system is defined by replacing the frequencies $\omega_1 = 1$ and $\omega_2 = \left(1+\sqrt{5}\right)\big/2$ with $\bar{\omega}_1 = 1.00310580$ and $\bar{\omega}_2 = 1.61611490$, respectively. Then, Eq. (4.13) reduces to the form

$$\ddot{z} + \left(a - 0.25d^2 + 3\tilde{y}^2\right)z = 0 \tag{4.14}$$

where, $\tilde{y}(t) = 0.1 + 0.25 sgn\left[\left(\cos 1.00310580t + 0.8\cos 1.61611490t\right)\right]$. Equation (4.14) is a periodic system with the principal period, $T_a = 112.747$ and hence, it can be analyzed using Floquet theory. From the form of $\tilde{y}^2(t)$ over the principal period, T_a, it is evident that Eq. (4.14) can be viewed as a set of ordinary differential equations with constant coefficients for which solutions can be expressed in terms of trigonometric or hyperbolic functions. An exact expression for the FTM of Eq. (4.14) in the original domain (e) is given by

$$\mathbf{\Phi}\left(T_a, k_1, k_2\right) = e^{-0.5dT_a}\begin{bmatrix} \bar{\phi}_{11} + 0.5d\bar{\phi}_{12} & \bar{\phi}_{12} \\ \bar{\phi}_{21} + 0.5d\bar{\phi}_{22} - 0.5d\left(\bar{\phi}_{11} + 0.5d\bar{\phi}_{12}\right) & \bar{\phi}_{22} - 0.5d\bar{\phi}_{12} \end{bmatrix} \tag{4.15}$$

where, $\begin{bmatrix} \bar{\phi}_{11} & \bar{\phi}_{12} \\ \bar{\phi}_{21} & \bar{\phi}_{22} \end{bmatrix} = \bar{\mathbf{\Phi}}\left(T_a, 0\right) = \prod_{s=1}^{N} \bar{\mathbf{\Phi}}\left(t_{N+1-s}, t_{N-s}\right)$. For positive coefficients of Eq. (4.14),

$$\bar{\mathbf{\Phi}}\left(t_{N+1-s}, t_{N-s}\right) = \begin{bmatrix} \cos\psi\left(t_{N+1-s} - t_{N-s}\right) & \left(1/\psi\right)\sin\psi\left(t_{N+1-s} - t_{N-s}\right) \\ -\psi\sin\psi\left(t_{N+1-s} - t_{N-s}\right) & \cos\psi\left(t_{N+1-s} - t_{N-s}\right) \end{bmatrix} \tag{4.16}$$

In the case of negative coefficients, trigonometric functions in Eq. (4.16) are replaced by hyperbolic functions. If $\cos\bar{\omega}_1 t + 0.8\cos\bar{\omega}_2 t \geq 0$, then $\psi = \alpha$. Otherwise, $\psi = \beta$. Here, $\alpha = \sqrt{a - 0.25d^2 + 0.3675}$, $\beta = \sqrt{a - 0.25d^2 + 0.0675}$, and $N = 41$ represents the total number of steps created due to the form of $\tilde{y}(t)$ over the principal period, T_a. N depends

upon the $\omega_{\min}$ and its value increases as $\omega_{\min}$ decreases. Once the FTM is known in terms of control gains k_1 and k_2, approximate stability diagram can be plotted for Eq. (4.12) using $Tr\left[\mathbf{\Phi}\left(T_a, k_1, k_2\right)\right] = \pm\left(1 + e^{-(0.4+k_2)T_a}\right)$ as shown in Fig. 4.4. For a typical set of k_1 and k_2 selected from the stable region, $e \to 0$ as $t \to \infty$ and therefore, $x \to y$. With $k_1 = 0.95$ and $k_2 = -0.1$, the chaos in Eq. (4.10) is controlled to the quasi-periodic square wave $y(t)$ as shown in Fig. 4.5.

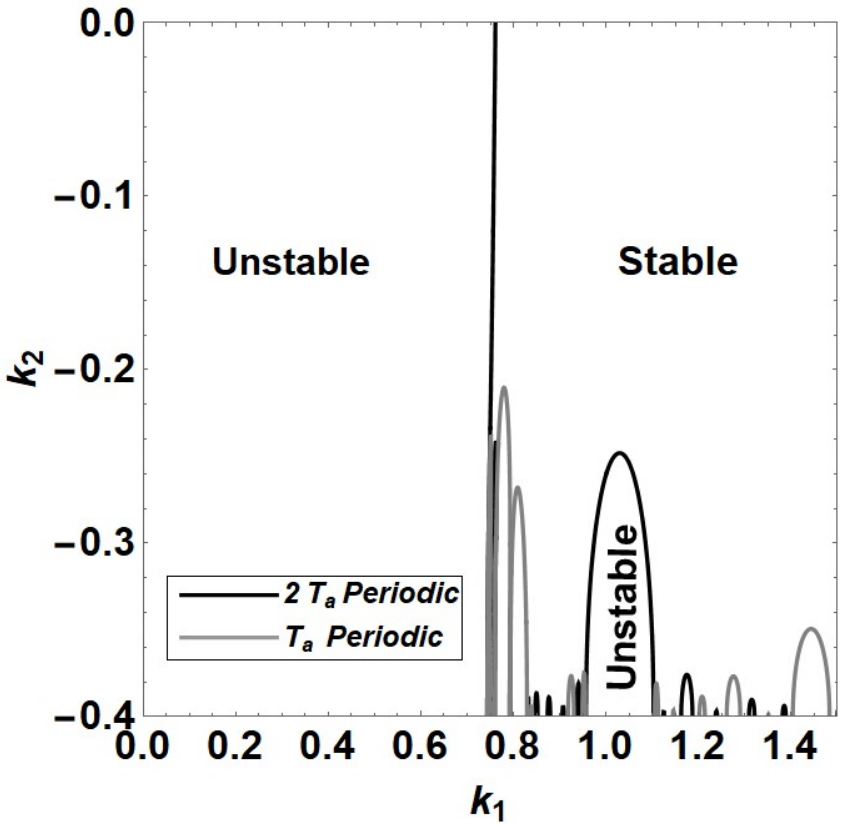

Fig. 4.4: Approximate stability diagram of linearized error equation (4.12) in $k_1 \sim k_2$ plane.

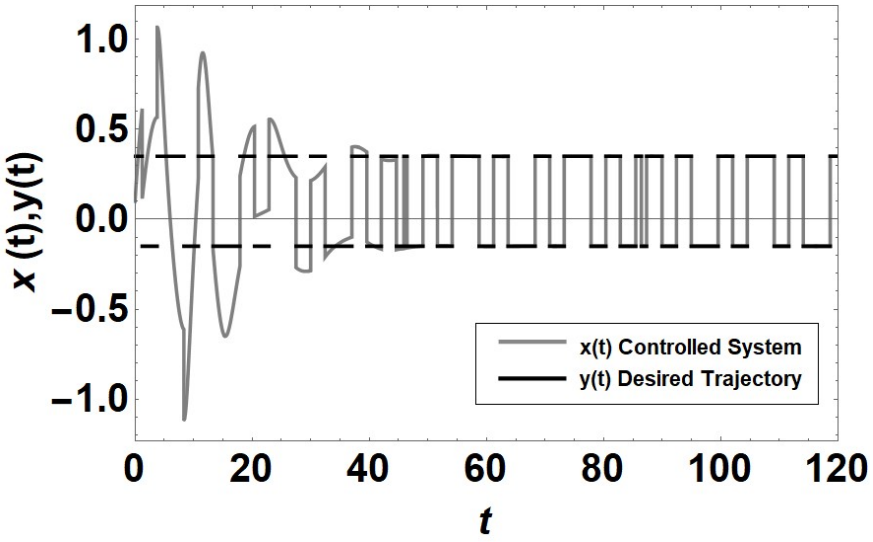

Fig. 4.5: Controlled motion of the chaotic forced Duffing oscillator to a quasi-periodic square wave $\left(y(t)=0.1+0.25sgn\left[\cos\omega_1 t+0.8\cos\omega_2 t\right]\right.$ where $\omega_1=1$ and $\omega_2=\left(1+\sqrt{5}\right)/2\Big)$.

4.3.1B Control to a fixed point through a logarithmic spiral trajectory

Consider a desired trajectory,

$$\mathbf{y}(t)=\begin{Bmatrix} y_1(t) \\ y_2(t) \end{Bmatrix}=\begin{Bmatrix} c_1+c_2\cos(c_3 t)e^{-c_4 t} \\ c_5+c_2\sin(c_3 t)e^{-c_4 t} \end{Bmatrix} \tag{4.17}$$

where, (c_1, c_5) are the coordinates of the fixed point in the parametric space, c_3 is the frequency of the motion, c_4 is the decay rate and c_2 accounts for the amplitude of the time-varying term. The logarithmic spiral trajectory is defined by setting $c_2=0.5$, $c_3=7$ and $c_4=0.18$. For the desired trajectory, $\mathbf{y}(t)$, the controlled system is defined in the state space form as

$$\begin{aligned} \dot{x}_1 &= x_2+u_{f1} \\ \dot{x}_2 &= x_1-x_1^3-0.4x_2+\sin t+u_{f2}+u_t \end{aligned} \tag{4.18}$$

where, $u_{f1} = \dot{y}_1 - y_2$ and $u_{f2} = \dot{y}_2 - y_1 + y_1^3 + 0.4y_2 - \sin t$. Following the procedure described in section 4.2, the linearized error equation is given by

$$\dot{\mathbf{e}} = \begin{bmatrix} 0 & 1 \\ 1-3y_1^2 & -0.4 \end{bmatrix} \mathbf{e} + \begin{Bmatrix} 0 \\ 1 \end{Bmatrix} \mathbf{u_t} \tag{4.19}$$

where, $\mathbf{u_t} = -\mathbf{Ke} = -\{k_1 \quad k_2\}\{e_1 \quad e_2\}^T$. Equation (4.19) is a time-varying equation and stability theorems proposed by Infante [83] can be used to analyze Eq. (4.19). Infante's theorems are applicable to linear systems with stochastic and deterministic temporal variations in parameters. It should be noted that the necessary condition for the stability theorems of Infante to hold is that the eigenvalues of the constant matrix have negative real parts. Equation (4.19) consists of three unknown parameters (c_1, k_1 and k_2) and these parameters can be utilized in numerous ways to satisfy the necessary condition. In the following two typical cases are discussed.

In the first case, parameters k_1 and c_1 are selected to satisfy the necessary condition and stability bounds on k_2 are determined using Infante's approach. The closed-loop form of Eq. (4.19) can be rearranged as

$$\mathbf{e}'(t) = \underbrace{\begin{bmatrix} 0 & 1 \\ 1-k_1-3c_1^2 & -0.4 \end{bmatrix}}_{\mathbf{A_0}} \mathbf{e} + \underbrace{\begin{bmatrix} 0 & 0 \\ -3\left[\left(0.5\cos(7t)e^{-0.18t}\right)^2 + c_1\cos(7t)e^{-0.18t}\right] & -k_2 \end{bmatrix}}_{\mathbf{A_t}} \mathbf{e} \tag{4.20}$$

The shaded region in Fig. 4.6 represents the values of k_1 and c_1 for which the constant matrix A_0 has eigenvalues with negative real parts. According to Infante's stability theorem, Eq. (4.20) is almost sure asymptotically stable if the following condition holds.

$$E\left\{\lambda_{\max}\left[\left(\mathbf{A_0}+\mathbf{A_t}\right)^{\mathbf{T}} + \mathbf{P}\left(\mathbf{A_0}+\mathbf{A_t}\right)\mathbf{P^{-1}}\right]\right\} \le 0 \tag{4.21}$$

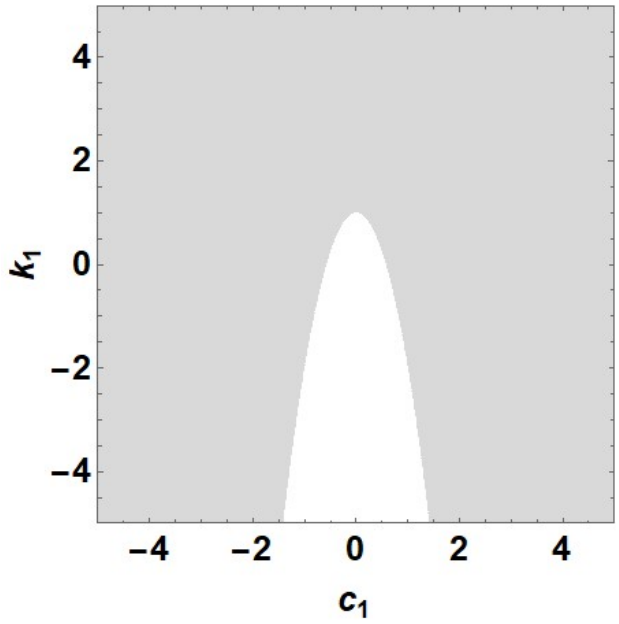

Fig. 4.6: Values of k_1 and c_1 for which the constant matrix $\mathbf{A}_0$ of Eq. (4.20) has eigenvalues with negative real parts (shaded area).

where, $E\{\bullet\}$ is the expectation operator, $\lambda_{\max}$ is the maximum real eigenvalue of the matrix pencil $\left[\left(\mathbf{A}_0+\mathbf{A}_t\right)^{\mathrm{T}}\mathbf{P}+\mathbf{P}\left(\mathbf{A}_0+\mathbf{A}_t\right)\mathbf{P}^{-1}\right]$ and $\mathbf{P}$ is the solution of the Lyapunov equation, $\mathbf{A}_0^{\mathrm{T}}\mathbf{P}+\mathbf{P}\mathbf{A}_0=-\mathbf{I}$. For $k_1=2.5$ and $c_1=-0.5$, the eigenvalues of $\mathbf{A}_0$ are $-0.2\pm1.48661i$ and $\mathbf{P}=\begin{bmatrix}13189/1680 & 2/21\\ 2/21 & 125/84\end{bmatrix}$. Using $\mathbf{A}_t$ from Eq. (4.20), inequality (4.21) produces

$$E\left\{-0.4-k_2+\sqrt{0.316738+0.395865k_2+1.00663k_2^2-2.14922y_1^2-0.323308k_2y_1^2+3.94031y_1^4}\right\}\le 0 \quad (4.22)$$

which can be rewritten as

$$E\left\{\sqrt{0.316738+0.395865k_2+1.00663k_2^2-2.14922y_1^2-0.323308k_2y_1^2+3.94031y_1^4}\right\}\le 0.4+k_2 \quad (4.23)$$

Using the Schwarz's inequality, $E\left\{\sqrt{X}\sqrt{Y}\right\}\le\sqrt{E\{X\}E\{Y\}}$,

$$0.872762+0.365555k_2+1.0662k_2^2-2.14922E\left\{y_1^2\right\}-0.323308k_2E\left\{y_1^2\right\}+3.94031E\left\{y_1^4\right\}\le\left(0.4+k_2\right)^2 \quad (4.24)$$

Since $E\left\{y_1^2\right\} = c_1^2$ and $E\left\{y_1^4\right\} = c_1^4$, inequality (4.24) yields

$$-0.275882 \le k_2 \le 73.4009 \tag{4.25}$$

Taking $c_5 = 1.25$ and selecting $k_2 = 2.5$, the system is controlled to the fixed point (-0.5,1.25) through the chosen logarithmic spiral trajectory as shown in Fig. 4.7.

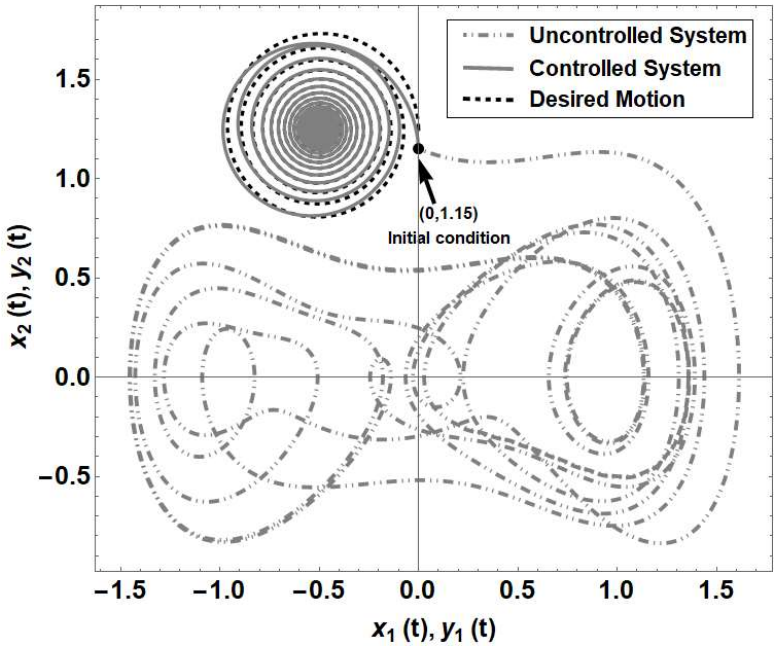

Fig. 4.7: Control of chaotic behavior of forced Duffing oscillator to a fixed point (-0.5,1.25) through a logarithmic spiral trajectory.

The same procedure can also be applied to examine the second case where parameters k_1 and k_2 are kept in the constant matrix to satisfy the necessary condition of Infante's stability theorem and then, stability bounds are calculated on c_1. The shaded area in Fig. 4.8 depicts the range of k_1 and k_2 for which the constant matrix has eigenvalues with negative reals parts. Choosing the control gains $k_1 = 3.5$ & $k_2 = 2.5$ and using the inequality (4.21) yields

$$E\left\{-2.9 + \sqrt{4.33933 - 4.8848y_1^2 + 2.13456y_1^4}\right\} \le 0 \tag{4.26}$$

An application of Schwarz's inequality leads to

$$-1.71395 \le c_1 \le 1.71395 \tag{4.27}$$

If $c_1 = 0$ and $c_5 = -1$, the coordinates of the fixed point are (0, -1) and the controlled dynamics is shown in Fig. 4.9.

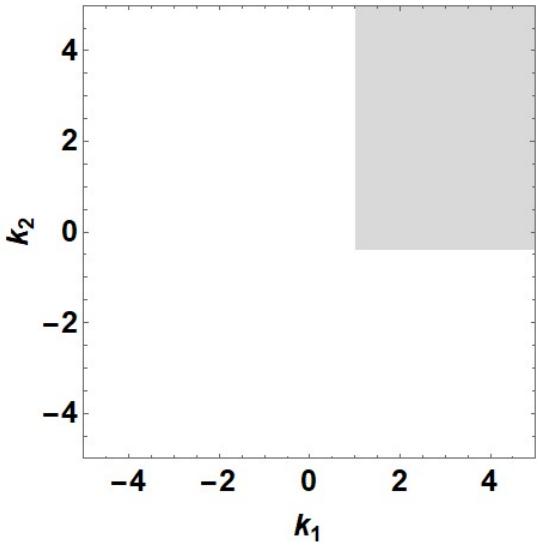

Fig. 4.8: Values of k_1 and k_2 for which the constant matrix has eigenvalues with negative real parts. (shaded area).

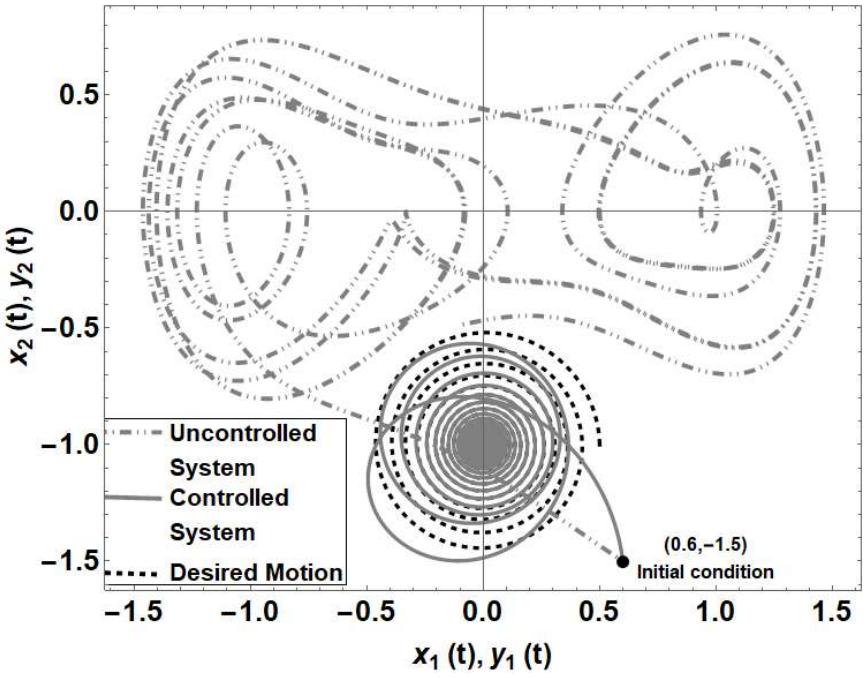

Fig. 4.9: Control of chaotic behavior of forced Duffing oscillator to a fixed point (0, -1) through a logarithmic spiral trajectory.

4.3.2 Parametrically Forced Lorenz System: Control to a desired periodic orbit

The dynamics of the flow in convective layers is represented by Lorenz equations. In many cases, the heat source/ sink may have time-dependence (periodic or quasi-periodic) which modifies the Lorenz equations to parametrically forced Lorenz equations [82] given by

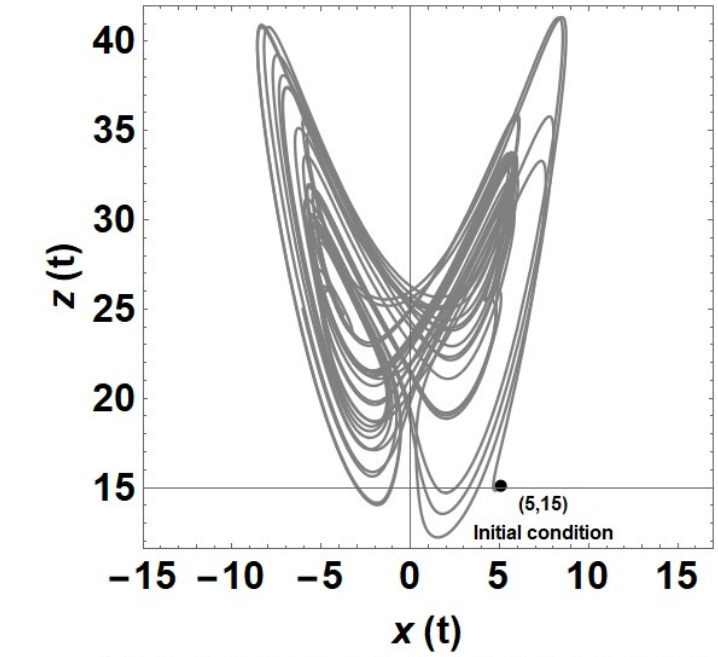

(i) $x \sim z$ projection

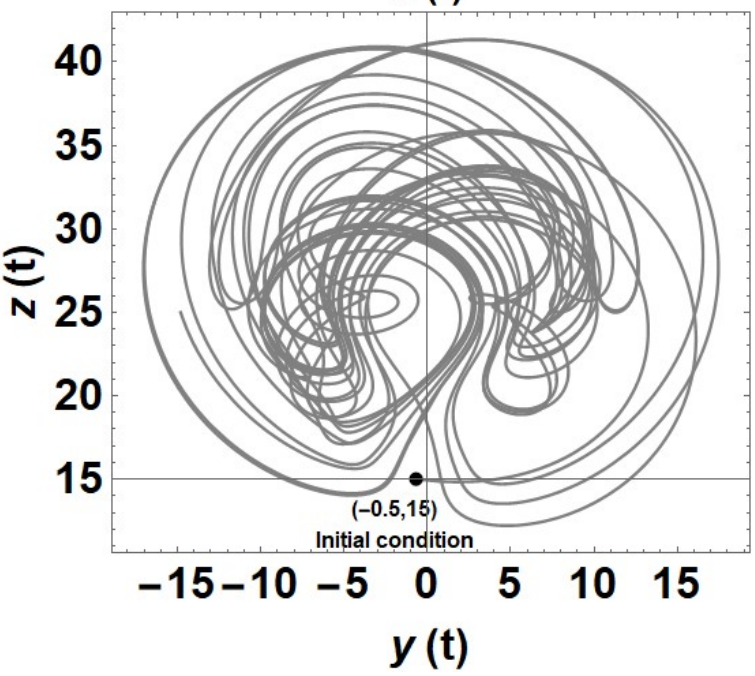

(ii) $y \sim z$ projection

Fig. 4.10: The 'shaken butterfly' chaotic attractor of the parametrically forced Lorenz equations.

$$\begin{aligned}\dot{x}(t) &= -\sigma x(t) + \sigma y(t)\\ \dot{y}(t) &= \left[\rho_0 + \rho_1 \cos\omega_1 t\right] x(t) - y(t) - x(t)z(t)\\ \dot{z}(t) &= x(t)y(t) - bz(t)\end{aligned} \tag{4.28}$$

The convection loops display a chaotic behavior when $\sigma = 2$, $\rho_0 = 26.5$, $\rho_1 = 5$, $b = 0.6$ and $\omega_1 = 2\pi$ as shown in Fig. 4.10. The controlled system with the feedforward control, u_f and the feedback control, u_t is assumed to be

$$\begin{aligned}\dot{x}(t) &= -2x(t) + 2y(t) + u_{f1}\\ \dot{y}(t) &= \left[26.5 + 5\cos\omega_1 t\right] x(t) - y(t) - x(t)z(t) + u_{f2} + u_t\\ \dot{z}(t) &= x(t)y(t) - 0.6z(t) + u_{f3}\end{aligned} \tag{4.29}$$

If the desired orbit is selected as

$$\begin{Bmatrix} y_1(t)\\ y_2(t)\\ y_3(t)\end{Bmatrix} = \begin{Bmatrix} \mathrm{Sin}\,\omega_2 t\\ \mathrm{Sin}\,\omega_2 t\\ 20 + \cos\omega_2 t\end{Bmatrix}, \tag{4.30}$$

the feedforward controls are given by

$$\begin{aligned}u_{f1} &= \omega_2 \cos\omega_2 t\\ u_{f2} &= \omega_2 \cos\omega_2 t - 5.5\sin\omega_2 t + 0.5\sin 2\omega_2 t + 2.5\left[\sin\left(\omega_1 - \omega_2\right)t - \sin\left(\omega_1 + \omega_2\right)t\right]\\ u_{f3} &= 11.5 + 0.6\cos\omega_2 t - \omega_2 \sin\omega_2 t + 0.5\cos 2\omega_2 t\end{aligned} \tag{4.31}$$

The linearized error dynamic e can be represented by

$$\begin{Bmatrix} \dot{e}_1(t)\\ \dot{e}_2(t)\\ \dot{e}_3(t)\end{Bmatrix} = \begin{bmatrix} -2 & 2 & 0\\ \left[\left(26.5 + 5\cos\omega_1 t\right) - 20\cos\omega_2 t\right] & -1 & -\sin\omega_2 t\\ \sin\omega_2 t & \sin\omega_2 t & -0.6\end{bmatrix} \begin{Bmatrix} e_1(t)\\ e_2(t)\\ e_3(t)\end{Bmatrix} + \begin{Bmatrix} 0\\ 1\\ 0\end{Bmatrix} u_t \tag{4.32}$$

Equation (4.32) represents a periodic (quasi-periodic) system if the frequencies, ω_1 and ω_2 are commensurate (incommensurate). In 2005, Sinha *et al.* controlled the chaos in a parametrically forced Lorenz equations to a periodic orbit. Their problem was simple as the periodic orbit had the same frequency as the parametric frequency. In the present

investigation $\omega_2 = \pi\left(1+\sqrt{5}\right)$ which is irrationally related to the parametric frequency, $\omega_1 = 2\pi$.

First, the transformation, $\omega_1 t = \bar{t}$ is applied to normalize the frequencies of the coefficient matrix to 1 and $\left(1+\sqrt{5}\right)/2$. Assuming $\mathbf{u_t} = -\mathbf{Ke} = -\{k_1 \quad k_2 \quad k_3\}\{e_1 \quad e_2 \quad e_3\}^T$, Eq. (4.32) takes the form

$$\begin{Bmatrix} e_1'(\bar{t}) \\ e_2'(\bar{t}) \\ e_3'(\bar{t}) \end{Bmatrix} = \frac{1}{\omega_1}\begin{bmatrix} -2 & 2 & 0 \\ \left[\left(26.5-k_1+5\cos\bar{t}\right)-20\cos\dfrac{\omega_2}{\omega_1}\bar{t}\right] & -1-k_2 & -k_3-\sin\dfrac{\omega_2}{\omega_1}\bar{t} \\ \sin\dfrac{\omega_2}{\omega_1}\bar{t} & \sin\dfrac{\omega_2}{\omega_1}\bar{t} & -0.6 \end{bmatrix}\begin{Bmatrix} e_1(\bar{t}) \\ e_2(\bar{t}) \\ e_3(\bar{t}) \end{Bmatrix} \tag{4.33}$$

where, $\mathbf{e}'(\bar{t}) = d\mathbf{e}/d\bar{t}$. The frequency basis of Eq. (4.33) is the same as the frequency basis of linearized error equation in the section 4.3.1A (see Eq. (4.12)). $\omega_{\min}$ over the range of j_1 & j_2 can be found in Table 4.1. Since Eq. (4.33) is a third order system, a relatively higher $\omega_{\min}$ is required in order to keep the computation time reasonable. If the upper limit of j_1, j_2 is fixed to 12, $\omega_{\min} = 0.0901699$ and $T_a = 68.6816$ (see Table 4.1). Using $\omega_{\min} = 0.0901699$, the approximate system is defined by replacing the frequencies, 1 & $\left(1+\sqrt{5}\right)/2$ in Eq. (4.33) with 0.99186890 & 1.62305820, respectively. Then, the approximate system takes the form

$$e'\left(\bar{t}\right) = A(\bar{t})e\left(\bar{t}\right) \tag{4.34}$$

where, $e\left(\bar{t}\right) = \left\{e_1\left(\bar{t}\right) \quad e_2\left(\bar{t}\right) \quad e_3\left(\bar{t}\right)\right\}^T$ and

$$A(\bar{t}) = \frac{1}{\omega_1}\begin{bmatrix} -2 & 2 & 0 \\ \left[\left(26.5 - k_1 + 5\cos 0.99186890\bar{t}\right) - 20\cos 1.62305820\bar{t}\right] & -1-k_2 & -k_3 - \sin 1.62305820\bar{t} \\ \sin 1.62305820\bar{t} & \sin 1.62305820\bar{t} & -0.6 \end{bmatrix}$$

This is a periodic system with the principal period $T_a = 68.6816$ and its stability can be determined using Floquet theory. For convenience, computations are performed by setting $k_3 = 0$.

The symbolic technique described in Section 2.5 is used to compute the FTM of Eq. (4.34) in terms of the control gains k_1 & k_2. In order to reduce the number of shifted Chebyshev polynomials, the principal period, $T_a = 68.6816$ is divided into 20 sub-intervals. FTM of each sub-interval is calculated using 10 shifted Chebyshev polynomials and 15 Picard iterations and the FTM over the principal period is computed using semigroup property of state transition matrices. The symbolic FTM obtained here is a relatively high degree polynomial in k_1 & k_2 and hence, computation of eigenvalues of the FTM for determining stability is not a trivial task even through the use of Schur-Cohen criteria [84, 85]. The problem can be circumvented by expressing the characteristic polynomial of the FTM as

$$\begin{aligned} &\mathrm{Det}\left[\mu\mathbf{I} - \mathbf{\Phi}\left(k_1, k_2, T_a\right)\right] = \mu^n - a_1\left(k_1, k_2\right)\mu^{n-1} + a_2\left(k_1, k_2\right)\mu^{n-2} - \ldots \\ &\ldots(-1)^{n-1} a_{n-1}\left(k_1, k_2\right)\mu + (-1)^n a_n\left(k_1, k_2\right) \end{aligned} \tag{4.35}$$

where, $a_i\left(k_1, k_2\right)$ is the sum of i^{th} order principal minors of $\mathbf{\Phi}\left(k_1, k_2, T_a\right)$. By introducing the complex fractional transformation, $\mu = \left(\eta + 1\right)/\left(\eta - 1\right)$, the unit circle in the complex plane can be mapped to the left half plane. The transformed expression is a polynomial in

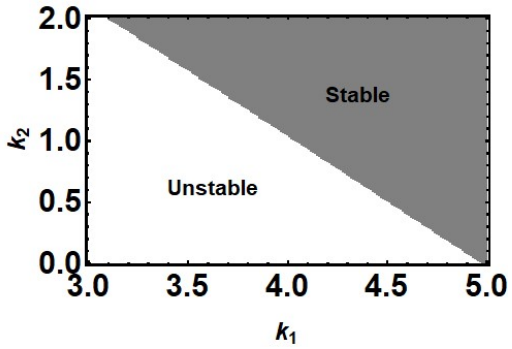

Fig. 4.11: Stability diagram of linearized error equation (39) in $k_1 \sim k_2$ plane.

η to which Routh Hurwitz stability criteria can be applied to determine the desired set of values of k_1 & k_2. The shaded area in Fig. 4.11 represents the region in the parametric space of k_1 & k_2 for which the equilibrium point of Eq. (4.34) is asymptotically stable. The null solution of Eq. (4.34) or (4.32) is unstable in the absence of k_1 & k_2. Selecting an arbitrary set of $(k_1, k_2) = (4.6,1)$, from the stable region, the chaotic dynamics in Eq. (4.28) can be controlled to the desired periodic orbit, Eq. (4.30) as shown in Fig. 4.12.

4.3.3 A Mathieu-Duffing Oscillator: Control to a two-frequency quasi-periodic motion Mathieu Duffing equation is one of the variants of nonlinear Mathieu equation and is used to explore the dynamics of parametrically excited Micro and Nano systems [86]. In this paper, the following form of Mathieu-Duffing equation is studied.

$$\ddot{x} + 2\xi\dot{x} - (\alpha + \beta \sin \omega_1 t)x + \gamma x^3 = 0 \tag{4.36}$$

The system undergoes chaotic motion for $\xi = 0.125, \alpha = 1, \beta = 5.3, \gamma = 1$ and $\omega_1 = 2$ as shown in Fig. 4.13. Chaos is considered undesirable for MEMS/NEMS devices as it restricts the signal strength and the output energy. Also, it limits the stable operating range of actuators. Therefore, the control of chaotic dynamics to a general periodic or quasi-

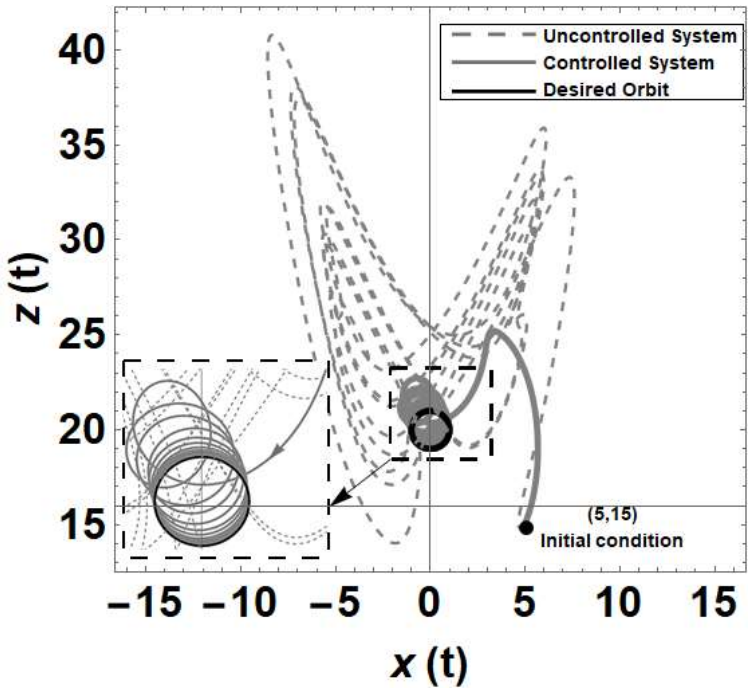

(i) $x \sim z$ projection

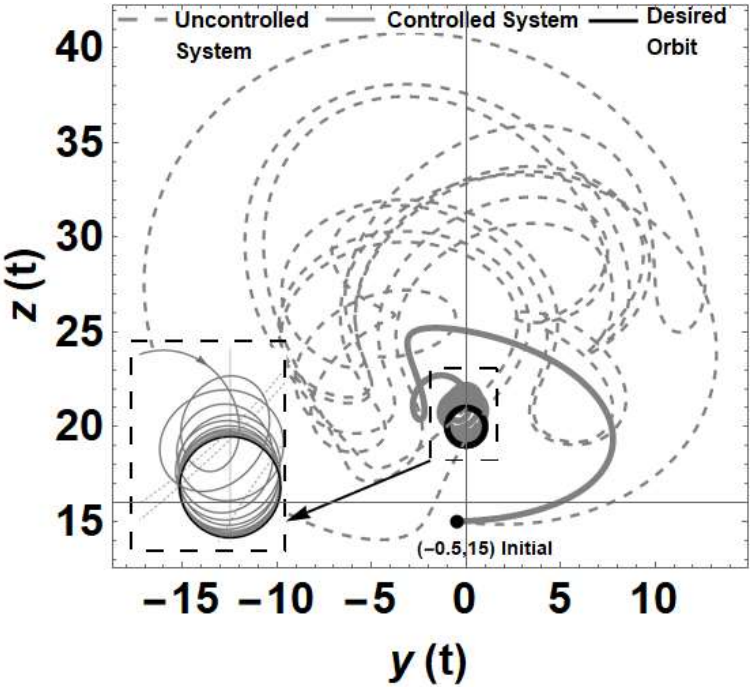

(ii) $y \sim z$ projection

Fig. 4.12: Control of chaotic behavior of parametrically forced Lorenz equations to a periodic orbit.

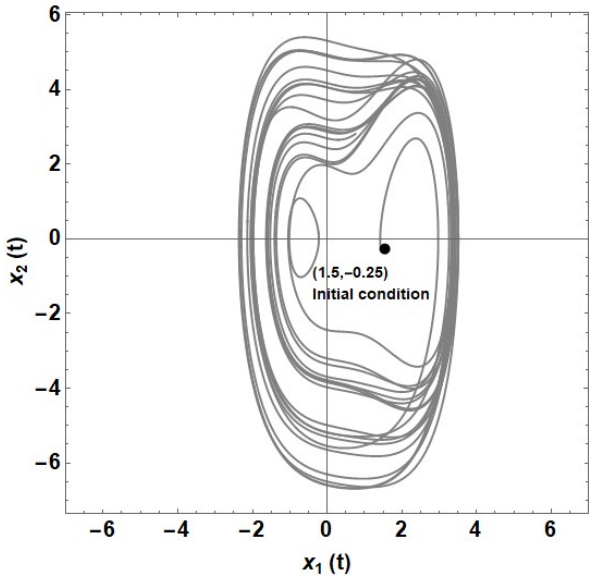

Fig. 4.13: Chaotic behavior of the uncontrolled Mathieu-Duffing oscillator in the phase plane.

periodic motion may be necessary. With a feedforward control, u_f and a linear feedback control, u_t , the controlled system can be written in the state space form as

$$\begin{aligned} \dot{x}_1 &= x_2 + u_{f1} \\ \dot{x}_2 &= \left(1 + 5.3\sin\omega_1 t\right) x_1 - 0.25x_2 - x_1^3 + u_{f2} + u_t \end{aligned} \tag{4.37}$$

where, $u_{f1} = y_1' - y_2$, $u_{f2} = y_2' - (1 + 5.3\sin\omega_1 t)y_1 + 0.25y_2 + y_1^3$ and let the desired two-frequency quasi-periodic motion, $\mathbf{y}(t)$ be defined as

$$\mathbf{y}(t) = \begin{Bmatrix} y_1(t) \\ y_2(t) \end{Bmatrix} = \begin{Bmatrix} \cos\omega_2 t + \cos\omega_3 t \\ \sin\omega_2 t \end{Bmatrix} \tag{4.38}$$

with $\omega_2 = \sqrt{2}$ and $\omega_3 = \sqrt{7}$. The linearized error equation can be shown to be

$$\begin{Bmatrix}\dot{e}_1\\ \dot{e}_2\end{Bmatrix}=\begin{bmatrix}0 & 0\\ -2+5.3\sin\omega_1 t-1.5\left(\cos 2\omega_2 t+\cos 2\omega_3 t\right)-3\left[\cos\left(\omega_2+\omega_3\right)t+\cos\left(\omega_3-\omega_2\right)t\right] & \\ 1 & \\ -0.25 & \end{bmatrix}\begin{Bmatrix}e_1\\ e_2\end{Bmatrix}+\begin{Bmatrix}0\\ 1\end{Bmatrix}\mathbf{u_t}$$

(4.39)

where, $\mathbf{u_t}=-\mathbf{Ke}=-\begin{Bmatrix}k_1\sin\omega_1 t & k_2\end{Bmatrix}\begin{Bmatrix}e_1 & e_2\end{Bmatrix}^T$. It is to be noted that unlike the previous cases, $\mathbf{K}$ is assumed to be a function of the parametric frequency ω_1. Since ω_1, ω_2 and ω_3 are irrationally related, Eq. (4.39) is a quasi-periodic system with ω_1, $\omega_2+\omega_3$ and $\omega_3-\omega_2$ forming the frequency basis of the coefficient matrix.

Following the methodology described in Chapter 2, various minimum frequencies, $\omega_{\min}$ are calculated over a range of j_1, j_2 & j_3 and are listed in Table 4.2. In order to select $\omega_{\min}$, convergence study of bifurcation points of main unstable regions corresponding to frequencies ω_1, $\left(\omega_3-\omega_2\right)$ and $\left(\omega_2+\omega_3\right)$ is performed as shown Fig. 4.14. $\omega_{\min}=0.0222059$ ($T_a=282.951$) is selected as the minimum frequency for further investigation. For this value of $\omega_{\min}$, the approximate system is constructed by replacing the frequencies of Eq. (44) with frequencies, $\bar{\omega}_1=1.998531$, $\left(\bar{\omega}_3-\bar{\omega}_2\right)=1.2213245$

Table 4.2: Minimum frequencies ($\omega_{\min}$) with their corresponding periods (T_a) and the frequencies of the approximate system (periodic system).

Entry Number (E. No.)	Range of j_1, j_2 & j_3 values	$\omega_{\min}$ ($\omega_{\min}\neq 0$)	$T_a=2\pi/\omega_{\min}$	$\bar{\omega}_1$	$\bar{\omega}_3-\bar{\omega}_2$	$\bar{\omega}_2+\bar{\omega}_3$
Col. 1	Col. 2	Col. 3	Col. 4	Col. 5	Col. 7	Col. 6
1	0 to 1	0.768462	8.17631	2.30538600	1.53692400	3.84231000
2	0 to 4	0.0599649	104.781	1.97884170	1.25926290	4.07761320
3	0 to 9	0.0222059	282.951	1.99853100	1.22132450	4.06367970
4	0 to 11	0.0155531	403.983	2.00634990	1.22869490	4.05935910
5	0 to 18	0.00556239	1129.58	2.00246040	1.22928819	4.06054470

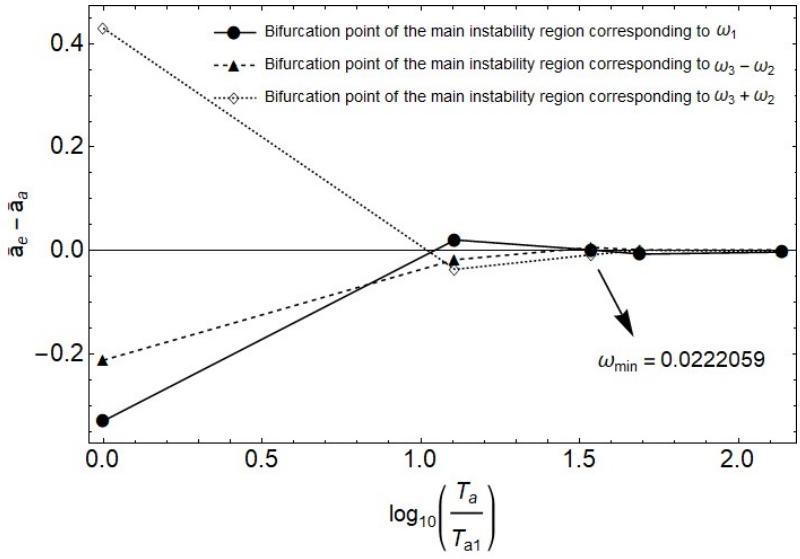

Fig. 4.14: Convergence diagram of bifurcation points of main instability regions of the linearized error equation (4.39).

and $\left(\bar{\omega}_2 + \bar{\omega}_3\right) = 4.0636797$. Thus, the approximate closed-loop system takes the form

$$e'(t) = A(t)e(t) \tag{4.40}$$

where $e(t) = \left\{e_1(t) \quad e_2(t)\right\}^T$ and

$$A(t) = \begin{bmatrix} 0 & 1 \\ -2 + (5.3 - k_1)\sin 1.998531t - 1.5\left(\cos 2.8423552t + \cos 5.2850042t\right) - 3\left[\cos 4.0636797t + \cos 1.2213245t\right] & -0.25 - k_2 \end{bmatrix}$$

Eq. (4.40) is a periodic system with principal period $T_a = 282.951$ and its stability diagram can be plotted using Floquet theory. The symbolic technique presented in Section 2.5 is utilized to compute the FTM of Eq. (4.40) using 80 sub-intervals with 30 shifted Chebyshev polynomials and 40 Picard iterations in each interval. Stability chart can be plotted using the expression, $Tr\left[\mathbf{\Phi}\left(T_a, k_1, k_2\right)\right] = \pm\left(1 + e^{-(0.25+k_2)T_a}\right)$ but it requires a large amount of memory due to the very long expression of $Tr\left[\mathbf{\Phi}\left(T_a, k_1, k_2\right)\right]$. This problem

could be overcome by computing $Tr\left[\mathbf{\Phi}\left(T_a, k_1, k_2\right)\right]$ and $\left(1+e^{-(0.25+k_2)T_a}\right)$ separately at equally spaced sampling points using a grid. Figure 4.15 shows the stability diagram of Eq. (4.40) in $k_1 \sim k_2$ plane in which the shaded area represents the stable region. Isolated stable regions are also observed in the unstable area and they occur due to the presence of instability pockets. It should be noted that in the absence of k_1 and k_2 *i.e.*, $k_1 = k_2 = 0$, Eq. (4.40) is unstable. In the case of $k_1 = 1.5$ and $k_2 = 1$, error e tends to zero and the chaotic behavior of Eq. (4.36) is controlled to the desired quasi-periodic motion (see Eq.(4.38)) as shown in Fig. 4.16.

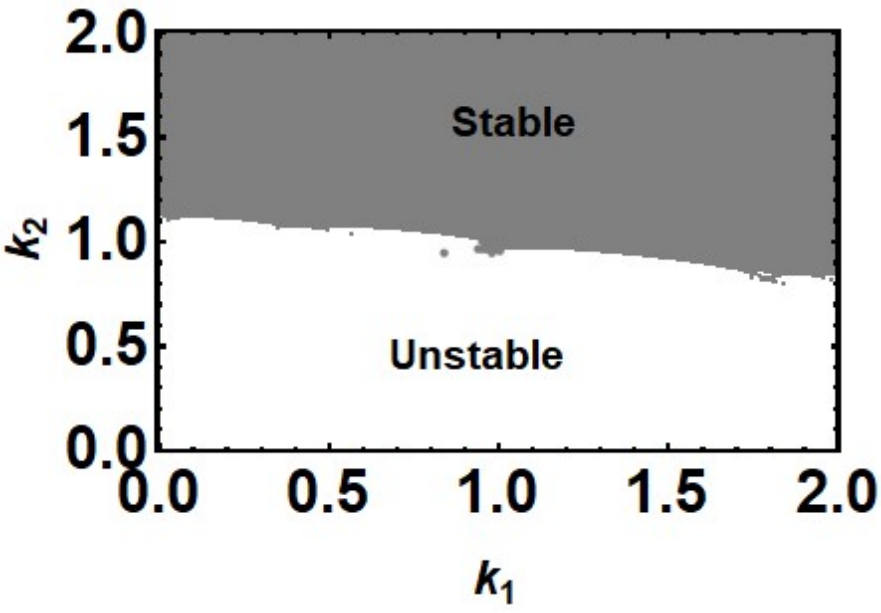

Fig. 4.15: Stability diagram of linearized error equation (4.40) in $k_1 \sim k_2$ plane.

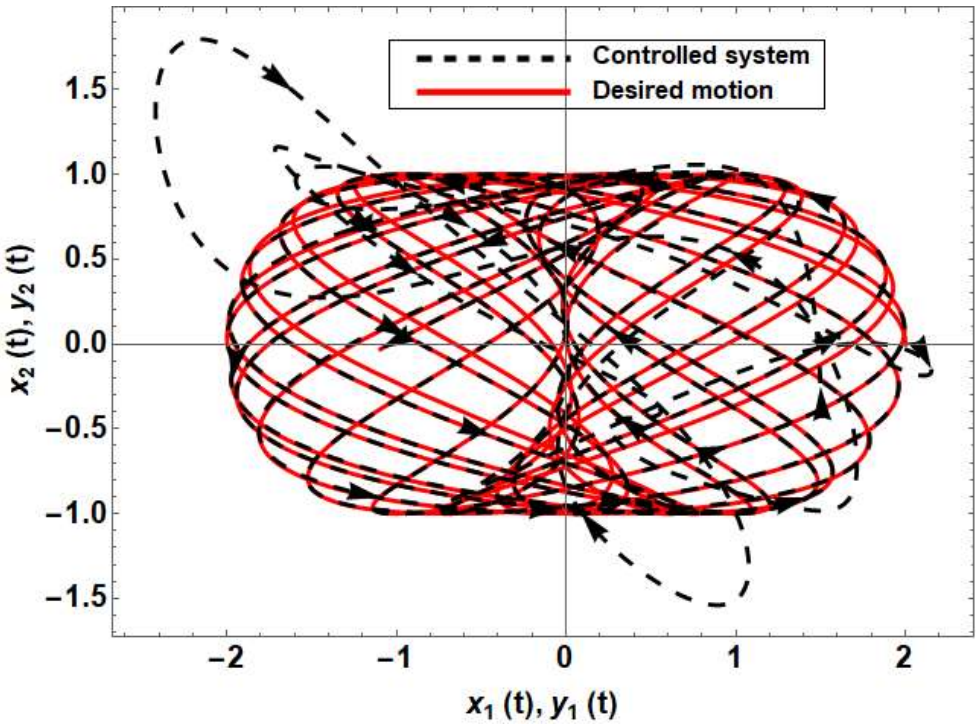

Fig. 4.16: Control of chaotic behavior of Mathieu-Duffing oscillator to a quasi-periodic motion with frequencies $\omega_2 = \sqrt{2}$ and $\omega_2 = \sqrt{7}$.

Chapter 5

Discussion and Conclusions

This dissertation proposes techniques to analyze and control dynamical systems with quasi-periodic systems. An approximate approach is proposed to determine the stability and response of quasi-periodic systems. Although Floquét theory is applicable only to periodic systems, it is suggested here that a quasi-periodic system may be replaced by a periodic system with an appropriately large principal period and thus making it suitable for an application of the Floquét theory. Based on this premise, a systematic approach has been developed and applied to three typical quasi-periodic systems. The approximate stability charts show excellent agreement with numerical results. A detailed analysis of 'instability pockets' appearing in stability diagrams of parametrically excited systems is also presented. In addition to this, the alterations in 'instability pockets' and stability diagrams, in general, due to addition of damping is systematically investigated. A control technique to drive nonlinear systems to desired periodic or quasi-periodic motions is also discussed in this work. Unlike perturbation and averaging, the techniques presented here are not restricted by an existence of a generating solution or a small parameter.

An approximate approach to determine stability and response of quasi-periodic systems has been presented in Chapter 2. The methodology is based on the proposition that a quasi-periodic system may be replaced by a periodic system with a 'suitable' large principal period to which Floquét theory can be applied. First, the '*minimum frequency*',

$\omega_{\min}$, in the truncated frequency module of coefficient matrix, $A(\omega t, \lambda)$ is defined to determine a 'suitable' principal period, T_a $(= 2\pi/\omega_{\min})$ of the parametric quasi-periodic term. This is achieved by performing a convergence study of the bifurcation points of main parametric instability regions. Once $\omega_{\min}$ has been selected, the original quasi-periodic system is approximated by a periodic system with principal period T_a. Excitation frequencies in the periodic system (approximate system) are integral multiplies of $\omega_{\min}$ and are close to respective excitation frequencies in the original quasi-periodic system. Due to the periodic nature of the approximate system its stability and response can be determined using the well-known Floquét theory.

Stability charts are plotted for three typical cases using the proposed technique based on Floquét theory. In case of undamped systems, a number of T_a and $2T_a$ unstable regions stem from a axis in the $a \sim b$ plane. These unstable regions occur because of individual excitation frequencies or due to various combinations of excitation frequencies present in the system and their number increases with a decrease in $\omega_{\min}$. In between the prominent instability regions, narrow strips of unstable regions are also observed (For instance, between R2 and R3 in Fig. 2.3). These narrow strips disappear for smaller values of b if damping is present in the system. Therefore, in engineering applications, these instability zones may not be important. Poincaré maps of approximate and exact solutions generated near the approximate stability boundaries are found to be qualitatively similar. Computations of maximal Lyapunov exponents and frequency spectra of the solutions demonstrate that the approximate boundaries are very close to the exact boundaries. The dominant frequencies in the frequency spectra of solutions are further used to identify

frequency combinations causing parametric resonances in the quasi-periodic systems considered here. The proposed approximate technique is able to capture the existence of '*instability loops*' or '*instability pockets*' in the stability diagrams of Case Study 2 ($\omega_1 = 1.0$ and $\omega_2 = \left(1+\sqrt{5}\right)\Big/2$) and Case Study 3 ($\omega_1 = 1.0$, $\omega_2 = \sqrt{3}$ and $\omega_3 = \sqrt{11}$). Such results have not been reported in the past.

A symbolic computation of state transition matrix (STM) in terms of system parameters is also presented in section 2.5. For Case Study 2, the STM was symbolically computed in terms of a and b and subsequently stability chart is plotted in the $a \sim b$ plane using the symbolic Floquét transition matrix (FTM). Using sufficient number of subintervals ($si = 30$), Picard iterations ($p = 30$) and Chebyshev polynomials ($m_c = 20$), the symbolic method produces a stability chart (Fig. 2.23) that is identical to Fig. 2.17 plotted using numerical computation. The symbolic form of STM would be extremely helpful in controller design and bifurcation analysis of nonlinear quasi-periodic systems.

It is understood that the accuracy of the proposed methodology depends upon the choice of $\omega_{\min}$. Smaller $\omega_{\min}$ implies larger T_a resulting in more accurate solutions. This is quite obvious since for a quasi-periodic system $T_a \to \infty$. However, larger periods require longer computation time. In some cases, the minimum frequencies could be so small that it would be practically impossible to use them, especially on a laptop computer that was used here. Nevertheless, this should not be considered a drawback as one can always use the processing power of supercomputers. It should also be noted that the selection of the $\omega_{\min}$ for a problem depends upon the type of investigation to be performed. For instance, a relatively larger $\omega_{\min}$ could be used in the presence of damping for control problems as

opposed to bifurcation studies. Control system designs generally require approximate location of stable/unstable regions in the parametric space. On the contrary, bifurcation studies require exact locations of stability boundaries in the parametric space.

Two features of parametrically excited linear systems have been investigated in chapter 3. Firstly, a detailed analysis of 'instability pockets' appearing in stability diagrams of such systems is presented. Secondly, the alterations in 'instability pockets' and stability diagrams, in general, due to addition of damping is systematically studied. In particular, the results for some typical cases of Mathieu, Meissner, three-frequency Hill and Quasi-Periodic Hill equations are presented in detail.

Instability pockets are observed in the stability charts of Meissner, three-frequency Hill and Quasi-Periodic Hill equations. These pockets do not exist for Mathieu equation. Since the instability pockets are formed by the intersections of boundary curves in the instability zones, two linearly independent solutions exist at these intersections, commonly known as 'coexistence points'. Therefore, the off-diagonal terms of Floquet transition matrix, FTM (or monodromy matrix) are set to zero to yield a pair of independent equations which are simultaneously solved to obtain the coexistence points. Since the FTMs are computed using a symbolic technique, the matrix elements are complicated algebraic expressions in terms of system parameters and therefore, numerical methods are used to determine these points. In the special case of Meissner equation with a square wave coefficient, simple expressions are generated for the number and locations of coexistence points in the parametric space.

In the second part of study, the effect of damping on these systems is investigated. With an increase in damping, instability pockets start turning into instability islands and eventually disappear from the parametric space when damping coefficient equals a critical

value. An expression relating the trace of FTM and damping coefficient is constructed to compute the minimum values of damping required for instability pockets to vanish from the parametric space.

The unexpected outcome of destabilization due to damping is also observed in all four systems. Under the influence of damping, unstable regions shift in the parametric space causing a crossover between damped and undamped boundaries, which leads to destabilization. The phenomenon of instability caused by damping is known to occur in parametrically excited systems with two degrees of freedom or higher. However, the present investigation shows that such a destabilization is very much possible in systems with one degree of freedom.

In Chapter 4, a methodology to control general nonlinear systems to desired motions is presented. The desired motion could be a periodic orbit, a quasi-periodic motion or a fixed point and does not need to be a solution of the nonlinear system. The applicability of the approach is demonstrated by controlling chaotic systems to desired motions.
The controller design is achieved using a combination of a nonlinear feedforward controller and a linear feedback controller. The feedforward component reduces the nonlinear control problem to a nonlinear stabilization problem which is linearized around the desired motion to yield a linear ordinary differential equation with time-varying coefficients. Depending upon the original chaotic system & the desired motion, the coefficients could be constant, periodic, or quasi-periodic functions of time. The resulting linear system obtained is stabilized using the full state feedback controller.

In the case of periodic coefficients, the well-known Floquet theory is utilized to compute the control gains via stability analysis of the system. An approximate technique

proposed in Chapter 2 is employed to compute the gains when the coefficients are quasi-periodic. In this approximate approach, the quasi-periodic system is replaced by a periodic system with an appropriate large principal period. Due to the periodic nature of the approximate system, its stability can be determined using the Floquet theory. The symbolic technique developed by Sinha and Butcher [17] is used to compute state transition matrices of these systems in terms of unknown control gains ($k_1, k_2, \ldots, k_i$) using shifted Chebyshev polynomials and Picard iterations. Symbolic STMs are used to plot stability diagrams in the $k_1 \sim k_2$ plane (restricted to two gains) and by choosing the appropriate values of k_1 and k_2 the system is stabilized. The symbolic technique is useful in the design of controllers as it guarantees the asymptotic stability of the feedback system for all possible values of control gains. Also, it is not restricted by the existence of a small parameter and a generating solution.

Successful applications of the control strategy are demonstrated by examining three typical chaotic systems. In these illustrative examples, the chaotic systems and the desired orbits are chosen in such a manner that each case represents a distinct class of problems. In the first case, chaos in a forced Duffing oscillator is driven to a two-frequency quasi-periodic square wave and a fixed point. Linearization of the feedforward-controlled system around the quasi-periodic square wave yielded a two-frequency quasi-periodic system which is analyzed using the technique discussed in Chapter 2. In the control to a fixed point, the controlled system is constrained to follow a logarithmic spiral trajectory. Due to this restriction, a linear ordinary differential equation with a time-varying coefficient is obtained whose stability is determined using Infante's stability theorems [83]. In the second case, the chaotic attractor of a parametrically forced Lorenz equation is controlled to a

periodic orbit whose frequency is irrationally related to the parametric excitation frequency. Although the dynamical system represents a periodic system and the desired motion is a periodic orbit, the linearized equation is a linear ordinary differential equation with quasi-periodic coefficients. In the last case, the chaotic behavior of a Mathieu-Duffing oscillator is driven to a two-frequency quasi-periodic motion. The frequencies of the quasi-periodic motion are irrationally related to the parametric frequency of the Mathieu-Duffing oscillator. In this case, linearization of the feedforward-controlled system resulted in a three-frequency quasi-periodic system. It should be noted that the control strategy is not limited to nonlinear systems exhibiting chaos.

Chapter 6

Future work

There are several opportunities to extend the work presented here beyond its current precincts and some of those are highlighted here.

A) Construction of Lyapunov-Perron transformation matrices

1.0 Introdcution

Parametrically excited systems have applications in every field of science and engineering. Some of the examples include structures subjected to periodic loads, asymmetric rotor bearing systems, ship dynamics, robots performing repetitive tasks, and cardiac dynamics, among others. Mathematically, parametrically excited systems are represented by linear/ nonlinear ordinary differential equations with time-varying coefficients.

There are several mathematical methods to analyze linear dynamical systems with periodic coefficients (so-called periodic systems). Hill's method of infinite determinants [1] is suitable for determining the stability boundaries of such systems. Hill's infinite determinants do not converge always, and the method is not computationally efficient for large order systems. Analytical techniques such as perturbation [14] and averaging [15] are restricted by the existence of a generating solution and a small parameter. In 1977, Friedmann et al. [13] employed Hsu's approach [10] and suggested a numerically efficient method that requires only a single integration pass scheme to calculate state transition

matrices (STMs). Sinha and his associates utilized shifted Chebyshev polynomials in conjunction with Floquet theory [9, 72] to compute STMs of periodic systems in semi-analytical [16] and symbolic forms [17].

Another way to deal with periodic systems is to use Lyapunov-Floquet theorem [49]. According to this theorem, a linear periodic system can be reduced to a time-invariant system using Lyapunov-Floquet (L-F) transformation. For special cases of periodic systems, called the commutative systems, L-F transformations can be computed in closed forms [87, 88]. In 1996, Sinha et al. [89] developed a technique for the computation of L-F transformation matrices for general periodic systems. They first computed the STM in the semi-analytical form using Ref. [16] and then, eigenanalysis is performed to the resulting STM to determine L-F transformation matrix. In 2009, Butcher et al. [90] attempted to calculate L-F transformation matrices in the symbolic form using Magnus expansions. Although their approach does not require the symbolic computation of STMs, it suffers from convergence issues even for relatively smaller values of system parameters. Recently, Kirkland and Sinha [18] presented a methodology for the symbolic computation of L-F transformations in terms of system parameters. Unlike Ref. [90], this approach is computationally efficient and convergent over a wide parametric space.

For linear ordinary differential equations with quasi-periodic coefficients (so-called quasi-periodic systems), a similar kind of transformations exists and are known as Lyapunov-Perron (L-P) transformations. These transformations reduce linear quasi-periodic systems to systems with constant coefficients. Several authors [75, 76, 91-93] have reported the existence of L-P transformations but, to this date, no one is able to compute them even in the approximate form. Unavailability of rigorous mathematical theory for

linear quasi-periodic systems could be one of the reasons for the absence of any attempt towards the computation of L-P transformations.

Very recently, Sharma and Sinha [94] proposed an approximate approach to analyze linear quasi-periodic systems. They replaced a quasi-periodic system by a periodic system with an appropriately large principal period to which Floquet theory can be applied. Their technique is novel in the sense that it allows the construction of the approximate STM of a quasi-periodic system which can be utilized to generate approximate stability diagrams, responses and L-P transformations. In this paper, an attempt has been made to develop approximate L-P transformations for quasi-periodic systems using Lyapunov-Floquet theorem and the symbolic STM computed by employing the methodology presented in Ref. [94]. First, L-F and L-P transformations are briefly outlined for completeness.

2.0 REDUCIBILITY OF PERIODIC AND QUASI-PERIODIC SYSTEMS

Consider a linear ordinary differential equation of the form

$$\dot{x} = A(\theta,\lambda)x \quad ; \quad \frac{d\theta}{dt} = \omega \qquad x(\theta,\lambda) = x_0 \tag{6.1}$$

where, $x(\theta,\lambda)\in\mathbb{R}^n$, $A(\theta,\lambda)$ is an $n\times n$ matrix that is 2π periodic in $\theta = \{\theta_1,\theta_2,\ldots,\theta_m\}$ and is a continuous function of a set of control parameters λ ; $\omega = \{\omega_1,\omega_2,\ldots,\omega_m\}$ (Unit: rad/s) is the frequency basis of $A(\theta,\lambda)$ and t is the time in seconds. For the sake of brevity, units of frequency, ω_i and time, t are omitted from the rest of the paper. Equation (6.1) is said to be reducible if a linear time-varying change of variable, $x = S(\theta,\lambda)z$ transforms Eq. (6.1) to the following form.

$$\dot{z} = A_0(\lambda)z \tag{6.2}$$

where, $A_0(\lambda) = S^{-1}(\theta,\lambda)\left[A(\theta,\lambda)S(\theta,\lambda) - \dot{S}(\theta,\lambda)\right]$ is a constant matrix.

2.1 Lyapunov-Floquet transformation

In the case of $m = 1$, $A(\theta,\lambda)$ in Eq. (6.1) is a periodic matrix with the principal period $T = 2\pi/\omega_1$ and thus, Eq. (6.1) is a linear periodic system and can be analyzed using Floquet theory. Let $\Phi(t,\lambda)$ be the STM such that it satisfies Eq. (6.1) with $\Phi(0,\lambda) = I$; then the solution can be written as

$$x(t,\lambda) = \Phi(t,\lambda)x_0 \qquad 0 \le t \le T \tag{6.3}$$

For $t \ge T$, the solution can be calculated using

$$x(t+sT,\lambda) = \Phi(t,\lambda)\Phi^s(T,\lambda)x_0 \qquad s = 1,2,3,\ldots \tag{6.4}$$

where, $0 \le t \le T$ and $\Phi(T,\lambda)$ is the Floquet transition matrix (FTM) or the monodromy matrix. The stability criteria for periodic systems depend upon the eigenvalues of $\Phi(T,\lambda)$, called the '*Floquet multipliers*' and the system is stable if all *Floquet multipliers* lie on or inside the unit circle, otherwise it is unstable.

According to the Lyapunov-Floquet theorem [49], the STM can be expressed as

$$\Phi(t,\lambda) = L(t,\lambda)e^{C(\lambda)t} \qquad L(t,\lambda) \in \mathbb{C}^{n\times n},\quad C(\lambda) \in \mathbb{C}^{n\times n} \tag{6.5}$$

or,

$$\Phi(t,\lambda) = Q(t,\lambda)e^{R(\lambda)t} \qquad Q(t,\lambda) \in \mathbb{R}^{n\times n},\quad R(\lambda) \in \mathbb{R}^{n\times n} \tag{6.6}$$

where, $L(t,\lambda)$ and $Q(t,\lambda)$ are T periodic and $2T$ periodic, respectively. $L(t,\lambda)$ and $Q(t,\lambda)$ are known as Lyapunov-Floquet (L-F) transformations. Using $x = L(t,\lambda)z$ or $x = Q(t,\lambda)z$, Eq. (6.1) (with $m = 1$) can be reduced to

$$\dot{z} = C(\lambda)z \quad \text{or} \quad \dot{z} = R(\lambda)z \quad \text{,respectively,} \tag{6.7}$$

where $C(\lambda)$ and $R(\lambda)$ are time-invariant matrices and can be expressed as

$$C(\lambda) = \frac{1}{T}\ln\Phi(T,\lambda) \quad \text{and} \quad R(\lambda) = \frac{1}{2T}\ln\Phi(2T,\lambda) \tag{6.8}$$

where, according to the semigroup property of the STM $\Phi(2T,\lambda) = \Phi^2(T,\lambda)$ [22].

A note of interest: If one of the Floquet multipliers lie in the left-half of the plane, $Q(t,\lambda)$ is $2T$ periodic. On the other hand, if all the Floquet multipliers lie in the right half of the complex plane, the complex and real L-F transformations coincide, both are T periodic and real.

2.2 Lyapunov-Perron transformation

When the coefficient matrix, $A(\theta,\lambda)$ has finite $(m \geq 2)$ incommensurate frequencies, Eq. (6.1) represents a linear quasi-periodic system. Unfortunately, there is no complete theory for the analysis of quasi-periodic systems and they cannot be analyzed using Floquet theory.

Linear quasi-periodic systems can also be reduced to systems with constant coefficients using Lyapunov-Perron (L-P) transformations. If $P(\theta,\lambda)$ is a L-P transformation, the change of variable $x = P(\theta,\lambda)z$ reduces Eq. (1) (with $m \geq 2$) to the following system [75, 76].

$$\dot{z} = B(\lambda)z \tag{6.9}$$

where, $B(\lambda)$ is a time-invariant matrix and is real for real $P(\theta,\lambda)$. It should be noted that the frequency basis of L-P transformation, $P(\theta,\lambda)$ is the same as the frequency basis of the coefficient matrix, $A(\theta,\lambda)$.

3.0 PROPOSED METHODOLOGY

A simple form of Eq. (6.1) (with $m \geq 2$) is the damped quasi-periodic Hill equation given by

$$\ddot{x} + d\,\dot{x} + \left(a + \sum_{i=1}^{m} b_i \cos(\omega_i t) \right) x = 0 \tag{6.10}$$

Equation (6.10) can be rewritten in the state space form as

$$\dot{x} = \begin{bmatrix} 0 & 1 \\ -\left(a + \sum_{i=1}^{m} b_i \cos(\omega_i t) \right) & -d \end{bmatrix} x \tag{6.11}$$

where, $x = \begin{bmatrix} x_1 & x_2 \end{bmatrix}^T$ and $\omega = \{\omega_1, \omega_2, \ldots, \omega_m\}$ is the frequency basis of the coefficient matrix.

Equation (6.11) cannot be directly analyzed using Floquet theory since the principal period of the coefficient matrix tends to infinity. However, an approximate principal period, T_a can be determined by truncating the frequency module of $A(\omega t, \lambda)$ defined as $|k_1\omega_1 \pm k_2\omega_2 \pm \ldots \pm k_m\omega_m|$; $k_i = 0,1,\ldots$ and $k_1 = k_2 = \ldots = k_m \neq 0$. The frequency module can be truncated by fixing the upper limit on k_i and the minimum frequency, '$\omega_{\min}$' in the truncated frequency module can be used to compute the approximate principal period of the quasi-periodic matrix function. $\omega_{\min}$ and T_a are defined as

$$\omega_{\min} = \text{Min}\left(\left|k_1\omega_1 \pm k_2\omega_2 \pm \ldots \pm k_m\omega_m\right|\right) \quad ; \quad \omega_{\min} \neq 0$$
$$\text{and} \tag{6.12}$$
$$T_a = 2\pi/\omega_{\min}$$

Various $\omega_{\min}$ (or T_a) can be computed over a range of values of k_i. The selection of $\omega_{\min}$ depends upon the convergence study of bifurcation points of main instability regions [94]. Once $\omega_{\min}$ and T_a have been selected, the original quasi-periodic system, Eq. (6.11) can be replaced by a periodic system given by

$$\dot{x} = \begin{bmatrix} 0 & 1 \\ -\left(a + \sum_{i=1}^{m} b_i \cos\left(\bar{\omega}_i t\right)\right) & -d \end{bmatrix} x \tag{6.13}$$

where, ω_i in Eq. (6.11) has been approximated by $\bar{\omega}_i$ such that $\bar{\omega}_i$ are integer multiples of $\omega_{\min}$, the minimum frequency of the approximate system. As Eq. (6.13) represents a periodic system, its stability and response can be determined by the Floquet theory. Ref. [94] demonstrates the feasibility of this approximate approach. They showed that the solutions of Eq. (6.13) are the approximate solutions of Eq. (6.11) and the accuracy of the approach depends upon the selection of minimum frequency. Readers are advised to see Ref. [94] for additional details.

In 1997, Sinha and Butcher [17] developed a symbolic technique that utilizes shifted Chebyshev polynomials of the first kind and Picard iterations to compute STMs of linear periodic systems. Their technique is used in this investigation to compute the STM of Eq. (6.13) in terms of system parameters and time, t. The symbolic approach is summarized in the next section for completeness.

Once the STM, $\Phi(t,\lambda)$ is known, Eq. (6.8) can be utilized to compute constant matrices $C(\lambda)$ and $R(\lambda)$. In this paper, only the real L-F transformation is considered. The constant matrix, $R(\lambda)$ is the approximation of $B(\lambda)$ and as $\omega_{\min} \to 0$, $R(\lambda) \to B(\lambda)$. $R(\lambda)$ can be substituted back in Eq. (6.6) to calculate the approximate L-P transformation, $Q(t,\lambda)$.

Investigation of nonlinear quasi-periodic systems requires $Q^{-1}(t,\lambda)$. $Q(t,\lambda)$ can be inverted by defining the adjoint system to Eq. (6.13) as

$$\dot{w} = -\overline{A}^T(t,\lambda)w \tag{6.14}$$

where, $\overline{A}(t,\lambda)$ is the coefficient matrix of Eq. (6.13). If $\Phi(t,\lambda)$ and $\Psi(t,\lambda)$ are the STMs of Eqs. (6.13) and (6.14), respectively, according to Ref. [49], the following relationship holds.

$$\Phi^{-1}(t,\lambda) = \Psi^T(t,\lambda) \tag{6.15}$$

Using Eq. (6.6), $Q^{-1}(t,\lambda)$ can be written as

$$Q^{-1}(t,\lambda) = e^{R(\lambda)t}\Phi^{-1}(t,\lambda) = e^{R(\lambda)t}\Psi^T(t,\lambda) \tag{6.16}$$

4.0 SYMBOLIC COMPUTATION OF STM

First, the principal period of Eq. (6.13) is normalized to 1 using the transformation $t = T_a\tau$. Then, the normalized system's matrix is expanded in m_c shifted Chebyshev polynomials of the first kind expressed in the interval [0,1] as $\overline{A}(\tau,\lambda) = \hat{T}^T(\tau)D(\lambda)$ where $\hat{T}(\tau)$ and $D(\lambda)$ are Chebyshev polynomial and Chebyshev coefficient matrices, respectively. An approximation to the true solution can be obtained by using the integral form of Eq. (6.13) and Picard iterative process. With the help of integration (G) and

product (Q_{d_i}) operation matrices associated with Chebyshev polynomials, an expression for the STM can be obtained as

$$\Phi^{(p,m_c)}(\tau,\lambda) = \hat{T}^T(\tau)\left[\hat{I} + \sum_{s=1}^{p}\left(\left[H(\lambda)\right]^{s\text{-}1}\right)V(\lambda)\right] \tag{6.17}$$

where, $\hat{I} = I_n \otimes \underbrace{[1\ 0\ 0\ \ldots\ 0]}_{m_c}^T$, $H(\lambda) = \sum_{i=1}^{r}\overline{A}_i(\lambda)\otimes\left(G^T Q_{d_i}\right)$, $V(\lambda) = \sum_{i=1}^{r}\overline{A}_i(\lambda)\otimes\left(G^T d_i\right)$ and

$\otimes$ denotes the Kronecker product (see Ref. [17] for more details). p and m_c are the number of Picard iterations and Chebyshev polynomials employed in the approximation. The FTM can be obtained in terms of system parameters by substituting $\tau = 1$ in Eq. (6.17). In the case of periodic systems with relatively large principal periods, the number of shifted Chebyshev polynomials and Picard iterations required for the computation of symbolic FTM can be reduced by dividing the principal period into several sub-intervals. FTM for each sub-interval can be calculated by following the procedure described above and can be combined using the semigroup property of state transition matrix [78] to obtain FTM over the principal period and is given by

$$\Phi(t_N, t_0, \lambda) = \prod_{s=1}^{N}\Phi(t_{N+1\text{-}s}, t_{N\text{-}s}, \lambda) \tag{6.18}$$

where, N is the total number of sub-intervals.

5.0 AN ILLUSTRATIVE EXAMPLE

The damped quasi-periodic Hill equation with excitation frequencies $\omega_1 = 1$ and $\omega_2 = \left(1+\sqrt{5}\right)\big/2$ can be represented in the state space form using Eq. (6.11) as

Table 6.1: Minimum frequencies ($\omega_{\min}$) with their corresponding periods (T_a) and the frequencies of the approximate system (periodic system).

Entry Number (E. No.)	Range of k_1, k_2 values	$\omega_{\min}$ ($\omega_{\min} \neq 0$)	$T_a = 2\pi/\omega_{\min}$	$\bar{\omega}_1$	$\bar{\omega}_2$
Col. 1	Col. 2	Col. 3	Col. 4	Col. 5	Col. 6
1	0 to 1	0.618034	10.1664	1.23606800	1.85410200
2	0 to 2	0.381966	16.4496	1.14589800	1.52786400
3	0 to 4	0.236068	26.616	0.94427200	1.65247600
4	0 to 7	0.145898	43.0656	1.02128600	1.60487800
5	0 to 12	0.0901699	69.6816	0.99186890	1.62305820
6	0 to 20	0.0557281	112.747	1.00310580	1.61611490
7	0 to 33	0.0344419	182.429	0.99881510	1.61876930
8	0 to 54	0.0212862	295.176	1.00045140	1.61775120
9	0 to 88	0.0131556	477.605	0.99982560	1.61813880
10	0 to 143	0.00813062	772.781	1.00006626	1.61799338

$$\dot{x} = \begin{bmatrix} 0 & 1 \\ -\left(a + b_1 \cos\omega_1 t + b_2 \cos\omega_2 t\right) & -d \end{bmatrix} x \tag{6.19}$$

As a first step, minimum frequencies are computed using Eq. (6.12) over a range of k_1 and k_2 and are tabulated in Table 6.1 along-with their corresponding periods, T_a. In order to approximate Eq. (6.19) by a periodic system, the original frequencies, $\omega_1 = 1$ and $\omega_2 = \left(1+\sqrt{5}\right)\big/2$ are replaced by $\bar{\omega}_1$ and $\bar{\omega}_2$, respectively, which are integer multiples of $\omega_{\min}$. Equation (6.19) reduces to the form

$$\dot{x} = \begin{bmatrix} 0 & 1 \\ -\left(a + b_1 \cos\bar{\omega}_1 t + b_2 \cos\bar{\omega}_2 t\right) & -d \end{bmatrix} x \tag{6.20}$$

Cols. 5 and 6 of Table 6.1 show $\bar{\omega}_1$ and $\bar{\omega}_2$ for various values of $\omega_{\min}$. According to Refs. [94] and [30], there are two main instability regions in the stability diagram of Eq. (6.19) and they correspond to frequencies $\omega_1 = 1$ and $\omega_2 = \left(1+\sqrt{5}\right)\big/2$. These regions stem from the bifurcation points, $a = \omega_1^2/4$ and $a = \omega_2^2/4$ on the a axis. It is well-known that

in a periodic system with excitation frequency ω_1 or ω_2 the main instability region originates from $a = \omega_1^2/4$ or $a = \omega_2^2/4$. Since the bifurcation points of main instability regions in quasi-periodic and periodic systems are the same, the convergence study of these bifurcation points can be used for the selection of $\omega_{\min}$. Figure 6.1 shows the convergence study of bifurcation points of the main instability regions of Eqs. (6.19) and (6.20). The $y-$axis denotes the difference between the exact $\left(a_e = \omega_1^2/4 \text{ and } a_e = \omega_2^2/4\right)$ and approximate $\left(a_a = \bar{\omega}_1^2/4 \text{ and } a_a = \bar{\omega}_2^2/4\right)$ bifurcation points, while the $x-$axis is represented by the expression, $\log_{10}\left(T_a/T_a^1\right)$ where, T_a^1 is the smallest T_a in Table 6.1 *i.e.*, 10.1664. From Fig. 6.1, it can be observed that for $\omega_{\min} < 0.0901699$, the difference $(a_e - a_a)$ is relatively small and as T_a increases (or $\omega_{\min}$ decreases) the difference converges to zero. Larger T_a causes an increase in computation time and hence, as a compromise, $\omega_{\min} = 0.0557281\,(T_a = 112.747)$ is selected as the minimum frequency for further investigations.

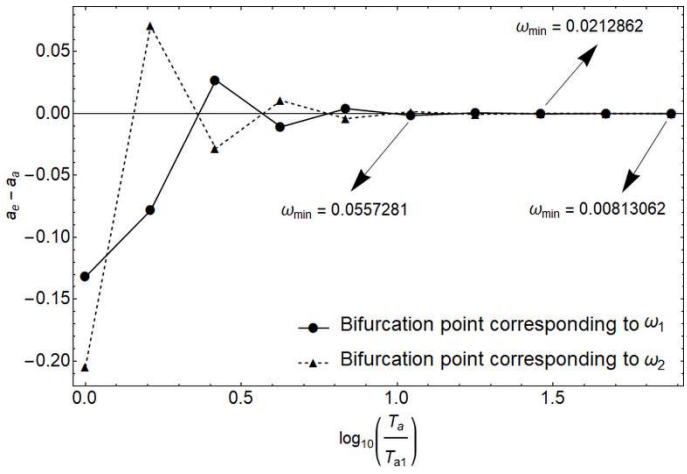

Fig. 6.1: Convergence diagram of bifurcation points of the main instability regions of Eqs. (6.19) and (6.20).

For $\omega_{\min} = 0.0557281$, the approximate system is defined by substituting $\bar{\omega}_1 = 1.00310580$ and $\bar{\omega}_2 = 1.61611490$ in Eq. (6.20). Since Eq. (6.20) is a periodic system with the principal period, $T_a = 112.747$, it can be analyzed using Floquet theory. For the sake of convenience, all computations are performed by setting $b_1 = b_2 = b$. The symbolic technique described in Section 4 is used to compute the STM, $\Phi(t, a, b, d)$ of Eq. (6.20) in terms of system parameters $\{a, b, d\}$ and t. In order to reduce the number of shifted Chebyshev polynomials of the first kind, the principal period, $T_a = 112.747$ is divided into 30 sub-intervals. STM in each sub-interval is determined in the symbolic form using 25 shifted Chebyshev polynomials and 35 Picard iterations. These STMs are combined using Eq. (6.18) to compute the STM over the principal period, T_a. All computations in this work are performed on a laptop computer with a 2.50 GHz i7-4710MQ 4-core processor and 32 GB of RAM.

Approximate L-P transformations are inverted by constructing an adjoint system to Eq. (6.20) (see Section 3.0) and is given by

$$\dot{w} = \begin{bmatrix} 0 & \left(a + b_1 \cos \bar{\omega}_1 t + b_2 \cos \bar{\omega}_2 t\right) \\ -1 & d \end{bmatrix} w \tag{6.21}$$

The symbolic technique presented in Section 4 is once again utilized to calculate the STM, $\Psi(t, a, b, d)$ of Eq. (6.21) in terms of system parameters and time using 30 sub-intervals, 25 shifted Chebyshev polynomials and 35 Picard iterations. In the following, approximate L-P transformations and their inverses are computed for three cases: Stable, Unstable and Critical.

5.1 Stable case

The stability of the approximate system *i.e.*, Eq. (6.20) is predicted by Floquet multipliers while the maximal Lyapunov exponent is computed to determine the stability of the quasi-periodic system, Eq. (6.19). For $a = 0.04$, $b = 0.21$ and $d = 0.1$, Floquet multipliers are $-0.000801826 \pm 0.00347088\,i$ and maximal Lyapunov exponent is negative. Hence, both the approximate system and the original quasi-periodic system are stable for these parameters. As multipliers lie in the left half of the complex plane, the approximate L-P transformation, $Q(t)$ is $2T_a$ periodic. Using $\Phi(T_a, a, b, d)$ and Eq. (6.8), the constant real matrix R can be calculated and is given by

$$R = \begin{bmatrix} -0.0691969 & -0.384229 \\ 0.00132882 & -0.0308031 \end{bmatrix} \tag{6.22}$$

It should be noted that R is the approximated form of B (see Eq. (6.9)). Once R is known, the approximate L-P transformation can be computed using the following expressions.

$$\begin{aligned} Q(t_{N+1-s}, t_{N-s}) &= \left[\prod_{s=1}^{N} \Phi(t_{N+1-s}, t_{N-s}) \right] e^{-R(t_{N+1-s} - t_{N-s})} \\ Q(T_a + t_{N+1-s}, T_a + t_{N-s}) &= \left[\prod_{s=1}^{N} \Phi(t_{N+1-s}, t_{N-s}) \right] Q(T_a)\, e^{-R(t_{N+1-s} - t_{N-s})} \end{aligned} \tag{6.23}$$

where, $0 \le t_{N-s} \le T_a$ and $0 \le t_{N+1-s} \le T_a$. In Fig. 6.2, all four elements of $Q(\tau)$ are plotted against normalized time.

Due to a very long expression of $Q(t_{N+1-s}, t_{N-s})$ it is impractical to invert it through *MATHEMATICA* and thus, an adjoint system defined by Eq. (6.21) is used to determine $Q^{-1}(t)$. At first, $\Psi(t, a, b, d)$ is explicitly expressed in terms of time, t for $a = 0.04$, $b = 0.21$ and $d = 0.1$. Then, $Q^{-1}(t)$ in each sub- interval can be calculated using

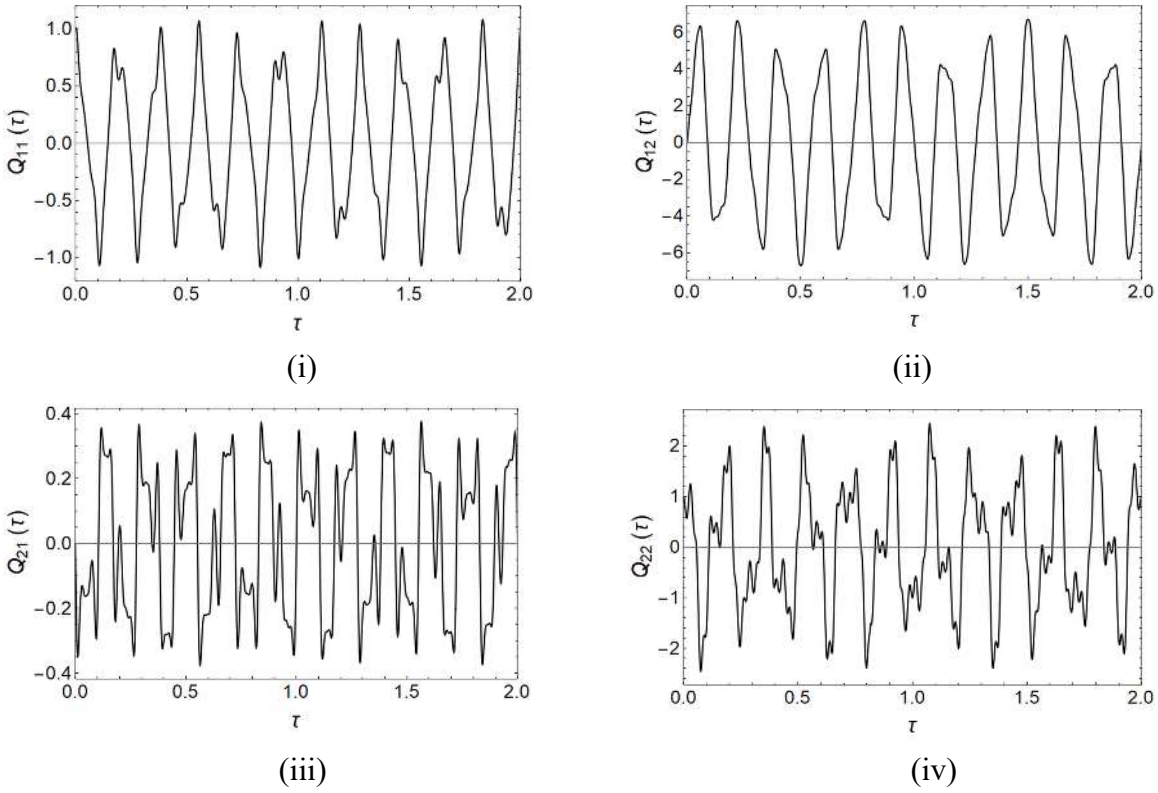

Fig. 6.2: Elements of $Q(\tau)$ for the stable case.

$$
\begin{aligned}
Q^{-1}(t_{N+1-s}, t_{N-s}) &= e^{R(t_{N+1-s}-t_{N-s})}\left[\prod_{s=1}^{N}\Psi^{T}(t_{N+1-s}, t_{N-s})\right] \\
Q^{-1}(T_a + t_{N+1-s}, T_a + t_{N-s}) &= e^{R(t_{N+1-s}-t_{N-s})}Q^{-1}(T_a)\left[\prod_{s=1}^{N}\Psi^{T}(t_{N+1-s}, t_{N-s})\right]
\end{aligned}
\tag{6.24}
$$

and are plotted against normalized time as shown in Fig. 6.3.

From Eqs. (6.23) and (6.24), it is clear that there is no single expression for $Q(t)$ or $Q^{-1}(t)$ that is valid over the principal period, T_a. This may pose a problem while dealing with nonlinear quasi-periodic systems. However, it could be circumvented by exploiting the periodic nature of $Q(t)$ and $Q^{-1}(t)$ and expressing them in the form of Fourier series as

$$
Q(t) \text{ or } Q^{-1}(t) = (a_0/2) + \sum_{j=1}^{j=r} a_j \cos j\hat{\omega}t + b_j \sin j\hat{\omega}t \tag{6.25}
$$

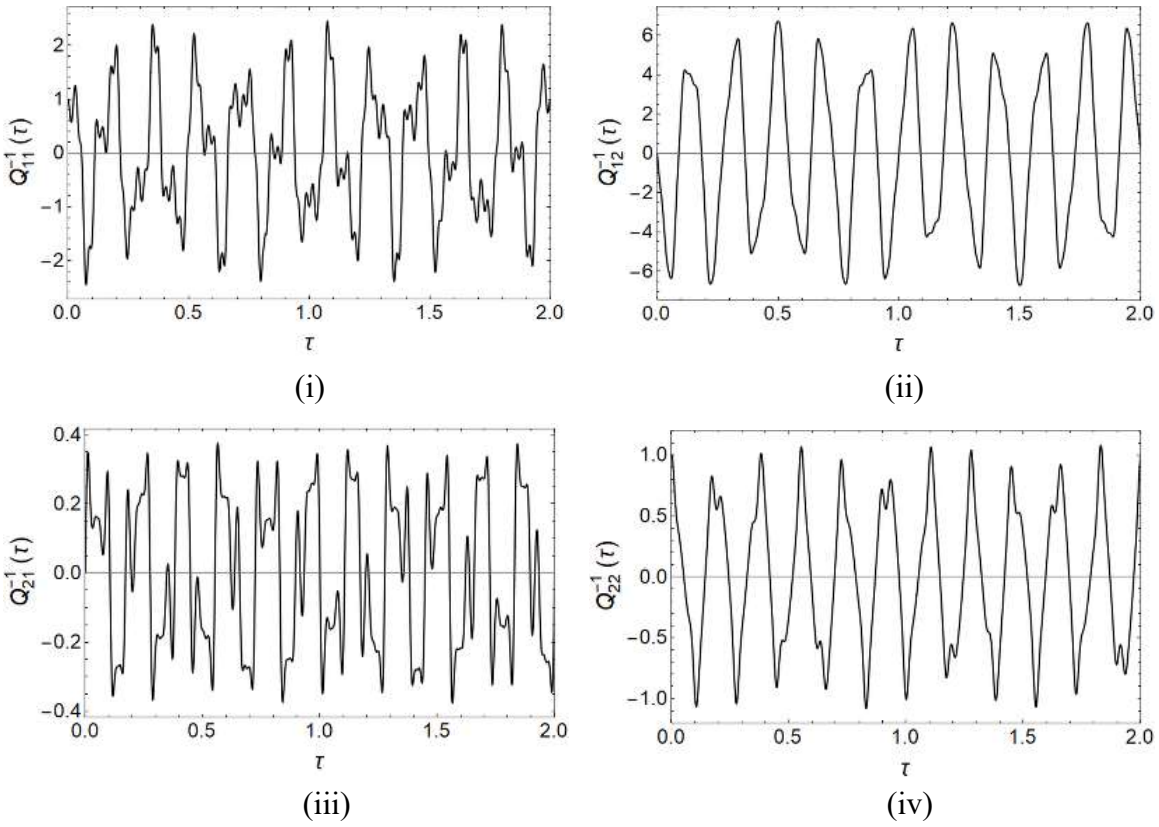

Fig. 6.3: Elements of $Q^{-1}(\tau)$ for the stable case.

where, $\hat{\omega} = \omega_{\min}$ (or $\omega_{\min}/2$) if $Q(t)$ and $Q^{-1}(t)$ is T_a (or $2T_a$) periodic. With $\hat{\omega} = \omega_{\min}/2$ in Eq. (6.25), Fourier coefficients are determined for $Q(t)$ and $Q^{-1}(t)$ for different values of r. The truncation of the Fourier series depends upon the relationship, $Q^{-1}(t)Q(t) = I$ which ensures that $Q(t)$ and $Q^{-1}(t)$ consist of enough number of frequencies to get a constant real matrix, R. Figures 6.4 and 6.5 show all four elements of $Q^{-1}(\tau)Q(\tau)$ for $r = 100$ and 125, respectively. It is observed that for both values of r, off-diagonal elements are almost zero. However, for diagonal elements, the error between the maximum amplitude and 1 is relatively small ($\approx 0.5\%$) when $r = 125$. This error can be reduced to

approximately 0.02% by choosing r as 150. For the sake of brevity, $Q^{-1}(\tau)Q(\tau)$ plot for $r = 150$ is not included. The truncated Fourier series of $Q(t)$ and $Q^{-1}(t)$ with $r = 125$ are found to be in close agreement with $Q(t)$ and $Q^{-1}(t)$ obtained from Eqs. (6.23) and (6.24), respectively.

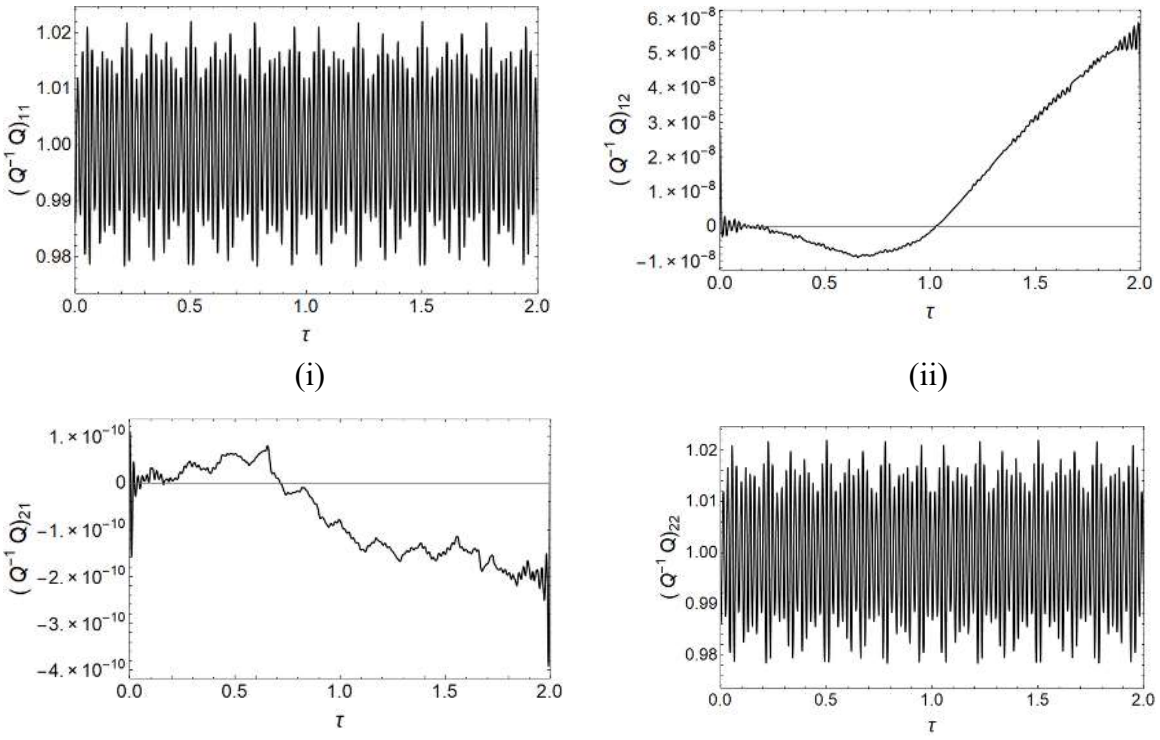

Fig. 6.4: Elements of $Q^{-1}(\tau)Q(\tau)$ for $r = 100$.

5.2 Unstable case

For the parameter set $a = 2.85$, $b = 1.4$ and $d = 0.1$, the approximate system (see Eq. (6.20)) produces Floquet multipliers $\{1.70167,\ 7.457 \times 10^{-6}\}$ and the original quasi-periodic system (see Eq. (6.19)) has a positive maximal Lyapunov exponent. Thus, both systems are unstable. Since Floquet multipliers lie in the right half of the complex plane,

$Q(t)$ is T_a periodic and the constant real matrix can be calculated using $R = \left(1/T_a\right)\ln\Phi\left(T_a, \lambda\right)$ (see Eq. (6.8)). R evaluates to

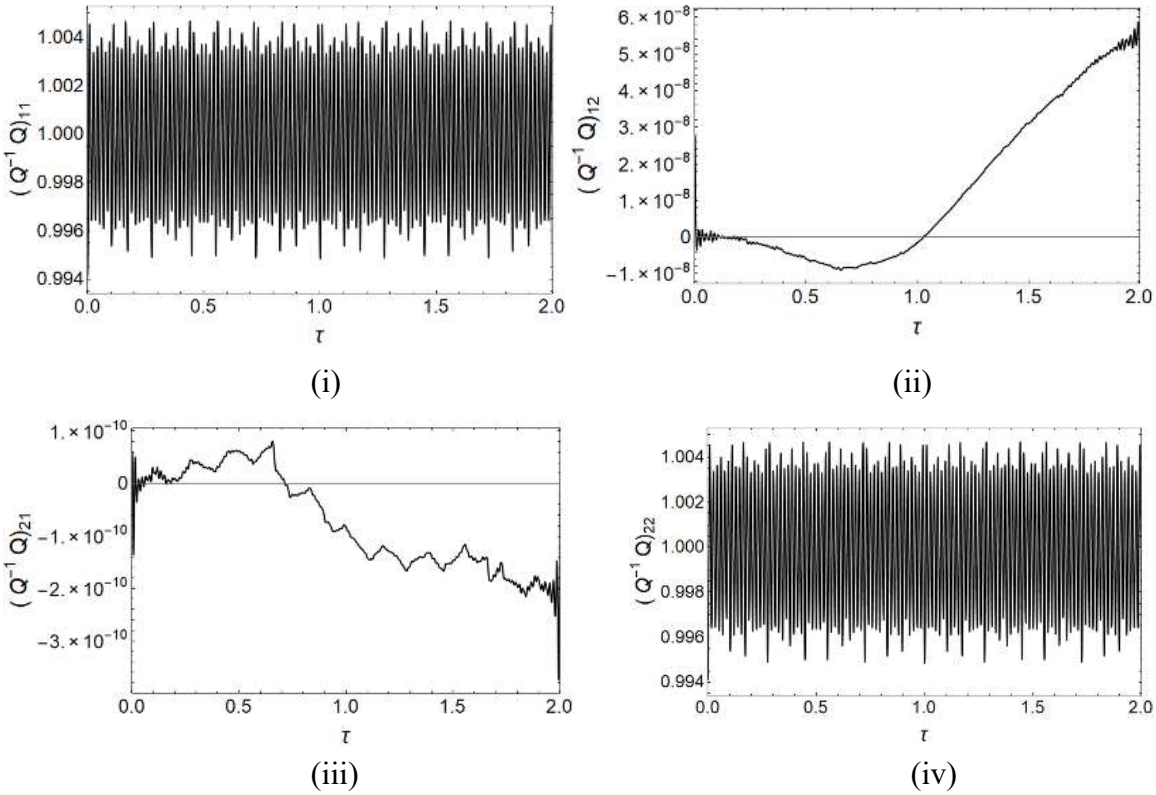

Fig. 6.5: Elements of $Q^{-1}(\tau)Q(\tau)$ for $r = 125$.

$$R = \begin{bmatrix} -0.0483396 & 0.0336694 \\ 0.0888338 & -0.0516604 \end{bmatrix} \tag{6.26}$$

Utilizing this R and the first expression of Eq. (6.23), approximate L-P transformation is determined over the principal period, T_a. The approximate L-P transformation is inverted with the help of the adjoint system *i.e.*, Eq. (6.21). Using $a = 2.85$, $b = 1.4$ and $d = 0.1$, the STM of Eq. (6.21) is determined in terms of t and substituted in the first expression of Eq. (6.24) to compute $Q^{-1}(t)$. Plots of $Q(t)$ and $Q^{-1}(t)$ are not included.

Single expressions for $Q(t)$ and $Q^{-1}(t)$ over the principal period, T_a are obtained by expressing them in Fourier series. Since $Q(t)$ and $Q^{-1}(t)$ are T_a periodic, Fourier coefficients are determined with $\hat{\omega} = \omega_{\min}$ in Eq. (6.25). The relationship, $Q^{-1}(t)Q(t) = I$ is utilized to determine the value of r in Eq. (6.25). It is found that for $r = 100$, off-diagonal elements are almost zero and for diagonal elements the error between the maximum amplitude and 1 is approximately 0.2%. A plot of $Q^{-1}(t)Q(t)$ for $r = 100$ is omitted for brevity. The truncated Fourier series of $Q(t)$ and $Q^{-1}(t)$ with $r = 100$ are found to be in good agreement with those obtained using Eqs. (6.23) and (6.24).

5.3 Critical case

The present sub-section discusses the construction of an approximate L-P transformation for a resonance condition. In contrast to stable and unstable cases, for the critical case it is important that the approximate and exact stability boundaries of an unstable region are very close. According to Ref. [94], the difference between the boundaries can be reduced by choosing relatively smaller $\omega_{\min}$. Due to computational limitation, $\omega_{\min} = 0.0212862$ (see E. No. 8 in Table 6.1) is selected here.

For $\omega_{\min} = 0.0212862$, $T_a = 295.176$, $\bar{\omega}_1 = 1.00045140$ and $\bar{\omega}_2 = 1.61775120$. Assuming $b_1 = b_2 = b$ (for convenience) in Eq. (6.20), once again, the symbolic technique discussed in Section 4 is employed to calculate $\Phi(t, a, b, d)$ of Eq. (6.20) using 60 sub-intervals with 30 shifted Chebyshev polynomials and 35 Picard iterations in each interval. With $a = 0.911986672$, $b = 0.5$ and $d = 0.03$, Floquet multipliers of Eq. (6.20) are found to be $\{0.9999998777, 0.0001426267\}$ indicating a resonance condition. For the same

values of b and d, it is found that the maximal Lyapunov exponent for the original quasi-periodic system i.e., Eq. (6.19) is positive at $a = 0.912155$ and negative at $a = 0.912156$ implying that the exact stability boundary lies between these two values of a. It should be noted that the difference between the approximate and exact boundaries is of the order of 10^{-4}. This difference can be of the order of 10^{-5} if $\omega_{\min} = 0.00813062$ (see E. No. 10 in Table 6.1) is chosen. However, this value of $\omega_{\min}$ is not used due to restrictive computational power.

Floquet multipliers indicate that $Q(t)$ is T_a periodic and the constant real matrix, R evaluates to

$$R = \begin{bmatrix} -0.0148778 & -0.000409736 \\ -0.549098 & -0.0151222 \end{bmatrix} \tag{6.27}$$

Substitution of R and $\Phi(t, 0.911986672, 0.5, 0.03)$ in the first expression of Eq. (6.23) yields $Q(t)$ over the principal period, T_a. In order to construct $Q^{-1}(t)$, first, the STM, $\Psi(t, a, b, d)$ of the adjoint system (see Eq. (6.21)) is computed using 60 sub-intervals with 30 shifted Chebyshev polynomials and 35 Picard iterations. Then, $\Psi(t, 0.911986672, 0.5, 0.03)$ and R are substituted in the first expression of Eq. (6.24) to obtain $Q^{-1}(t)$. Once again, plots of $Q(t)$ and $Q^{-1}(t)$ are not included.

In order to generate single expressions for $Q(t)$ and $Q^{-1}(t)$, they are expressed in Fourier series. With $\hat{\omega} = \omega_{\min}$ in Eq. (6.25), Fourier coefficients are calculated and the series is truncated using the relationship, $Q^{-1}(t)Q(t) = I$. The truncated Fourier series obtained with $r = 175$ are found to be in excellent agreement with $Q(t)$ and $Q^{-1}(t)$ computed using Eqs. (6.23) and (6.24), respectively.

6.0 DISCUSSION AND CONCLUSIONS

A methodology to compute approximate Lyapunov-Perron (L-P) transformations has been presented. These transformations reduce linear quasi-periodic systems to systems with constant coefficients. Very recently, Sharma and Sinha [94] proposed an approximate approach to analyze quasi-periodic systems using the well-known Floquet theory. Their technique allows the computation of approximate state transition matrices (STMs) for general quasi-periodic systems which can be used to construct stability diagrams, responses and L-P transformations.

This paper utilizes the methodology presented in Ref. [94] to compute the STM of a quasi-periodic system and uses it further to calculate approximate L-P transformations with the help of Lyapunov-Floquet theorem. First, the minimum frequency, $\omega_{\min}$ in the truncated frequency module of the coefficient matrix of a quasi-periodic system is determined to calculate the principal period, $T_a = 2\pi/\omega_{\min}$. A 'suitable' principal period is selected based on the convergence study of bifurcation points of main instability regions. Once $\omega_{\min}$ and T_a have been selected, the original quasi-periodic system is replaced by a periodic system in which the excitation frequencies are integer multiples of $\omega_{\min}$. Since the approximate system is periodic in nature, it can be analyzed using Floquet theory. The symbolic technique presented in Section 4 is utilized to compute the STM, $\Phi(t,\lambda)$ of the periodic system in the symbolic form. According to the Lyapunov-Floquet theorem, the STM can be expressed in terms of a periodic matrix and a time-invariant matrix. The constant real matrix, $R(\lambda)$ can be computed using Eq. (6.8). Substitution of $R(\lambda)$ in Eq. (6.6) yields an approximate L-P transformation, $Q(t)$. $Q^{-1}(t)$ which is important for the

analysis of nonlinear quasi-periodic systems can be obtained by constructing an adjoint system to the periodic system *i.e.*, Eq. (6.20). A two-frequency quasi-periodic system with excitation frequencies $\omega_1 = 1$ and $\omega_2 = \left(1+\sqrt{5}\right)\Big/2$ is investigated in this paper and $Q(t)$ and $Q^{-1}(t)$ are computed for stable, unstable and critical cases. A relatively smaller $\omega_{\min}$ is chosen for the critical case to make sure that the approximate and exact stability boundaries of an unstable region are very close to each other. The periodic nature of $Q(t)$ and $Q^{-1}(t)$ is utilized to express approximate L-P transformations in the form of truncated Fourier series for all three cases.

In summary, Lyapunov-Perron transformations have been computed for the first time. The proposed methodology is applicable to general quasi-periodic systems and is not limited by the existence of a generating solution and a small parameter. These transformations can be helpful in the design of controllers using time-invariant methods. Also, L-P transformations would serve as a powerful tool in the bifurcation studies of nonlinear quasi-periodic systems.

B. Normal forms for nonlinear quasi-periodic systems

Study of nonlinear quasi-periodic systems requires the development of normal forms theory and it could be done by following the procedure given below.

Consider a nonlinear quasi-periodic system of the form,

$$\dot{x} = A(t)x + \overline{f}_2(x,t) + \cdots + \overline{f}_k(x,t) + O\left(|x|^{k+1}, t\right) \tag{6.4}$$

where, $A(t)$ and $\overline{f}_k(x,t)$ are quasi-periodic functions. Using the approximate technique proposed in this work, Eq. (6.4) can be approximated by a periodic system. Application of

Lyapunov-Perron transformation and modal transformation reduce this periodic system to the following form.

$$\dot{z} = Jz + f_2(z,t) + \cdots + f_k(z,t) + \mathrm{O}\left(|z|^{k+1}, t\right) \tag{6.5}$$

where, the linear term is time-invariant and has Jordan canonical form, J. Due to the time-independent form of the linear term, a near-identity transformation, $z = v + h_r(v,t)$ can be applied to obtain the homological equation which can be solved to yield solvability condition.

C) Birfurcation analysis of nonlinear quasi-periodic systems

There are only a few studies related to the bifurcation analysis of quasi-periodic systems and those studies are either numerical or involve small parameter techniques such as perturbation and averaging. The approximate approach presented in this work allows symbolic computation of state transition matrices in terms of systems parameters and enable bifurcation analysis at any point in the parametric space. The investigation requires the application of Lyapunov-Perron transformation, center manifold theory and normal form theory. Bifurcation point obtained through the approximate technique is the approximate bifurcation point and its closeness to the exact bifurcation point depends upon the value of minimum frequency. As the value of minimum frequency decreases, the difference between the exact and approximate bifurcation point decreases.

D) Applications

Once nonlinear techniques to analyze quasi-periodic systems have been developed (Points 1 through 3), they can be applied to solve problems associated with ship dynamics, wind turbines, ion traps, MEMS, etc.

References

[1] Bolotin, V.V., 1964, The Dynamic Stability of Elastic Systems, Holden-Day Inc., San Francisco.

[2] Johnson, W., 1980, Helicopter Theory, Princeton University Press, Princeton, NJ.

[3] Roseau, M., 1987, Vibration in Mechanical Systems: Analytical Methods and Applications, Springer-Verlag, New York.

[4] Streit, D.A., Krousgrill, C.M., and Bajaj, A.K., 1989, "Nonlinear Response of Flexible Robotic Manipulators Performing Repetitive Tasks," J. Dyn. Syst.-T ASME, 111(3), pp. 470-479.

[5] Sanchez, N.E., and Nayfeh, A.H., 1990, "Nonlinear Rolling Motion of Ships in Longitudinal Waves," International Shipbuilding Progress, 37(411), pp. 247-272.

[6] Mingori, D.L., 1969, "Effects of Energy Dissipation on the Attitude Stability of Dual Spin Satellite," AIAA J., 7(1), pp. 20-27.

[7] Glass, L., 1991, "Cardiac Arrhythmias and Circle Maps-A Classical Problem," Chaos, 1(1), pp. 13-19.

[8] Powell, J.L., and Crasemann, B., 1961, Quantum Mechanics, Addinson-Wesley, Boston, MA.

[9] Floquét. G., 1883," Sur les equations differentials lineaires a coefficients periodiques," Annales Scientifiques de l'Ecole Normale Superieue, 12(2), pp. 47-88.

[10] Hsu, C.S., 1974, "On Approximating a General Linear Periodic System," J. Mathematical Analysis and Applications, 45(1), pp. 234-251.

[11] Sinha, S.C., Chou, C.C., and Denman, H.H., 1979, "Stability Analysis of Systems with Periodic Coefficients: An Approximate Approach," J. Sound and Vibration, 64(4), pp. 515-527.

[12] Hammond, C.E., 1974, "An Application of Floquet Theory to prediction of mechanical instability," J. American Helicopter Society, 19(4), pp. 14-23.

[13] Friedmann, P., Hammond, C.E., and Woo, T.H., 1977, "Efficient numerical treatment of periodic systems with application to stability problems," Int. J. Numerical Methods in Engineering, 11(7), pp. 1117-1136.

[14] Nayfeh, A.H., and Mook. D.T., 1979, Nonlinear Oscillations, John Wiley, New York.

[15] Sanders, J.A., and Verhulst, F., 1985, Averaging Methods in Nonlinear Dynamical Systems, Springer, New York.

[16] Sinha, S.C., and Wu, D.H., 1991, "An Efficient Computational Scheme for the Analysis of Periodic Systems," J. Sound and Vibration, 151(1), pp. 91-117.

[17] Sinha, S.C., and Butcher, E.A., 1997, "Symbolic Computation of Fundamental Solution Matrices for Time Periodic Dynamical Systems," J. Sound and Vibration, 206(1), pp.61-85.

[18] Kirkland, G.W., and Sinha, S.C., 2016, "Symbolic Computation of Quantities Associated with Time-Periodic Dynamical Systems," J. Comput. Nonlin. Dyn., 11(4), pp. 041022-041022-10.

[19] Sinha, S. C., Ravindra, B., and Henrichs, J. T., 2000, "A General Approach in the Design of Active Controllers for Nonlinear Systems Exhibiting Chaos," Int. J. Bifurcation Chaos, 10(1), pp. 165-178.

[20] Dávid, A., and Sinha, S. C., 2003, "Bifurcation Control of Nonlinear Systems with Time-Periodic Coefficients," J. Dyn. Syst.-T ASME, 125(4), pp. 541-548.

[21] Ko, W., and Stockie, J.M., 2016, "Parametric Resonance in Spherical Immersed Elastic Shells," SIAM J. Applied Mathematics, 76(1), pp. 58-86.

[22] Ko, W., and Stockie, J.M., 2015, "An Immersed Boundary Model of the Cochlea with Parametric Forcing," SIAM J. Applied Mathematics, 75(3), pp. 1065-1089.

[23] Karavitaki, K.D., and Mountain, D.C., 2007, "Evidence for outer hair cell driven oscillatory fluid flow in the Tunnel of Corti," Biophysical J., 92(9), pp.3284-3293.

[24] Robles, L., Ruggero, M.A., and L., Rich, N.C., 1997, "Two-tone distortion on the Basilar Membrane of the Chinchilla Cochlea," J. Neurophysiology, 77(5), pp.2385-2399.

[25] Ruggero, M.A., Robles, L., Rich, N.C., and Recio, A., 1992, "Basilar Membrane responses to two-tone and broadband stimuli," Philosophical transactions of the Royal Society of London Series B, Biological sciences, 336(1278), pp. 307-315.

[26] Ben-Haim,S., Darvish, N., Mika, Y., Rousso, B., Felzen, B., and Malonek,D., 2002, " Local Cardiac Motion Control Using Applied Electrical Signals," U.S. Patent 6,442,424, Washington, DC: U.S. Patent and Trademark Office.

[27] Matheny, R.G., and Taylor, C.S., 1997, "Method of Using Vagal Nerve Stimulation in Surgery," U.S. Patent 5651378A, Washington, DC: U.S. Patent and Trademark Office.

[28] Davis, S.H., and Rosenblat, S., 1980, "A Quasiperiodic Mathieu-Hill Equation," SIAM J. Applied Mathematics, 38(1), pp. 139-155.

[29] Johnson, R.A., and Moser, J., 1982, "The Rotation Number for Almost Periodic Potentials," Communications in Mathematical Physics, 84(3), pp. 403-438.

[30] Zounes, R.S., and Rand, R.H., 1998, "Transition Curves for the Quasi-Periodic Mathieu Equation," SIAM J. Applied Mathematics, 58(4), pp. 1094-1115.

[31] Broer, H., and Simó, C., 1998, "Hill's Equation with Quasi-Periodic Forcing: Resonance Tongues, Instability Pockets and Global Phenomena," Boletim da Sociedade Brasileira de Matemática-Bulletin/Brazilian Mathematical Society, 29(2), pp. 253-293.

[32] Puig, J., and Simó, C., 2011, "Resonance Tongues in Quasi-Periodic Hill-Schrödinger Equation with Three Frequencies," Regular and Chaotic Dynamics, 16(1), pp. 61-78.

[33] Waters, T.J., 2010, "Stability of a 2-Dimensional Mathieu Type System with Quasiperiodic Coefficients," Nonlinear Dynamics, 60(3), pp. 341-356.

[34] Mathieu, É., 1868, "Mémoire Sur Le Mouvement Vibratoire D'une Membrane De Forme Elliptique," Journal de Mathématiques Pures et Appliquées, **13**, pp. 137-203.

[35] Hill, G.W., 1886, "On the Part of the Motion of the Lunar Perigee which is a Function of the Mean Motions of the Sun and Moon," Acta Mathematica, **8**, pp. 1-36.

[36] Richards, J.A., 1983, *Analysis of Periodically Time-Varying Systems*, Springer-Verlag Berlin Heidelberg, Germany.

[37] Trypogeorgos, D., and Foot, C.J., 2016, "Cotrapping Different Species in Ion Traps using Multiple Radio Frequencies," Physical Review A, **94** (2), pp. 023609.

[38] Meissner, E., 1918, "Ueber Schüttelerscheinungen in Systemen mit periodisch veränderlicher Elastizität," Schweizerische Bauzeitung, **71/72** (11), pp. 95-98.

[39] Lin, J., and Parker, R.G., 2002, "Mesh Stiffness Variation Instabilities in Two-Stage Gear Systems," Journal of Vibration and Acoustics, **124** (1), pp. 68-76.

[40] Shmulevich, S., and Elata, D., 2017, "A MEMS Implementation of the Classic Meissner Parametric Resonator: Exploring High Order Windows of Unbounded Response," Journal of Microelectromechanical Systems, **26** (2), pp. 325-332.

[41] Gasparetto, C., and Gazzola, F., 2018, "Resonance Tongues for the Hill Equation with Duffing Coefficients and Instabilities in a Nonlinear Beam Equation," Communications in Contemporary Mathematics, **20** (1), pp. 1750022.

[42] Arscott, F. M., 1964, *Periodic Differential Equations*, Pergamon Press Limited, Oxford, England.

[43] Broer, H., and Levi, M., 1995, "Geometrical aspects of stability theory of Hill's equations," Archive for Rational Mechanics and Analysis, **131** (3), pp. 225-240.

[44] Broer, H., and Simó, C., 2000, "Resonance Tongues in Hill's Equations: A Geometric Approach," Journal of Differential Equations, **166** (2), pp. 290–327.

[45] Gan, S., and Zhang, M., 2000, "Resonance Pockets of Hill's Equations with Two-Step Potentials," SIAM Journal of Applied Mathematics, **32** (3), pp. 651-664.

[46] Franco, C., and Collado, J., 2017, "Minimum Damping Needed for Vanishing an Unstable Pocket of a Hill Equation," Proceedings of 9th European Nonlinear Dynamics Conference (ENOC 2017), Budapest, June 25-30, 2017, ID: 200.

[47] Thomson, W., and Tait, P.G., 1888, *Treatise on Natural Philosophy, Vol. I, Part I*, Cambridge University Press, Cambridge.

[48] Ziegler, H., 1952, "Die Stabilitätskriterien der Elastomechanik," Ingenieur-Archiv, **20**, pp. 49–56.

[49] Yakubovich, V.A., and Starzhinski, V.M., 1975, *Linear Differential Equations with Periodic Coefficients*, *Parts II*, John Wiley & Sons, New York.

[50] Franco, C., and Collado, J., 2015, "Ziegler Paradox and Periodic Coefficient Differential Equations," 12th International Conference on Electrical Engineering, Computing Science and Automatic Control (CCE), Mexico City, October 28-30, 2015, pp. 1-5.

[51] Schiehlen, W., Guse, N.: Control of limit cycle oscillations. In: Rega G., Vestroni F. (eds.) IUTAM Symposium on Chaotic Dynamics and Control of Systems and Processes in Mechanics, pp. 429-439. Springer, Netherlands (2005)

[52] Younis, M.I.: MEMS Linear and Nonlinear Statics and Dynamics. Springer, New York (2011)

[53] Föllinger, O.: Design of Time Varying Systems by Pole Assignment. at – Automatisierungstechnik. 26, 189-196 (1978)

[54] D'Angelo, H.: Linear Time-Varying Systems: Analysis and Synthesis. Allyn and Bacon, MA (1970)

[55] Calico, R.A., Wiesel, W.E.: Control of Time-Periodic Systems. Journal of Guidance, Control, and Dynamics. 7, 671-676 (1984)

[56] Alfhaid, M.S., Lee, G.K.F.: Pole Assignment in Linear Time-Varying Systems Using State Feedback. Twenty-Second Asilomar Conference on Signals, Systems and Computers, Pacific Grove, CA, USA. 241-245 (1988)

[57] Kwakernaak, H., Sivan, R.: Linear Optimal Control Systems. Wiley-Interscience, New York (1972)

[58] Sinha, S.C., Joseph, P.: Control of General Dynamic Systems with periodically varying parameters via Liapunov-Floquet transformation. ASME Journal of Dynamic Systems, Measurement, and Control. 116, 650-658 (1994)

[59] Lee, Y.J., Balas, M.J.: Controller Design of Periodic Time-Varying Systems via Time-Invariant Methods. Journal of Guidance, Control, and Dynamics. 22, 486-488 (1999)

[60] Montagnier, P., Spiteri, R.J., Angeles, J.: Pitfalls of a Least-Squares-Equivalent Controller for Linear, Time-Periodic Systems. International Journal of Control. 74, 199-204 (2001)

[61] Middleton, R.H., Goodwin, G.C.: Adaptive Control of Time-Varying Linear Systems. IEEE Transactions on Automatic Control. 33, 150-155 (1988)

[62] Zhang, Y, Sinha, S.C.: Development of a Feedback Linearization Technique for Parametrically Excited Nonlinear Systems via Normal Forms. ASME Journal of Computational and Nonlinear Dynamics. 2, 124-131 (2006)

[63] Pettini M.: Controlling Chaos through parametric excitations. In: Lima R., Streit L., Vilela Mendes R. (eds) Dynamics and Stochastic Processes Theory and Applications. 355, 242-250 (1988)

[64] Lima, R., Pettini, M.: Parametric Resonant Control of Chaos. International Journal of Bifurcation and Chaos. 8, 1675–1684 (1998)

[65] Hübler, A., Lüscher, E.: Resonant Stimulation and Control of Nonlinear Oscillators. Naturwissenschaft. 76, 67–72 (1989)

[66] Jackson, E. A., Grosu, I.: An Open-Plus-Closed-Loop (OPCL) Control of Complex Dynamic Systems. Physica D: Nonlinear Phenomena. 85, 1–9 (1995)

[67] Ott, E., Grebogi, C, Yorke, J.A.: Controlling Chaos. Physical review Letters. 64, 1196-1199 (1990)

[68] Pyragas, K.: Continuous Control of Chaos by Self Controlling Feedback. Physics Letters A. 170, 421-428 (1992)

[69] Chen, C.C.: Direct Chaotic Dynamics to Any Desired Orbits via a Closed-Loop Control. Physics Letters A. 213, 148-154 (1996)

[70] Sinha, S.C., Henrichs, J.T., Ravindra, B.: A General Approach in the Design of Active Controllers for Nonlinear Systems Exhibiting Chaos. International Journal of Bifurcation and Chaos. 10, 165-178 (2000)

[71] Sinha, S.C., Gourdon, E., Zhang, Y.: Control of Time-Periodic Systems via Symbolic Computation with Application to Chaos Control. Communications in Nonlinear Science and Numerical Simulation. 10, 835-854 (2005)

[72] Grimshaw, R., 1990, Nonlinear Ordinary Differential Equations, Blackwell Scientific Publications, Massachusetts.

[73] Yakubovich, V.A., and Starzhinski, V.M., 1975, Linear Differential Equations with Periodic Coefficients, Parts I and Parts II, John Wiley & Sons, New York.

[74] Butcher, E., and Sinha, S.C., 1998, "Symbolic Computation of Local Stability and Bifurcation Surfaces of Time-Periodic Nonlinear Systems," Nonlinear Dynamics, 17(1), pp. 1-21.

[75] Bogoljubov, N.N., Mitropoliskii, Ju. A., and Samoilenko, A.M., 1976, Methods of Accelerated Convergence in Nonlinear Mechanics, Hindustan Publishing Corporation, Delhi.

[76] Murdock, J.A., 1978, "On the Floquet problem for Quasiperiodic Systems," Proceedings of the American Mathematical Society, 68(2), pp. 179-184.

[77] Sato, C., 1966, "Correction of Stability Curves in Hill-Meissner's Equation," Mathematics of Computation, 20(93), pp. 98-106.

[78] Brogan, W.L., 1991, Modern Control theory, Prentice Hall, New Jersey.

[79] Verhulst, F., 2012, "Perturbation Analysis of Parametric Resonance," *Mathematics of Complexity and Dynamical Systems*. R.A. Meyers, 2012, Springer, New York, pp. 1251-1264.

[80] Magnus, W., and Winkler, S., 1966, *Hill's Equation*, John Wiley & Sons, Inc., New York.

[81] Vidyasagar, M: Nonlinear Systems Analysis. Prentice Hall, New Jersey (1993)

[82] Dorning, J.J., Decker, W.J., Holloway, J.P.: Controlling the Dynamics of Chaotic Convective Flows. In: Kim, J.H., Stringer, J. (eds.) Applied chaos, pp.189-206. John Wiley & Sons, Inc., New York (1992)

[83] Infante, E.F.: On the Stability of Some Linear Nonautonomous Random Systems. ASME Journal of Applied Mechanics. 35, 7-12 (1968)

[84] Schur, J.: Über Potenzreihen, die im Innern des Einheitskreises beschränkt sind. Journal für die reine und angewandte Mathematik (Crelle's Journal). 147, 205-232 (1917)

[85] Cohn, A.: Über die Anzahl der Wurzeln einer algebraischen Gleichung in einem Kreise. Mathematische Zeitschrift. 14, 110-148 (1922)

[86] Rhoads, J. F., Guo, C., Fedder, G. K.: Parametrically Excited Micro- and Nanosystems. In: Brand, O., Dufour, I., Heinrich, S. M., Josse, F. (eds.) Resonant MEMS, pp. 73-95. Wiley-VCH Verlag GmbH & Co. KGaA, Weinheim (2015)

[87] Lukes, Dahlard L. Differential Equations: Classical to Controlled. Academic Press, New York (1982).

[88] Wu, Min-Yen. "Transformation of a Linear Time-varying System into a Linear Time-Invariant System." International Journal of Control Vol. 27 No. 4 (1978): pp. 589-602.

[89] Sinha, Subhash C., Pandiyan, R. and Bibb, J.S. “Liapunov-Floquet Transformation: Computation and Applications to Periodic Systems.” ASME Journal of Vibration and Acoustics Vol. 118 No. 2 (1996): pp. 209-219.

[90] Butcher, Eric A., Sari, Ma’en S. and Carlson, Tim. “Magnus’ Expansion for Time-Periodic Systems: Parameter-dependent Approximation.” Communications in Nonlinear Science and Numerical Simulation Vol. 14 No. 12 (2009): pp. 4226-4245.

[91] Johnson. Russell A. and Sell, George R. “Smoothness of Spectral Bundles and reducibility of Quasi-Periodic Linear Differential Systems.” Journal of Differential Equations Vol. 41 No. 2 (1981): pp. 262-288.

[92] Jorba, Àngel and Simó, Carles. “On the Reducibility of Linear Differential Equations with Quasi-Periodic Coefficients.” Journal of Differential Equations Vol. 98 No. 1 (1992): pp. 111-124.

[93] Jorba, Àngel, Ramirez-Ros, Rafael and Villanueva, Jordi. “Effective Reducibility of Quasi-Periodic Linear Equations Close to Constant Coefficients.” SIAM Journal of Mathematical Analysis Vol. 28 No. 1 (1997): pp. 178- 188.

[94] Sharma, Ashu and Sinha, Subhash C. “An Approximate Analysis of Quasi- periodic Systems Via Floquét Theory.” ASME Journal of Computational and Nonlinear Dynamics Vol. 13 No. 2 (2018): pp. 021008-021008-18.

Appendix A

The symbolic computation of FTM for Case Study 2 ($\omega_1 = 1.0$ and $\omega_2 = \left(1+\sqrt{5}\right)\Big/2$) is presented in section 2.5. Approximate principal period, $T_a = 112.747$ was divided into 30 equal sub-intervals and then, FTM over the approximate principal period, $T_a = 112.747$ is computed using Eq. (2.34) with 30 Picard iterations and 20 Chebyshev polynomials in each sub-interval. For brevity, only one element of the FTM for the third sub-interval is shown below.

$\Phi_{11}^{(30,20)}(t_3, t_2, a, b) =$ 1. -7.06216 a+8.31235 a^2-3.91354 a^3+0.987073 a^4-0.154908 a^5+0.0165755 a^6-0.00128636 a^7+0.0000757042 a^8-3.49435*10^{-6} a^9+1.29882*10^{-7} a^{10}-3.97078*10^{-9} a^{11}+1.01602*10^{-10} a^{12}-2.20779*10^{-12} a^{13}+4.12481*10^{-14} a^{14}-6.69677*10^{-16} a^{15}+2.57727 b-7.71097 a b+5.81431 a^2 b-2.01022 a^3 b+0.400073 a^4 b-0.05181 a^5 b+0.0047167 a^6 b-0.000318433 a^7 b+0.0000165802 a^8 b-6.86127*10^{-7} a^9 b+2.31097*10^{-8} a^{10} b-6.45863*10^{-10} a^{11} b+1.52189*10^{-11} a^{12} b-3.06429*10^{-13} a^{13} b+5.32817*10^{-15} a^{14} b-2.04847 b^2+0.349669 a b^2+0.402521 a^2 b^2-0.188342 a^3 b^2+0.0384945 a^4 b^2-0.00478743 a^5 b^2+0.000409623 a^6 b^2-0.0000258172 a^7 b^2+1.25376*10^{-6} a^8 b^2-4.84605*10^{-8} a^9 b^2+1.52819*10^{-9} a^{10} b^2-4.01051*10^{-11} a^{11} b^2+8.9231*10^{-13} a^{12} b^2-1.72963*10^{-14} a^{13} b^2-1.46636 b^3+0.788637 a b^3-0.167801 a^2 b^3+0.0176971 a^3 b^3-0.000770441 a^4 b^3-0.0000359646 a^5 b^3+8.0592*10^{-6} a^6 b^3-6.55484*10^{-7} a^7 b^3+3.51141*10^{-8} a^8 b^3-1.40316*10^{-9} a^9 b^3+4.40618*10^{-11} a^{10} b^3-1.13087*10^{-12} a^{11} b^3+2.73084*10^{-14} a^{12} b^3-…

Appendix B

Computer Codes

B.1 Mathematica code for convergence diagram of bifurcation points.

B.2 Mathematica code for Discrete Fourier Transform of a quasi-periodic system.

B.3 Mathematica code for plotting Poincaré maps of a quasi-periodic system.

B.4 Mathematica code for symbolic computation of the state transition matrix of an approximate periodic system.

B.5 Mathematica code containing supporting functions for **B.4**

B.6 Mathematica code to drive Duffing's oscillator to a quasi-periodic square wave.

Note: Mathematica code for symbolic computation of feedback gains to drive the chaotic behavior of a Mathieu-Duffing oscillator to a two-frequency quasi-periodic motion is not included here for the sake of brevity. The code goes over 40 pages and one could utilize **B.4** to write this code.

B.1

```
ClearAll["Global`*"]
SetDirectory[NotebookDirectory[]]

w1 = 1.; w2 = (1/2)*(Sqrt[5] + 1);

wmin = {0.618034, 0.381966, 0.236068, 0.145898, 0.0901699, 0.0557281, 0.0344419,
0.0212862};

ta = {10.1664, 16.4496, 26.616, 43.0656, 69.6816, 112.747, 182.429, 295.176};
tan = ta/10.1664;

i1 = {2, 3, 4, 7, 11, 18, 29, 47};
i2 = {3, 4, 7, 11, 18, 29, 47, 76};

w1n = SetPrecision[Table[i1[[i]]*wmin[[i]], {i, 1, Length[wmin]}], 16];
w2n = SetPrecision[Table[i2[[i]]*wmin[[i]], {i, 1, Length[wmin]}], 16];

ae1 = SetPrecision[(w1*w1)/4, 16];
ae2 = SetPrecision[(w2*w2)/4, 16];
aa1 = (w1n*w1n)/4;
aa2 = (w2n*w2n)/4;

err1 = ae1 - aa1;
err2 = ae2 - aa2;
xaxis = Log10[tan];

ListLinePlot[Table[Table[{xaxis[[i]], f[[i]]}, {i, 1, Length[wmin]}], {f, {err1, err2}}],
PlotTheme -> "Monochrome", Frame -> True, MaxPlotPoints -> Infinity, PlotStyle ->
{Black, Dashed}, PlotRange -> All, PlotLegends -> Placed[{"Bifurcation point of region
R1", "Bifurcation point of region R2"}, {0.5, 0.5}], FrameLabel ->
{Style[TraditionalForm[HoldForm[Log10[Subscript[T, a]/Subscript[T, a1]]]], FontSize ->
> 20, Black], Style[HoldForm[Subscript[a, e] - Subscript[a, a]], FontSize -> 20, Black]},
FrameTicksStyle -> Directive[Black, 22], PlotMarkers -> {{●, 18}, {▲, 18}}]
```

B.2

```
ClearAll["Global`*"]
SetDirectory[NotebookDirectory[]]

toi = 58505;
a = 1.01977;
b = 0.25;
d = 0.;
w1 = 1;
w2 = Sqrt[3];
w3 = Sqrt[11];

A1 = {{0., 1.}, {-a, -d}};
A2 = {{0., 0.}, {(-b)*Cos[w1*y], 0.}};
A3 = {{0., 0.}, {(-b)*Cos[w2*y] - b*Cos[w3*y], 0.}};
A = A1 + A2 + A3

si = 0.001;
sf = 1/si;
st = 53928;

xsol = NDSolve[{Derivative[1][x1][y] == A[[1,1]]*x1[y] + A[[1,2]]*x2[y],
Derivative[1][x2][y] == A[[2,1]]*x1[y] + A[[2,2]]*x2[y], x1[0] == 0.1, x2[0] == 0.1},
{x1, x2}, {y, 0, toi}, InterpolationOrder -> All, MaxSteps -> Infinity];

tdata = Flatten[Table[t, {t, 0, st - si, si}]];
x1data = Flatten[Table[x1[y] /. xsol, {y, 0, st - si, si}]];
x1datan = Flatten[Table[(x1[y] /. xsol)*HannWindow[(y - st/2)/st], {y, 0, st - si, si}]];
y1 = Length[x1datan];
x1data = Flatten[Join[x1datan]];
x1four = Chop[Flatten[2*2*(Length[x1data]/y1)*Abs[Fourier[x1data, FourierParameters
-> {-1, 1}]]], 10^(-6)];
x1data1 = Take[x1four, Length[x1four]/2];
freq1 = Flatten[Table[(sf/Length[x1data])*2*Pi*z, {z, 0, Length[x1data1] - 1, 1}]];
nqfreq = N[2*Pi*(sf/2)];
Print["Nyquist frequency is  ", nqfreq];

ListLinePlot[Table[{freq1[[i]], x1data1[[i]]}, {i, 1, Length[freq1]}], PlotRange -> {{0,
10}, All}, PlotStyle -> {Black}, Frame -> True, FrameLabel ->
{Style[HoldForm[Frequency], FontSize -> 22, Black], Style[HoldForm[Amplitude],
FontSize -> 22, Black]}, FrameTicksStyle -> Directive[Black, 22]]
sot2 = Sort[x1data1, Greater];
pp2 = Position[x1data1, sot2[[1]]];
N[(pp2 - 1)*((sf/Length[x1data])*2*Pi)]
```

B.3

```
ClearAll["Global`*"]
SetDirectory[NotebookDirectory[]]

toi = 91*289.934 + 5;
a = 0.19589
b = 0.1
d = 0.;
w = 0.0216711;
w1 = 46*w;
w2 = 80*w;
w3 = 153*w;
P = N[2*(Pi/w)]
P = 289.934;
Print[Style["Period is ", 15, Black, Bold], Style[P, 15, Black, Bold], Style[" seconds ",
15, Black, Bold]];

A1 = {{0., 1.}, {-a, -d}};
A2 = {{0., 0.}, {(-b)*Cos[1*y], 0.}};
A3 = {{0., 0.}, {(-b)*Cos[Sqrt[3]*y] - b*Cos[Sqrt[11]*y], 0.}};
A = A1 + A2 + A3;

top = toi
int = 1.
xsol = NDSolve[{Derivative[1][x1][y] == A[[1,1]]*x1[y] + A[[1,2]]*x2[y],
      Derivative[1][x2][y] == A[[2,1]]*x1[y] + A[[2,2]]*x2[y], x1[0] == 0.1, x2[0] ==
0.1}, {x1, x2}, {y, 0, toi}, InterpolationOrder -> All, MaxSteps -> Infinity];

xT = Flatten[{x1[y] /. xsol, x2[y] /. xsol}];
Edata = Table[xT, {y, 0, top, int}];

p1 = ListPlot[Edata, PlotRange -> All, PlotStyle -> {PointSize[0.01], Black},
PlotMarkers -> {Automatic, Tiny}, Frame -> True, PlotLegends ->
Placed[{Style[HoldForm["Original system"], FontSize -> 18, Black]}, {0.9, 0.8}]];

xplot1 = Plot[Evaluate[x1[y] /. xsol], {y, 0., top}, PlotRange -> All, PlotStyle -> {Black,
Dashed}]
vplot1 = Plot[Evaluate[x2[y] /. xsol], {y, 0., top}, PlotRange -> All, PlotStyle -> {Black,
Dashed}]

nop = Quotient[toi, P]
an = a;
bn = b;
dn = d;
```

```
B1 = {{0., 1.}, {-an, -dn}};
B2 = {{0., 0.}, {(-bn)*Cos[w1*y], 0.}};
B3 = {{0., 0.}, {(-bn)*Cos[w2*y] - bn*Cos[w3*y], 0.}};
B = B1 + B2 + B3;

icφ = {{1., 0.}, {0., 1.}};
icx = {{0.1}, {0.1}};

φsol1 = NDSolve[{Derivative[1][φ11][y] == B[[1,1]]*φ11[y] + B[[1,2]]*φ21[y],
      Derivative[1][φ21][y] == B[[2,1]]*φ11[y] + B[[2,2]]*φ21[y], φ11[0] ==
icφ[[All,1]][[1]], φ21[0] == icφ[[All,1]][[2]]}, {φ11, φ21}, {y, 0, toi}, MaxSteps ->
Infinity, InterpolationOrder -> All];
φsol2 = NDSolve[{Derivative[1][φ12][y] == B[[1,1]]*φ12[y] + B[[1,2]]*φ22[y],
      Derivative[1][φ22][y] == B[[2,1]]*φ12[y] + B[[2,2]]*φ22[y], φ12[0] ==
icφ[[All,2]][[1]], φ22[0] == icφ[[All,2]][[2]]}, {φ12, φ22}, {y, 0, toi}, MaxSteps ->
Infinity, InterpolationOrder -> All];

eT = Flatten[{φ11[y] /. φsol1 /. y -> P, φ12[y] /. φsol2 /. y -> P, φ21[y] /. φsol1 /. y -> P,
      φ22[y] /. φsol2 /. y -> P}];
et = Flatten[{φ11[y] /. φsol1, φ12[y] /. φsol2, φ21[y] /. φsol1, φ22[y] /. φsol2}];
φT = {{eT[[1]], eT[[2]]}, {eT[[3]], eT[[4]]}}
φt = {{et[[1]], et[[2]]}, {et[[3]], et[[4]]}};

Eigenvalues[φT]
Abs[Eigenvalues[φT]]

φδ[n_] := φt . MatrixPower[φT, n - 1];
figure1[n_] := ListPlot[Table[Flatten[φδ[n] . icx], {y, 0, P, int}], PlotRange -> All,
    PlotStyle -> {PointSize[0.01], Black}, PlotMarkers -> {Automatic, Tiny}, Frame ->
True];
xplot2[n_] := Plot[Evaluate[(φδ[n] . icx)[[1,1]] /. y -> t - (n - 1)*P], {t, (n - 1)*P, n*P},
PlotRange -> All, PlotStyle -> {Red, Dashed}, AxesOrigin -> {0, 0}];
vplot2[n_] := Plot[Evaluate[(φδ[n] . icx)[[2,1]] /. y -> t - (n - 1)*P], {t, (n - 1)*P, n*P},
PlotRange -> All, PlotStyle -> {Red, Dashed}, AxesOrigin -> {0, 0}];

x = ListPlot[Table[Flatten[φt . icx], {y, 0, P, int}], PlotRange -> All, PlotStyle ->
{PointSize[0.01], Black}, PlotMarkers -> {Automatic, Tiny}, Frame -> True,
    PlotLegends -> Placed[{Style[HoldForm["Approximate system"], FontSize -> 18,
Black]}, {0.8, 0.8}]];

xplot = Plot[(φt . icx)[[1,1]], {y, 0, P}, PlotRange -> All, PlotStyle -> {Red, Dashed}];
vplot = Plot[(φt . icx)[[2,1]], {y, 0, P}, PlotRange -> All, PlotStyle -> {Red, Dashed}];

For[i = 2, i <= nop, i++, x = Show[figure1[i], x, PlotRange -> All];
```

```
   xplot = Show[xplot2[i], xplot, PlotRange -> All]; vplot = Show[vplot2[i], vplot,
PlotRange -> All]; ]

Show[x, p1, PlotRange -> All, FrameLabel -> {Style[HoldForm[x1], FontSize -> 22,
Black], Style[HoldForm[x2], FontSize -> 22, Black]}, FrameTicksStyle ->
Directive[Black, 22], AxesOrigin -> {0, 0}]

Show[xplot, xplot1, PlotRange -> All]

Show[vplot, vplot1, PlotRange -> All]

Show[x, PlotRange -> All, FrameLabel -> {Style[HoldForm[x1], FontSize -> 22, Black],
      Style[HoldForm[x2], FontSize -> 22, Black]}, FrameTicksStyle -> Directive[Black,
22], AxesOrigin -> {0, 0}]

Show[p1, PlotRange -> All, FrameLabel -> {Style[HoldForm[x1], FontSize -> 22,
Black], Style[HoldForm[x2], FontSize -> 22, Black]}, FrameTicksStyle ->
Directive[Black, 22], AxesOrigin -> {0, 0}]
```

B.4

```
ClearAll["Global`*"]
ClearSystemCache[]
SetDirectory[NotebookDirectory[]]

Get["subfunctions2`"]

w=0.0557281;
(* Frequencies present in a system *)
w1=18*w;w2=29*w;
(*a11=1.8;
b11=0.72;
d11=0.1;*)
ch=20;
pc=30;

(*Period of quasi periodic system *)
P=112.747;


(* Sub-Intervals *)
nos=30;
P0=0/nos;
P1=P/nos;P2=2P/nos;P3=3P/nos;P4=4P/nos;P5=5P/nos;P6=6P/nos;P7=7P/nos;
P8=8P/nos;P9=9P/nos;P10=10 P/nos;P11=11 P/nos;P12=12 P/nos;P13=13 P/nos;
P14=14 P/nos;P15=15 P/nos;P16=16 P/nos;P17=17P/nos;P18=18P/nos;P19=19P/nos;
P20=20 P/nos;P21=21P/nos;P22=22P/nos;P23=23P/nos;P24=24P/nos;P25=25P/nos;
P26=26P/nos;P27=27P/nos;P28=28P/nos;P29=29P/nos;P30=30 P/nos;(*P31=31 P/nos;*)

(* τ1 , τ2 , τ3 varies from 0 to 1 *)
y1=P0+(P1-P0)*τ1;y2=P1+(P2-P1)*τ2;y3=P2+(P3-P2)*τ3;y4=P3+(P4-P3)*τ4;
y5=P4+(P5-P4)*τ5;y6=P5+(P6-P5)*τ6;y7=P6+(P7-P6)*τ7;y8=P7+(P8-P7)*τ8;
y9=P8+(P9-P8)*τ9;y10=P9+(P10-P9)*τ10;y11=P10+(P11-P10)*τ11;
y12=P11+(P12-P11)*τ12;y13=P12+(P13-P12)*τ13;y14=P13+(P14-P13)*τ14;
y15=P14+(P15-P14)*τ15;y16=P15+(P16-P15)*τ16;y17=P16+(P17-P16)*τ17;
y18=P17+(P18-P17)*τ18;y19=P18+(P19-P18)*τ19;y20=P19+(P20-P19)*τ20;
y21=P20+(P21-P20)*τ21;y22=P21+(P22-P21)*τ22;y23=P22+(P23-P22)*τ23;
y24=P23+(P24-P23)*τ24;y25=P24+(P25-P24)*τ25;y26=P25+(P26-P25)*τ26;
y27=P26+(P27-P26)*τ27;y28=P27+(P28-P27)*τ28;y29=P28+(P29-P28)*τ29;
y30=P29+(P30-P29)*τ30;(*y31=P30+(P31-P30)*τ31;*)

eqsubw1τ1=Chop[TrigExpand[N[Cos[w1 y1]]]];
eqsubw1τ2=Chop[TrigExpand[N[Cos[w1 y2]]]];
eqsubw1τ3=Chop[TrigExpand[N[Cos[w1 y3]]]];
```

```
eqsubw1τ4=Chop[TrigExpand[N[Cos[w1 y4]]]];
eqsubw1τ5=Chop[TrigExpand[N[Cos[w1 y5]]]];
eqsubw1τ6=Chop[TrigExpand[N[Cos[w1 y6]]]];
eqsubw1τ7=Chop[TrigExpand[N[Cos[w1 y7]]]];
eqsubw1τ8=Chop[TrigExpand[N[Cos[w1 y8]]]];
eqsubw1τ9=Chop[TrigExpand[N[Cos[w1 y9]]]];
eqsubw1τ10=Chop[TrigExpand[N[Cos[w1 y10]]]];
eqsubw1τ11=Chop[TrigExpand[N[Cos[w1 y11]]]];
eqsubw1τ12=Chop[TrigExpand[N[Cos[w1 y12]]]];
eqsubw1τ13=Chop[TrigExpand[N[Cos[w1 y13]]]];
eqsubw1τ14=Chop[TrigExpand[N[Cos[w1 y14]]]];
eqsubw1τ15=Chop[TrigExpand[N[Cos[w1 y15]]]];
eqsubw1τ16=Chop[TrigExpand[N[Cos[w1 y16]]]];
eqsubw1τ17=Chop[TrigExpand[N[Cos[w1 y17]]]];
eqsubw1τ18=Chop[TrigExpand[N[Cos[w1 y18]]]];
eqsubw1τ19=Chop[TrigExpand[N[Cos[w1 y19]]]];
eqsubw1τ20=Chop[TrigExpand[N[Cos[w1 y20]]]];
eqsubw1τ21=Chop[TrigExpand[N[Cos[w1 y21]]]];
eqsubw1τ22=Chop[TrigExpand[N[Cos[w1 y22]]]];
eqsubw1τ23=Chop[TrigExpand[N[Cos[w1 y23]]]];
eqsubw1τ24=Chop[TrigExpand[N[Cos[w1 y24]]]];
eqsubw1τ25=Chop[TrigExpand[N[Cos[w1 y25]]]];
eqsubw1τ26=Chop[TrigExpand[N[Cos[w1 y26]]]];
eqsubw1τ27=Chop[TrigExpand[N[Cos[w1 y27]]]];
eqsubw1τ28=Chop[TrigExpand[N[Cos[w1 y28]]]];
eqsubw1τ29=Chop[TrigExpand[N[Cos[w1 y29]]]];
eqsubw1τ30=Chop[TrigExpand[N[Cos[w1 y30]]]];
(*eqsubw1τ31=Chop[TrigExpand[N[Cos[w1 y31]]]];*)

eqsubw2τ1=Chop[TrigExpand[N[Cos[w2 y1]]]];
eqsubw2τ2=Chop[TrigExpand[N[Cos[w2 y2]]]];
eqsubw2τ3=Chop[TrigExpand[N[Cos[w2 y3]]]];
eqsubw2τ4=Chop[TrigExpand[N[Cos[w2 y4]]]];
eqsubw2τ5=Chop[TrigExpand[N[Cos[w2 y5]]]];
eqsubw2τ6=Chop[TrigExpand[N[Cos[w2 y6]]]];
eqsubw2τ7=Chop[TrigExpand[N[Cos[w2 y7]]]];
eqsubw2τ8=Chop[TrigExpand[N[Cos[w2 y8]]]];
eqsubw2τ9=Chop[TrigExpand[N[Cos[w2 y9]]]];
eqsubw2τ10=Chop[TrigExpand[N[Cos[w2 y10]]]];
eqsubw2τ11=Chop[TrigExpand[N[Cos[w2 y11]]]];
eqsubw2τ12=Chop[TrigExpand[N[Cos[w2 y12]]]];
eqsubw2τ13=Chop[TrigExpand[N[Cos[w2 y13]]]];
eqsubw2τ14=Chop[TrigExpand[N[Cos[w2 y14]]]];
eqsubw2τ15=Chop[TrigExpand[N[Cos[w2 y15]]]];
eqsubw2τ16=Chop[TrigExpand[N[Cos[w2 y16]]]];
eqsubw2τ17=Chop[TrigExpand[N[Cos[w2 y17]]]];
```

```
eqsubw2τ18=Chop[TrigExpand[N[Cos[w2 y18]]]];
eqsubw2τ19=Chop[TrigExpand[N[Cos[w2 y19]]]];
eqsubw2τ20=Chop[TrigExpand[N[Cos[w2 y20]]]];
eqsubw2τ21=Chop[TrigExpand[N[Cos[w2 y21]]]];
eqsubw2τ22=Chop[TrigExpand[N[Cos[w2 y22]]]];
eqsubw2τ23=Chop[TrigExpand[N[Cos[w2 y23]]]];
eqsubw2τ24=Chop[TrigExpand[N[Cos[w2 y24]]]];
eqsubw2τ25=Chop[TrigExpand[N[Cos[w2 y25]]]];
eqsubw2τ26=Chop[TrigExpand[N[Cos[w2 y26]]]];
eqsubw2τ27=Chop[TrigExpand[N[Cos[w2 y27]]]];
eqsubw2τ28=Chop[TrigExpand[N[Cos[w2 y28]]]];
eqsubw2τ29=Chop[TrigExpand[N[Cos[w2 y29]]]];
eqsubw2τ30=Chop[TrigExpand[N[Cos[w2 y30]]]];
(*eqsubw2τ31=Chop[TrigExpand[N[Cos[w2 y31]]]];*)

(* Angles for expansion *)

xw11=N[w1(P1-P0)];xw12=N[w1(P2-P1)];xw13=N[w1(P3-P2)];xw14=N[w1(P4-P3)];
xw15=N[w1(P5-P4)];xw16=N[w1(P6-P5)];xw17=N[w1(P7-P6)];xw18=N[w1(P8-P7)];
xw19=N[w1(P9-P8)];xw110=N[w1(P10-P9)];xw111=N[w1(P11-P10)];
xw112=N[w1(P12-P11)];xw113=N[w1(P13-P12)];xw114=N[w1(P14-P13)];
xw115=N[w1(P15-P14)];xw116=N[w1(P16-P15)];xw117=N[w1(P17-P16)];
xw118=N[w1(P18-P17)];xw119=N[w1(P19-P18)];xw120=N[w1(P20-P19)];
xw121=N[w1(P21-P20)];xw122=N[w1(P22-P21)];xw123=N[w1(P23-P22)];
xw124=N[w1(P24-P23)];xw125=N[w1(P25-P24)];xw126=N[w1(P26-P25)];
xw127=N[w1(P27-P26)];xw128=N[w1(P28-P27)];xw129=N[w1(P29-P28)];
xw130=N[w1(P30-P29)];(*xw131=N[w1(P31-P30)];*)


xw21=N[w2(P1-P0)];xw22=N[w2(P2-P1)];xw23=N[w2(P3-P2)];xw24=N[w2(P4-P3)];
xw25=N[w2(P5-P4)];xw26=N[w2(P6-P5)];xw27=N[w2(P7-P6)];xw28=N[w2(P8-P7)];
xw29=N[w2(P9-P8)];xw210=N[w2(P10-P9)];xw211=N[w2(P11-P10)];
xw212=N[w2(P12-P11)];xw213=N[w2(P13-P12)];xw214=N[w2(P14-P13)];
xw215=N[w2(P15-P14)];xw216=N[w2(P16-P15)];xw217=N[w2(P17-P16)];
xw218=N[w2(P18-P17)];xw219=N[w2(P19-P18)];xw220=N[w2(P20-P19)];
xw221=N[w2(P21-P20)];xw222=N[w2(P22-P21)];xw223=N[w2(P23-P22)];
xw224=N[w2(P24-P23)];xw225=N[w2(P25-P24)];xw226=N[w2(P26-P25)];
xw227=N[w2(P27-P26)];xw228=N[w2(P28-P27)];xw229=N[w2(P29-P28)];
xw230=N[w2(P30-P29)];(*xw231=N[w2(P31-P30)];*)

α=0.0;
β=1.0;
γ1=(β+α)/2;
γ2=(β-α)/2;
ξ=(2.0*τ-α-β)/(β-α);
```

```
(* m = Number of chebyshev terms *)
m=ch;
If[EvenQ[m]==True,
 n1=(m)/2;
 n2=n1-1;,
 n1=(m+1)/2;
 n2=n1-2;
 ]

cosxτ[x_]:=Simplify[Cos[γ1*x]*(Sum[2*(((-1)^n)*BesselJ[2*n,γ2*x]*T[2*n]),{n,1,n1-
1}])+Cos[γ1*x]*BesselJ[0,γ2*x]*T[0]-Sin[γ1*x]*2*(Sum[(((-
1)^n)*BesselJ[2*n+1,γ2*x]*T[2*n+1]),{n,0,n2}])];
sinxτ[x_]:=Simplify[(Cos[γ1 x]*2*Sum[(((-
1)^n)*BesselJ[2*n+1,γ2*x]*T[2*n+1]),{n,0,n2}])+Sin[γ1
x]*BesselJ[0,γ2*x]*T[0]+Sin[γ1 x]*2*Sum[(((-
1)^n)*BesselJ[2*n,γ2*x]*T[2*n]),{n,1,n1-1}]];

eqw11=Simplify[eqsubw1τ1/.{Cos[xw11 τ1]->cosxτ[xw11],Sin[xw11 τ1]
        ->sinxτ[xw11]}];
eqw12=Simplify[eqsubw1τ2/.{Cos[xw12 τ2]->cosxτ[xw12],Sin[xw12 τ2]
        ->sinxτ[xw12]}];
eqw13=Simplify[eqsubw1τ3/.{Cos[xw13 τ3]->cosxτ[xw13],Sin[xw13 τ3]
        ->sinxτ[xw13]}];
eqw14=Simplify[eqsubw1τ4/.{Cos[xw14 τ4]->cosxτ[xw14],Sin[xw14 τ4]
        ->sinxτ[xw14]}];
eqw15=Simplify[eqsubw1τ5/.{Cos[xw15 τ5]->cosxτ[xw15],Sin[xw15 τ5]
        ->sinxτ[xw15]}];
eqw16=Simplify[eqsubw1τ6/.{Cos[xw16 τ6]->cosxτ[xw16],Sin[xw16 τ6]
        ->sinxτ[xw16]}];
eqw17=Simplify[eqsubw1τ7/.{Cos[xw17 τ7]->cosxτ[xw17],Sin[xw17 τ7]
        ->sinxτ[xw17]}];
eqw18=Simplify[eqsubw1τ8/.{Cos[xw18 τ8]->cosxτ[xw18],Sin[xw18 τ8]
        ->sinxτ[xw18]}];
eqw19=Simplify[eqsubw1τ9/.{Cos[xw19 τ9]->cosxτ[xw19],Sin[xw19 τ9]
        ->sinxτ[xw19]}];
eqw110=Simplify[eqsubw1τ10/.{Cos[xw110 τ10]->cosxτ[xw110],Sin[xw110 τ10]
        ->sinxτ[xw110]}];
eqw111=Simplify[eqsubw1τ11/.{Cos[xw111 τ11]->cosxτ[xw111],Sin[xw111 τ11]
        ->sinxτ[xw111]}];
eqw112=Simplify[eqsubw1τ12/.{Cos[xw112 τ12]->cosxτ[xw112],Sin[xw112 τ12]
        ->sinxτ[xw112]}];
eqw113=Simplify[eqsubw1τ13/.{Cos[xw113 τ13]->cosxτ[xw113],Sin[xw113 τ13]
        ->sinxτ[xw113]}];
eqw114=Simplify[eqsubw1τ14/.{Cos[xw114 τ14]->cosxτ[xw114],Sin[xw114 τ14]
        ->sinxτ[xw114]}];
```

```
eqw115=Simplify[eqsubw1τ15/.{Cos[xw115 τ15]->cosxτ[xw115],Sin[xw115 τ15]
        ->sinxτ[xw115]}];
eqw116=Simplify[eqsubw1τ16/.{Cos[xw116 τ16]->cosxτ[xw116],Sin[xw116 τ16]
        ->sinxτ[xw116]}];
eqw117=Simplify[eqsubw1τ17/.{Cos[xw117 τ17]->cosxτ[xw117],Sin[xw117 τ17]
        ->sinxτ[xw117]}];
eqw118=Simplify[eqsubw1τ18/.{Cos[xw118 τ18]->cosxτ[xw118],Sin[xw118 τ18]
        ->sinxτ[xw118]}];
eqw119=Simplify[eqsubw1τ19/.{Cos[xw119 τ19]->cosxτ[xw119],Sin[xw119 τ19]
        ->sinxτ[xw119]}];
eqw120=Simplify[eqsubw1τ20/.{Cos[xw120 τ20]->cosxτ[xw120],Sin[xw120 τ20]
        ->sinxτ[xw120]}];
eqw121=Simplify[eqsubw1τ21/.{Cos[xw121 τ21]->cosxτ[xw121],Sin[xw121 τ21]
        ->sinxτ[xw121]}];
eqw122=Simplify[eqsubw1τ22/.{Cos[xw122 τ22]->cosxτ[xw122],Sin[xw122 τ22]
        ->sinxτ[xw122]}];
eqw123=Simplify[eqsubw1τ23/.{Cos[xw123 τ23]->cosxτ[xw123],Sin[xw123 τ23]
        ->sinxτ[xw123]}];
eqw124=Simplify[eqsubw1τ24/.{Cos[xw124 τ24]->cosxτ[xw124],Sin[xw124 τ24]
        ->sinxτ[xw124]}];
eqw125=Simplify[eqsubw1τ25/.{Cos[xw125 τ25]->cosxτ[xw125],Sin[xw125 τ25]
        ->sinxτ[xw125]}];
eqw126=Simplify[eqsubw1τ26/.{Cos[xw126 τ26]->cosxτ[xw126],Sin[xw126 τ26]
        ->sinxτ[xw126]}];
eqw127=Simplify[eqsubw1τ27/.{Cos[xw127 τ27]->cosxτ[xw127],Sin[xw127 τ27]
        ->sinxτ[xw127]}];
eqw128=Simplify[eqsubw1τ28/.{Cos[xw128 τ28]->cosxτ[xw128],Sin[xw128 τ28]
        ->sinxτ[xw128]}];
eqw129=Simplify[eqsubw1τ29/.{Cos[xw129 τ29]->cosxτ[xw129],Sin[xw129 τ29]
        ->sinxτ[xw129]}];
eqw130=Simplify[eqsubw1τ30/.{Cos[xw130 τ30]->cosxτ[xw130],Sin[xw130 τ30]
        ->sinxτ[xw130]}];


eqw21=Simplify[eqsubw2τ1/.{Cos[xw21 τ1]->cosxτ[xw21],Sin[xw21 τ1]
        ->sinxτ[xw21]}];
eqw22=Simplify[eqsubw2τ2/.{Cos[xw22 τ2]->cosxτ[xw22],Sin[xw22 τ2]
        ->sinxτ[xw22]}];
eqw23=Simplify[eqsubw2τ3/.{Cos[xw23 τ3]->cosxτ[xw23],Sin[xw23 τ3]
        ->sinxτ[xw23]}];
eqw24=Simplify[eqsubw2τ4/.{Cos[xw24 τ4]->cosxτ[xw24],Sin[xw24 τ4]
        ->sinxτ[xw24]}];
eqw25=Simplify[eqsubw2τ5/.{Cos[xw25 τ5]->cosxτ[xw25],Sin[xw25 τ5]
        ->sinxτ[xw25]}];
eqw26=Simplify[eqsubw2τ6/.{Cos[xw26 τ6]->cosxτ[xw26],Sin[xw26 τ6]
        ->sinxτ[xw26]}];
```

```
eqw27=Simplify[eqsubw2τ7/.{Cos[xw27 τ7]->cosxτ[xw27],Sin[xw27 τ7]
        ->sinxτ[xw27]}];
eqw28=Simplify[eqsubw2τ8/.{Cos[xw28 τ8]->cosxτ[xw28],Sin[xw28 τ8]
        ->sinxτ[xw28]}];
eqw29=Simplify[eqsubw2τ9/.{Cos[xw29 τ9]->cosxτ[xw29],Sin[xw29 τ9]
        ->sinxτ[xw29]}];
eqw210=Simplify[eqsubw2τ10/.{Cos[xw210 τ10]->cosxτ[xw210],Sin[xw210 τ10]
        ->sinxτ[xw210]}];
eqw211=Simplify[eqsubw2τ11/.{Cos[xw211 τ11]->cosxτ[xw211],Sin[xw211 τ11]
        ->sinxτ[xw211]}];
eqw212=Simplify[eqsubw2τ12/.{Cos[xw212 τ12]->cosxτ[xw212],Sin[xw212 τ12]
        ->sinxτ[xw212]}];
eqw213=Simplify[eqsubw2τ13/.{Cos[xw213 τ13]->cosxτ[xw213],Sin[xw213 τ13]
        ->sinxτ[xw213]}];
eqw214=Simplify[eqsubw2τ14/.{Cos[xw214 τ14]->cosxτ[xw214],Sin[xw214 τ14]
        ->sinxτ[xw214]}];
eqw215=Simplify[eqsubw2τ15/.{Cos[xw215 τ15]->cosxτ[xw215],Sin[xw215 τ15]
        ->sinxτ[xw215]}];
eqw216=Simplify[eqsubw2τ16/.{Cos[xw216 τ16]->cosxτ[xw216],Sin[xw216 τ16]
        ->sinxτ[xw216]}];
eqw217=Simplify[eqsubw2τ17/.{Cos[xw217 τ17]->cosxτ[xw217],Sin[xw217 τ17]
        ->sinxτ[xw217]}];
eqw218=Simplify[eqsubw2τ18/.{Cos[xw218 τ18]->cosxτ[xw218],Sin[xw218 τ18]
        ->sinxτ[xw218]}];
eqw219=Simplify[eqsubw2τ19/.{Cos[xw219 τ19]->cosxτ[xw219],Sin[xw219 τ19]
        ->sinxτ[xw219]}];
eqw220=Simplify[eqsubw2τ20/.{Cos[xw220 τ20]->cosxτ[xw220],Sin[xw220 τ20]
        ->sinxτ[xw220]}];
eqw221=Simplify[eqsubw2τ21/.{Cos[xw221 τ21]->cosxτ[xw221],Sin[xw221 τ21]
        ->sinxτ[xw221]}];
eqw222=Simplify[eqsubw2τ22/.{Cos[xw222 τ22]->cosxτ[xw222],Sin[xw222 τ22]
        ->sinxτ[xw222]}];
eqw223=Simplify[eqsubw2τ23/.{Cos[xw223 τ23]->cosxτ[xw223],Sin[xw223 τ23]
        ->sinxτ[xw223]}];
eqw224=Simplify[eqsubw2τ24/.{Cos[xw224 τ24]->cosxτ[xw224],Sin[xw224 τ24]
        ->sinxτ[xw224]}];
eqw225=Simplify[eqsubw2τ25/.{Cos[xw225 τ25]->cosxτ[xw225],Sin[xw225 τ25]
        ->sinxτ[xw225]}];
eqw226=Simplify[eqsubw2τ26/.{Cos[xw226 τ26]->cosxτ[xw226],Sin[xw226 τ26]
        ->sinxτ[xw226]}];
eqw227=Simplify[eqsubw2τ27/.{Cos[xw227 τ27]->cosxτ[xw227],Sin[xw227 τ27]
        ->sinxτ[xw227]}];
eqw228=Simplify[eqsubw2τ28/.{Cos[xw228 τ28]->cosxτ[xw228],Sin[xw228 τ28]
        ->sinxτ[xw228]}];
eqw229=Simplify[eqsubw2τ29/.{Cos[xw229 τ29]->cosxτ[xw229],Sin[xw229 τ29]
        ->sinxτ[xw229]}];
```

```
eqw230=Simplify[eqsubw2τ30/.{Cos[xw230 τ30]->cosxτ[xw230],Sin[xw230 τ30]
        ->sinxτ[xw230]}];

ptable=Table[T[i],{i,0,m}];
tst=Table[ChebyshevT[i,ξ],{i,0,m}];
sol=Solve[ptable-tst==0,ptable];

x11=Cos[w1 y];
x22=Cos[w2 y];

yw11=N[(eqw11/.sol)/.τ->((y-P0)/(P1-P0))];
yw12=N[(eqw12/.sol)/.τ->((y-P1)/(P2-P1))];
yw13=N[(eqw13/.sol)/.τ->((y-P2)/(P3-P2))];
yw14=N[(eqw14/.sol)/.τ->((y-P3)/(P4-P3))];
yw15=N[(eqw15/.sol)/.τ->((y-P4)/(P5-P4))];
yw16=N[(eqw16/.sol)/.τ->((y-P5)/(P6-P5))];
yw17=N[(eqw17/.sol)/.τ->((y-P6)/(P7-P6))];
yw18=N[(eqw18/.sol)/.τ->((y-P7)/(P8-P7))];
yw19=N[(eqw19/.sol)/.τ->((y-P8)/(P9-P8))];
yw110=N[(eqw110/.sol)/.τ->((y-P9)/(P10-P9))];
yw111=N[(eqw111/.sol)/.τ->((y-P10)/(P11-P10))];
yw112=N[(eqw112/.sol)/.τ->((y-P11)/(P12-P11))];
yw113=N[(eqw113/.sol)/.τ->((y-P12)/(P13-P12))];
yw114=N[(eqw114/.sol)/.τ->((y-P13)/(P14-P13))];
yw115=N[(eqw115/.sol)/.τ->((y-P14)/(P15-P14))];
yw116=N[(eqw116/.sol)/.τ->((y-P15)/(P16-P15))];
yw117=N[(eqw117/.sol)/.τ->((y-P16)/(P17-P16))];
yw118=N[(eqw118/.sol)/.τ->((y-P17)/(P18-P17))];
yw119=N[(eqw119/.sol)/.τ->((y-P18)/(P19-P18))];
yw120=N[(eqw120/.sol)/.τ->((y-P19)/(P20-P19))];
yw121=N[(eqw121/.sol)/.τ->((y-P20)/(P21-P20))];
yw122=N[(eqw122/.sol)/.τ->((y-P21)/(P22-P21))];
yw123=N[(eqw123/.sol)/.τ->((y-P22)/(P23-P22))];
yw124=N[(eqw124/.sol)/.τ->((y-P23)/(P24-P23))];
yw125=N[(eqw125/.sol)/.τ->((y-P24)/(P25-P24))];
yw126=N[(eqw126/.sol)/.τ->((y-P25)/(P26-P25))];
yw127=N[(eqw127/.sol)/.τ->((y-P26)/(P27-P26))];
yw128=N[(eqw128/.sol)/.τ->((y-P27)/(P28-P27))];
yw129=N[(eqw129/.sol)/.τ->((y-P28)/(P29-P28))];
yw130=N[(eqw130/.sol)/.τ->((y-P29)/(P30-P29))];

yw21=N[(eqw21/.sol)/.τ->((y-P0)/(P1-P0))];
yw22=N[(eqw22/.sol)/.τ->((y-P1)/(P2-P1))];
yw23=N[(eqw23/.sol)/.τ->((y-P2)/(P3-P2))];
yw24=N[(eqw24/.sol)/.τ->((y-P3)/(P4-P3))];
yw25=N[(eqw25/.sol)/.τ->((y-P4)/(P5-P4))];
```

```
yw26=N[(eqw26/.sol)/.τ->((y-P5)/(P6-P5))];
yw27=N[(eqw27/.sol)/.τ->((y-P6)/(P7-P6))];
yw28=N[(eqw28/.sol)/.τ->((y-P7)/(P8-P7))];
yw29=N[(eqw29/.sol)/.τ->((y-P8)/(P9-P8))];
yw210=N[(eqw210/.sol)/.τ->((y-P9)/(P10-P9))];
yw211=N[(eqw211/.sol)/.τ->((y-P10)/(P11-P10))];
yw212=N[(eqw212/.sol)/.τ->((y-P11)/(P12-P11))];
yw213=N[(eqw213/.sol)/.τ->((y-P12)/(P13-P12))];
yw214=N[(eqw214/.sol)/.τ->((y-P13)/(P14-P13))];
yw215=N[(eqw215/.sol)/.τ->((y-P14)/(P15-P14))];
yw216=N[(eqw216/.sol)/.τ->((y-P15)/(P16-P15))];
yw217=N[(eqw217/.sol)/.τ->((y-P16)/(P17-P16))];
yw218=N[(eqw218/.sol)/.τ->((y-P17)/(P18-P17))];
yw219=N[(eqw219/.sol)/.τ->((y-P18)/(P19-P18))];
yw220=N[(eqw220/.sol)/.τ->((y-P19)/(P20-P19))];
yw221=N[(eqw221/.sol)/.τ->((y-P20)/(P21-P20))];
yw222=N[(eqw222/.sol)/.τ->((y-P21)/(P22-P21))];
yw223=N[(eqw223/.sol)/.τ->((y-P22)/(P23-P22))];
yw224=N[(eqw224/.sol)/.τ->((y-P23)/(P24-P23))];
yw225=N[(eqw225/.sol)/.τ->((y-P24)/(P25-P24))];
yw226=N[(eqw226/.sol)/.τ->((y-P25)/(P26-P25))];
yw227=N[(eqw227/.sol)/.τ->((y-P26)/(P27-P26))];
yw228=N[(eqw228/.sol)/.τ->((y-P27)/(P28-P27))];
yw229=N[(eqw229/.sol)/.τ->((y-P28)/(P29-P28))];
yw230=N[(eqw230/.sol)/.τ->((y-P29)/(P30-P29))];


h11=Plot[x11,{y,0,P},PlotRange->All,PlotStyle->{Black}];
hw12=Plot[{yw11},{y,P0,P1},PlotRange->All,PlotStyle->{Red,Dashed}];
hw13=Plot[{yw12},{y,P1,P2},PlotRange->All,PlotStyle->{Red,Dashed}];
hw14=Plot[{yw13},{y,P2,P3},PlotRange->All,PlotStyle->{Red,Dashed}];
hw15=Plot[{yw14},{y,P3,P4},PlotRange->All,PlotStyle->{Red,Dashed}];
hw16=Plot[{yw15},{y,P4,P5},PlotRange->All,PlotStyle->{Red,Dashed}];
hw17=Plot[{yw16},{y,P5,P6},PlotRange->All,PlotStyle->{Red,Dashed}];
hw18=Plot[{yw17},{y,P6,P7},PlotRange->All,PlotStyle->{Red,Dashed}];
hw19=Plot[{yw18},{y,P7,P8},PlotRange->All,PlotStyle->{Red,Dashed}];
hw110=Plot[{yw19},{y,P8,P9},PlotRange->All,PlotStyle->{Red,Dashed}];
hw111=Plot[{yw110},{y,P9,P10},PlotRange->All,PlotStyle->{Red,Dashed}];
hw112=Plot[{yw111},{y,P10,P11},PlotRange->All,PlotStyle->{Red,Dashed}];
hw113=Plot[{yw112},{y,P11,P12},PlotRange->All,PlotStyle->{Red,Dashed}];
hw114=Plot[{yw113},{y,P12,P13},PlotRange->All,PlotStyle->{Red,Dashed}];
hw115=Plot[{yw114},{y,P13,P14},PlotRange->All,PlotStyle->{Red,Dashed}];
hw116=Plot[{yw115},{y,P14,P15},PlotRange->All,PlotStyle->{Red,Dashed}];
hw117=Plot[{yw116},{y,P15,P16},PlotRange->All,PlotStyle->{Red,Dashed}];
hw118=Plot[{yw117},{y,P16,P17},PlotRange->All,PlotStyle->{Red,Dashed}];
hw119=Plot[{yw118},{y,P17,P18},PlotRange->All,PlotStyle->{Red,Dashed}];
```

```
hw120=Plot[{yw119},{y,P18,P19},PlotRange->All,PlotStyle->{Red,Dashed}];
hw121=Plot[{yw120},{y,P19,P20},PlotRange->All,PlotStyle->{Red,Dashed}];
hw122=Plot[{yw121},{y,P20,P21},PlotRange->All,PlotStyle->{Red,Dashed}];
hw123=Plot[{yw122},{y,P21,P22},PlotRange->All,PlotStyle->{Red,Dashed}];
hw124=Plot[{yw123},{y,P22,P23},PlotRange->All,PlotStyle->{Red,Dashed}];
hw125=Plot[{yw124},{y,P23,P24},PlotRange->All,PlotStyle->{Red,Dashed}];
hw126=Plot[{yw125},{y,P24,P25},PlotRange->All,PlotStyle->{Red,Dashed}];
hw127=Plot[{yw126},{y,P25,P26},PlotRange->All,PlotStyle->{Red,Dashed}];
hw128=Plot[{yw127},{y,P26,P27},PlotRange->All,PlotStyle->{Red,Dashed}];
hw129=Plot[{yw128},{y,P27,P28},PlotRange->All,PlotStyle->{Red,Dashed}];
hw130=Plot[{yw129},{y,P28,P29},PlotRange->All,PlotStyle->{Red,Dashed}];
hw131=Plot[{yw130},{y,P29,P30},PlotRange->All,PlotStyle->{Red,Dashed}];


h22=Plot[x22,{y,0,P},PlotRange->All,PlotStyle->{Black}];
hw22=Plot[{yw21},{y,P0,P1},PlotRange->All,PlotStyle->{Red,Dashed}];
hw23=Plot[{yw22},{y,P1,P2},PlotRange->All,PlotStyle->{Red,Dashed}];
hw24=Plot[{yw23},{y,P2,P3},PlotRange->All,PlotStyle->{Red,Dashed}];
hw25=Plot[{yw24},{y,P3,P4},PlotRange->All,PlotStyle->{Red,Dashed}];
hw26=Plot[{yw25},{y,P4,P5},PlotRange->All,PlotStyle->{Red,Dashed}];
hw27=Plot[{yw26},{y,P5,P6},PlotRange->All,PlotStyle->{Red,Dashed}];
hw28=Plot[{yw27},{y,P6,P7},PlotRange->All,PlotStyle->{Red,Dashed}];
hw29=Plot[{yw28},{y,P7,P8},PlotRange->All,PlotStyle->{Red,Dashed}];
hw210=Plot[{yw29},{y,P8,P9},PlotRange->All,PlotStyle->{Red,Dashed}];
hw211=Plot[{yw210},{y,P9,P10},PlotRange->All,PlotStyle->{Red,Dashed}];
hw212=Plot[{yw211},{y,P10,P11},PlotRange->All,PlotStyle->{Red,Dashed}];
hw213=Plot[{yw212},{y,P11,P12},PlotRange->All,PlotStyle->{Red,Dashed}];
hw214=Plot[{yw213},{y,P12,P13},PlotRange->All,PlotStyle->{Red,Dashed}];
hw215=Plot[{yw214},{y,P13,P14},PlotRange->All,PlotStyle->{Red,Dashed}];
hw216=Plot[{yw215},{y,P14,P15},PlotRange->All,PlotStyle->{Red,Dashed}];
hw217=Plot[{yw216},{y,P15,P16},PlotRange->All,PlotStyle->{Red,Dashed}];
hw218=Plot[{yw217},{y,P16,P17},PlotRange->All,PlotStyle->{Red,Dashed}];
hw219=Plot[{yw218},{y,P17,P18},PlotRange->All,PlotStyle->{Red,Dashed}];
hw220=Plot[{yw219},{y,P18,P19},PlotRange->All,PlotStyle->{Red,Dashed}];
hw221=Plot[{yw220},{y,P19,P20},PlotRange->All,PlotStyle->{Red,Dashed}];
hw222=Plot[{yw221},{y,P20,P21},PlotRange->All,PlotStyle->{Red,Dashed}];
hw223=Plot[{yw222},{y,P21,P22},PlotRange->All,PlotStyle->{Red,Dashed}];
hw224=Plot[{yw223},{y,P22,P23},PlotRange->All,PlotStyle->{Red,Dashed}];
hw225=Plot[{yw224},{y,P23,P24},PlotRange->All,PlotStyle->{Red,Dashed}];
hw226=Plot[{yw225},{y,P24,P25},PlotRange->All,PlotStyle->{Red,Dashed}];
hw227=Plot[{yw226},{y,P25,P26},PlotRange->All,PlotStyle->{Red,Dashed}];
hw228=Plot[{yw227},{y,P26,P27},PlotRange->All,PlotStyle->{Red,Dashed}];
hw229=Plot[{yw228},{y,P27,P28},PlotRange->All,PlotStyle->{Red,Dashed}];
hw230=Plot[{yw229},{y,P28,P29},PlotRange->All,PlotStyle->{Red,Dashed}];
hw231=Plot[{yw230},{y,P29,P30},PlotRange->All,PlotStyle->{Red,Dashed}];
```

```
Show[h11,hw12,hw13,hw14,hw15,hw16,hw17,hw18,hw19,hw110,hw111,hw112,hw113
,hw114,hw115,hw116,hw117,hw118,hw119,hw120,hw121,hw122,hw123,hw124,hw125,
hw126,hw127,hw128,hw129,hw130,hw131(*,hw132*)]
Show[h22,hw22,hw23,hw24,hw25,hw26,hw27,hw28,hw29,hw210,hw211,hw212,hw213
,hw214,hw215,hw216,hw217,hw218,hw219,hw220,hw221,hw222,hw223,hw224,hw225,
hw226,hw227,hw228,hw229,hw230,hw231(*,hw232*)]


(* ---------------------------------------- STM CALCULATION ----------------------------------
------ *)
(* Length of sub-intervals *)
l1=P1-P0;
l2=P2-P1;
l3=P3-P2;
l4=P4-P3;
l5=P5-P4;
l6=P6-P5;
l7=P7-P6;
l8=P8-P7;
l9=P9-P8;
l10=P10-P9;
l11=P11-P10;
l12=P12-P11;
l13=P13-P12;
l14=P14-P13;
l15=P15-P14;
l16=P16-P15;
l17=P17-P16;
l18=P18-P17;
l19=P19-P18;
l20=P20-P19;
l21=P21-P20;
l22=P22-P21;
l23=P23-P22;
l24=P24-P23;
l25=P25-P24;
l26=P26-P25;
l27=P27-P26;
l28=P28-P27;
l29=P29-P28;
l30=P30-P29;
(*l31=P31-P30;*)

l77={l1,l2,l3,l4,l5,l6,l7,l8,l9,l10,l11,l12,l13,l14,l15,l16,l17,l18,l19,l20,l21,l22,l23,l24,l25
,l26,l27,l28,l29,l30(*,l31*)};
```

```
l88={P0,P1,P2,P3,P4,P5,P6,P7,P8,P9,P10,P11,P12,P13,P14,P15,P16,P17,P18,P19,P20,P
20,P21,P22,P23,P24,P25,P26,P27,P28,P29,P30(*,P31*)};

eqw1={eqw11,eqw12,eqw13,eqw14,eqw15,eqw16,eqw17,eqw18,eqw19,eqw110,eqw11
1,eqw112,eqw113,eqw114,eqw115,eqw116,eqw117,eqw118,eqw119,eqw120,eqw121,eq
w122,eqw123,eqw124,eqw125,eqw126,eqw127,eqw128,eqw129,eqw130(*,eqw131*)};
eqw2={eqw21,eqw22,eqw23,eqw24,eqw25,eqw26,eqw27,eqw28,eqw29,eqw210,eqw21
1,eqw212,eqw213,eqw214,eqw215,eqw216,eqw217,eqw218,eqw219,eqw220,eqw221,eq
w222,eqw223,eqw224,eqw225,eqw226,eqw227,eqw228,eqw229,eqw230(*,eqw231*)};

(*a=a11;
b=b11;
d=0.1;*)


stm[u1_]:=
 Block[{u=u1},
  Ac={{0,1},{-a,-d}};
  Ap1={{0,0},{-b,0}};
  Ap2={{0,0},{-b,0}};
  (* 'A' matrix in state space form - with normalization *)
  A1=l77[[u]]*Ac;
  A2=l77[[u]]*Ap1;
  A3=l77[[u]]*Ap2;

  (*Coefficients of shifted chebyshev polynomials*)
  d1=UnitVector[m,1];
  d2=Coefficient[eqw1[[u]],Variables[eqw1[[u]]]];
  d3=Coefficient[eqw2[[u]],Variables[eqw2[[u]]]];

  (*Transpose of Integration Opertaional Matrix*)
  Gt=Transpose[Iom[m]];

  (*Product Matrix*)
  Qd1=pqmat[m,d1];
  Qd2=pqmat[m,d2];
  Qd3=pqmat[m,d3];
  (*Calculation for P[a]*)

Pa=Simplify[KroneckerProduct[A1,Gt.Transpose[{d1}]]+KroneckerProduct[A2,Gt.Tran
spose[{d2}]]+KroneckerProduct[A3,Gt.Transpose[{d3}]]];

  (*Calculation for L[a]*)

La=Simplify[KroneckerProduct[A1,Gt.Qd1]+KroneckerProduct[A2,Gt.Qd2]+Kronecker
Product[A3,Gt.Qd3]];
```

```
(*-----------------------------------------------------------------------------------------------------*)
(*Calculation for B*)
n=Length[A1];
i=IdentityMatrix[n*m];
Ihat=KroneckerProduct[IdentityMatrix[n],Transpose[{d1}]];

(*Performing iterations on La*)
p=pc;
For[k=2;s=i;s1=i,k<=p,k++,
 Lk=Expand[s.La];
 s1=Expand[s1+Lk];
 s=Lk
 ];

 ba=s1.Pa+Ihat;
(*-----------------------------------------------------------------------------------------------------*)
(*Calculation for That*)
Tstar=Transpose[{Table[ChebyshevT[i,ξ],{i,0,m-1}]}];
That=KroneckerProduct[IdentityMatrix[n],Tstar];

(*Determine STM-------------------------------------------------*)
Print["start"];
stm1=((Transpose[That].ba)/.τ->1.0);
stm111=HornerForm[stm1[[1,1]]];
stm112=HornerForm[stm1[[1,2]]];
stm121=HornerForm[stm1[[2,1]]];
stm122=HornerForm[stm1[[2,2]]];
stm1={{stm111,stm112},{stm121,stm122}}

 ]
stmt1=(*(stm[31]).*)(stm[30]).(stm[29]).(stm[28]).(stm[27]).(stm[26]);
stmt2=(stm[25]).(stm[24]).(stm[23]).(stm[22]).(stm[21]);
stmt3=(stm[20]).(stm[19]).(stm[18]).(stm[17]).(stm[16]);
stmt4=(stm[15]).(stm[14]).(stm[13]).(stm[12]).(stm[11]);
stmt5=(stm[10]).(stm[9]).(stm[8]).(stm[7]).(stm[6]);
stmt6=(stm[5]).(stm[4]).(stm[3]).(stm[2]).(stm[1]);
stmt7=stmt1.stmt2.stmt3;
stmt8=stmt4.stmt5.stmt6;
stmt9=stmt7.stmt8;
tr=Tr[stmt9];
stmt10=Chop[stmt9,10^-30];

Export["habdftmp30m20.txt",stmt9]
Export["habdftmp30m20chop-30.txt",stmt10]
Export["habdtrp30m20.txt",tr]
```

B.5

```
BeginPackage["subfunctions2`"]

schebycoeff::usage="schebycoeff returns the coefficient of shidfted chebyT where fun_ is
put in form Cos[2 Pi #]& "

pqmat::usage="Product Matrix"

Iom::usage="Integration Operational Matrix"

Begin["`Private`"]

schebycoeff[fun_,m1_]:=
 Module[{m=m1},
  f[t]=fun[t];   (*f[t]= function which is to be expanded using chebyshev polynomials*)
  w[t]=1/Sqrt[t-t^2];    (*w[t]=Weight function*)
  Tn[t]=ChebyshevT[n,2*t-1]; (*Tn[t]=Shifted chebyshev Polynomial of order n *)
  c=Table[Chop[ParallelNIntegrate[f[t]*Tn[t]*w[t], {t, 0, 1}]/(Pi/2),10^-20], {n, 0, m -
1}]; (*c= coefficient  of Tn[t]*)
  c[[1]]=c[[1]]/2; (*Replace (1,1) to its half in order to apply orthogonality rule*)
  c
  ]

pqmat[x0_,y0_]:=
        Module[{m=x0,c=y0},
                mult[i_,j_]:=mult[i,j]=(tstar[Abs[i-j]]+tstar[i+j-2])/2;  (*function to form
symmetric matrix which is a matrix multiplication of Transpose[T] and [T]*)
                cofmat=Table[Coefficient[Table[Sum[g[i-
1]*mult[i,j],{i,m}],{j,m}][[y]],tstar[i-1],1],{y,m},{i,m}]//Transpose; (*Give you the
Product Matrix*)

  nwcofmat=cofmat/.Table[g[i]->c[[i+1]],{i,0,m-1}]  (*replace the elements of cofmat
matrix by the coefficients calculated in package schebycoeff*)
  ]
```

B.6

```
ClearAll["Global`*"]

c1=0.1;c2=0.25;c3=0.8;
yt=(c1+c2*Sign[(Cos[18*0.0557281*t]+c3*Cos[29*0.0557281*t])])^2;

T[0]=0;
T[1]=N[1.2331020534858776`];
T[2]=N[3.7898309275289983`];
T[3]=N[8.339927384996278`];
T[4]=N[10.809644287801543`];
T[5]=N[13.30851559066226`];
T[6]=N[17.90543280792838`];
T[7]=N[20.387532387012143`];
T[8]=N[22.864216245005764`];
T[9]=N[27.453305983532445`];
T[10]=N[29.965162181751648`];
T[11]=N[32.43289449546345`];
T[12]=N[35.12087555086121`];
T[13]=N[35.77048072012568`];
T[14]=N[36.94080881938995`];
T[15]=N[39.54082733801231`];
T[16]=N[42.007408699287005`];
T[17]=N[44.53741157850583`];
T[18]=N[49.111952667679496`];
T[19]=N[51.58459616643635`];
T[20]=N[54.07388491152966`];
T[21]=N[58.6732804714564`];
T[22]=N[61.16256921654972`];
T[23]=N[63.635212715306565`];
T[24]=N[68.20975380448023`];
T[25]=N[70.73975668369906`];
T[26]=N[73.20633804497375`];
T[27]=N[75.80635656359611`];
T[28]=N[76.97668466286046`];
T[29]=N[77.62628983212484`];
T[30]=N[80.31427088752261`];
T[31]=N[82.78200320123442`];
T[32]=N[85.29385939945362`];
T[33]=N[89.8829491379803`];
T[34]=N[92.35963299597393`];
T[35]=N[94.84173257505768`];
T[36]=N[99.43864979232407`];
T[37]=N[101.93752109518452`];
```

```
T[38]=N[104.40723799798978`];
T[39]=N[108.95733445545707`];
T[40]=N[111.51406332950019`];
T[41]=112.747;

ϕ1[s_]:={{Cos[al*(T[42-s]-T[41-s])],(1/al)*Sin[al*(T[42-s]-T[41-s])]},{-
al*Sin[al*(T[42-s]-T[41-s])],Cos[al*(T[42-s]-T[41-s])]}};
ϕ2[s_]:={{Cos[bt*(T[42-s]-T[41-s])],(1/bt)*Sin[bt*(T[42-s]-T[41-s])]},{-
bt*Sin[bt*(T[42-s]-T[41-s])],Cos[bt*(T[42-s]-T[41-s])]}};

aftm1=ϕ1[1].ϕ2[2].ϕ1[3].ϕ2[4].ϕ1[5].ϕ2[6].ϕ1[7].ϕ2[8].ϕ1[9].ϕ2[10];
aftm2=ϕ1[11].ϕ2[12].ϕ1[13].ϕ2[14].ϕ1[15].ϕ2[16].ϕ1[17].ϕ2[18].ϕ1[19].ϕ2[20];
aftm3=ϕ1[21].ϕ2[22].ϕ1[23].ϕ2[24].ϕ1[25].ϕ2[26].ϕ1[27].ϕ2[28].ϕ1[29].ϕ2[30];
aftm4=ϕ1[31].ϕ2[32].ϕ1[33].ϕ2[34].ϕ1[35].ϕ2[36].ϕ1[37].ϕ2[38].ϕ1[39].ϕ2[40].ϕ1[41];
aftm=aftm1.aftm2.aftm3.aftm4;

tr1=(aftm[[1,1]]+aftm[[2,2]])*Exp[-0.5*d*T[41]];
tr2=tr1/.{al->Sqrt[k1-1-0.25*d*d+3*0.1225],bt->Sqrt[k1-1-0.25*d*d+3*0.0225]};
tr3=tr2/.{d->(0.4+k2)};

plo1=ContourPlot[{tr3==(1+Exp[-(0.4+k2)*T[41]]),tr3==-(1+Exp[-
(0.4+k2)*T[41]])},{k1,-0.2,1.5},{k2,-0.4,0.4},PlotRange->{{-0.2,1.5},{-
0.4,0.4}},PlotPoints->200,ContourStyle-
>{Directive[Black,Bold,Thickness[0.006]],Directive[Gray,Bold,Thickness[0.006]]},Axe
s->True,AxesStyle->Directive[Gray, Thin],FrameLabel-
>{Style[Subscript[k,1],Black],Style[Subscript[k,2],Black]},LabelStyle-
>Directive[20,Black,Bold]]


ClearAll["Global`*"]
SetDirectory[NotebookDirectory[]]

P=112.747;toi=85*P;k1=0.95;k2=-0.1;c1=0.1;c2=0.25;c3=0.8;

yt=c1+c2*(Cos[1*t]+c3*Cos[((1+Sqrt[5])/2)*t]);
yte=c1+c2*Sign[(Cos[1*t]+c3*Cos[((1+Sqrt[5])/2)*t])];

plo4=Plot[{yte},{t,0,150},PlotStyle-
>Directive[Black,Bold,Thickness[0.005]],FrameLabel->{t,HoldForm[y
"(t)"]},LabelStyle->Directive[25,Black,Bold],Frame->True,PlotPoints->2200,PlotRange-
>{{0,80},All},Exclusions->None,FrameStyle->Directive[Black]];

sol=NDSolve[{e''[t]+(0.4+k2)*e'[t]+(3*yte*yte+k1-
1)*e[t]+3*yte*e[t]*e[t]+e[t]*e[t]*e[t]==0,e[0]==-0.25,e'[0]==0.5},e,{t,0,toi}];
x=yte+(e[t]/.sol);
```

```
plo5=Plot[{x,yte},{t,0,150},PlotStyle-
>{Directive[Gray,Bold,Thickness[0.005]],Directive[Black,Bold,Thickness[0.005]],Red},
FrameLabel->{t,HoldForm[x "(t),y(t)"]},LabelStyle->Directive[25,Black,Bold],Frame-
>True,PlotLegends->Placed[{HoldForm[x "(t)"],HoldForm[y "(t)"]},{Scaled[{0.5,0.0}],
{0.5, 0.0}}],PlotPoints->3200,PlotRange->{{0,120},All}]
```